EFFECT OF CENTRIFUGAL AND INTERFACIAL FORCES ON COLLOID TRANSPORT AND MOBILIZATION

By

PRABHAKAR SHARMA

A dissertation submitted in partial fulfillment of
the requirements for the degree of

DOCTOR OF PHILOSOPHY

WASHINGTON STATE UNIVERSITY
Program of Engineering Science

December 2007

To the Faculty of Washington State University:

The members of the Committee appointed to examine the dissertation of PRABHAKAR SHARMA find it satisfactory and recommend that it be accepted.

_____
Chair

_____

_____

_____

Acknowledgements

I would like to extend my gratitude and appreciation to several individuals. First, I would like to thank my major advisor, Dr. Markus Flury for his guidance, support, encouragement, and great patience during the course of my studies. Without his assistance and supervision, this research would not have been possible. I would like to thank my academic committee members, Dr. Joan Wu and Dr. Earl Mattson, and Dr. David Yonge for their valuable advice, guidance, and consistent encouragement. I am very fortunate to have them on my academic committee. I extend my special thank to Dr. Wu for selecting me as a graduate student in the Department of Biological Systems Engineering. I would like to thank specially Dr. Mattson for his assistance during the Geocentrifuges experiment. I would like to express my sincere appreciation to Jon Mathison and Jeffery Boyle for their technical assistance that substantially help to complete this study. My special thanks goes to Dr. Abadou , visiting scientists in our lab, who worked with me during colloid mobilization experiments. I am also grateful to Chris Davitt from Franceschi Microscopy and Imaging Center at Washington State University for her assistance during confocal microscopy. I thank my fellow lab-mate Jianying Shang and Prabhakar Singh for discussion during my research and their friendship.

I gratefully acknowledge the financial supports from the Inland Northwest Research Alliance, the Water Research Center of the State of Washington, and Washington State University.

I would like to extend my deepest gratitude to my parents, who have sacrificed towards my education. Finally, I would like to thank my wife, Archana, for her love, moral support, and understanding while I completed this dissertation.

EFFECT OF CENTRIFUGAL AND INTERFACIAL FORCES ON COLLOID TRANSPORT AND MOBILIZATION

Abstract

by Prabhakar Sharma, Ph.D.

Washington State University

December 2007

Chair: Markus Flury

Knowledge of colloid fate and transport in saturated and unsaturated porous media is important for management of ground- and surface-water contamination, because many contaminants attach and migrate with colloids. In this dissertation, I applied theoretical and experimental techniques to evaluate the forces responsible for deposition and removal of colloids in saturated and unsaturated porous media.

The main objectives of this dissertation were:

1. To test the suitability of geocentrifuges for studying colloid transport in porous media and to determine the critical accelerations when colloid transport through a saturated porous media is altered compared to normal gravity;

2. To study the effect of different boundary conditions imposed at the column outflow on *in situ* colloid mobilization in porous media and to elucidate the mechanisms of colloid mobilization; and

3. To quantify the effect of moving liquid-gas interfaces on the detachment of colloidal

particles from collector surfaces.

I studied the suitability of geocentrifuges for investigating colloid transport. Forces exerted by centrifugation and the thermodynamic energy were considered to develop a theoretical relationship to determine the critical centrifugal acceleration at which sedimentation dominates diffusion. Experiments using a geocentrifuge were carried out to verify the theory.

I demonstrated the importance of the lower boundary of unsaturated porous media on colloid mobilization. Several column experiments were conducted to identify the effect of the boundary conditions. The hydrological conditions and solution chemistry were also varied. In unsaturated porous media, liquid-gas interface played an important role in colloid mobilization. This research demonstrated the paramount role of liquid-gas interfaces on colloid mobilization.

To obtain mechanistic information on the role the liquid-gas interface, I used confocal microscopy to directly visualize and quantify how many colloids can be removed from a solid surface by a moving liquid-gas interface. Theoretical calculations using adhesive forces and surface tension forces were used to support the experimental results.

Table of Contents

List of Tables

List of Figures

Chapter 1

Introduction

1.1 Background

Colloid transport in subsurface environments has received increased attention in the last two decades because mobile colloids can act as carriers of otherwise immobile contaminants. Colloids are commonly defined as particles less than 10 μm in diameter that can remain suspended in aqueous solution for considerable amount of time. Many of the contaminants are colloids themselves, such as viruses and bacteria; or attach to soil colloids, such as heavy metals, radionuclides, or pesticides. Colloids, and attached contaminants, can be transported deep into subsurface systems and cause ground-water pollution. It is therefore important to understand the mechanisms of colloid transport in soils.

Usually, column studies are conducted to represent the subsurface systems for colloid transport. Flow and transport experiments can take extremely long time because of the low hydraulic conductivity of soils, particularly under unsaturated conditions. Geocentrifuges can be used to reduce the experimental time for soils with low hydraulic conductivity and low water content. In geocentrifuges, the driving force can be changed without affecting the

water content [*Nimmo et al.,* 1987]. Geocentrifuges (≈1.5 to 9-m radius, loading capacity up to 200 *g*-tons) were used primarily for geo-technical applications [*Wu et al.,* 1996*; Mitchell,* 1998*; Dewoolkar et al.,* 1999], but they more and more used to study flow and transport in porous media [*Culligan et al.,* 2002]. It was expected that colloid behavior would be changed under centrifugal acceleration (by using geocentrifuges) compared to under normal gravitational acceleration.

In situ colloid mobilization from unsaturated soils is commonly studied by column experiments in the laboratory. In column experiments, the outflow is either open to the atmosphere (seepage boundary) [*Jacobsen et al.,* 1997*; Laegdsmand et al.,* 1999*; Schelde et al.,* 2002] or controlled by a suction (suction-controlled boundary) [*Lenhart and Saiers,* 2003*; Kjaergaard et al.,* 2004*; Levin et al.,* 2006]. At the seepage boundary, the unsaturated flow profile is disturbed and water often flows horizontally along the outflow boundary before outflow occurs [*Abdou and Flury,* 2004]. The increased water content caused by a seepage boundary can lead to colloid mobilization.

The air-water interface can play an important role in colloid mobilization [*Saiers et al.,* 2003]. Several mechanisms have been proposed to explain how the liquid-gas interface affects colloid transport, such as attachment to the liquid-gas interface [*Wan and Wilson,* 1994b], straining in thin water films [*Crist et al.,* 2005], and storage in immobile water regions [*Saiers and Lenhart,* 2003]. Usually, colloids interact strongly with the air-water interface. This principle is used in many applications to separate and fractionate particles. Example of such applications is removal of contaminants in soil remediation, water purification, paper recycling, coal, mining, and medical industries [*Ralston et al.,* 1999*; Gomez-Suarez et al.,* 1999b]. In these applications, air-bubbles are used to separate suspended particles from

each other. The balance among gravity, buoyancy, interfacial, and adhesive forces controls these separation processes [*Huh and Mason,* 1974]. For colloidal-size particles, gravity and buoyancy forces can be neglected [*Scheludko et al.,* 1976*; Preuss and Butt,* 1998*; Pitois and Chateau,* 2002]. It is expected that colloids can detach from the solid surfaces due to moving liquid-gas interfaces, but only if the adhesive forces exceed the interfacial forces [*Noordmans et al.,* 1997].

This dissertation focuses on the effect of different types of forces exerted upon colloidal particles in porous media. I investigated the usefulness of geocentrifuges to study the colloid transport in porous media. A central question was how centrifugal forces change the behavior of colloid in porous media. I also investigated the impact of different types of boundary conditions applied at the column outflow on colloid mobilization. The liquid-gas interface plays an important role in the colloid mobilization. I thus studied the impact of the liquid-gas interface on the detachment of colloid from a solid surface by considering the forces exerted on a single particle.

1.2 Scope and Objectives

This research was conducted to attain a better understanding of the fundamental mechanisms of colloid transport in soils. The ultimate goal of this research was to evaluate the effect of centrifugal and interfacial forces on colloid transport and mobilization in porous media. The specific objectives of this study were:

1. *To test the suitability of geocentrifuges for studying colloid transport in porous media and to determine the critical accelerations when colloid transport through a saturated*

porous media is altered as compared to normal gravity:

The flow rate is low under unsaturated flow; so the study of colloid movement in soils is time-consuming. Geocentrifuges can be used as a tool to study colloid transport in soils and sediments to speed up experiments. Colloidal processes are relevant for the understanding of fate and transport of pathogenic microorganisms, heavy metals, radionuclides, pesticides, and pharmaceuticals; and geocentrifuges can potentially be a useful tool to study these processes.

2. *To study the effect of different boundary conditions imposed at the column outflow on in situ colloid mobilization in porous media and to elucidate the mechanisms of colloid mobilization:*

   The boundary conditions affect the water content distribution, which in turn affects colloid mobilization. The mechanism of colloid mobilization strongly depends on moving liquid-gas interfaces, which occur in soils and near-surface sediments during infiltration and drainage caused by rainfall, snowmelt, or irrigation events.

3. *To quantify the effect of moving liquid-gas interfaces on the detachment of colloidal particles from collector surfaces:*

   Moving liquid-gas interfaces can remove adhered colloidal particles to surfaces. Several factors influence the detachment of colloids from surfaces, such as chemical conditions of solutions, surface charge of colloids and solid surfaces, and multiple passage and velocity of the liquid-gas interface.

1.3 Thesis Outline

This dissertation consists of an introduction and three main chapters; two of which have been submitted, and the third one is ready to be submitted, to peer-reviewed journals. Chapter 1 (Introduction) provides an overview and the major objectives of the dissertation. Chapter 2 presents the use of geocentrifuges to study colloid transport. This chapter describes the importance of sedimentation and diffusion forces on movement of colloids, and the effect of higher gravity (generated by a geocentrifuge) on the behavior of colloids in column transport experiments. In Chapter 3, the effect of the hydraulic boundary conditions on colloid mobilization in the vadose zone are presented. The effect of different flow rates and infiltrating solutions were considered on colloid mobilization. This chapter also elucidates the effect of flotation on colloid mobilization in unsaturated porous media. Chapter 4 describes the detachment of colloidal particles from the solid surface due to moving liquid-gas interfaces. This chapter describes the amount of colloids detached by moving liquid-gas interfaces. Finally, Chapter 5 contains the major conclusions of this study. Tables and figures are included at the end of each chapter in conformity with the format used for manuscript submission to a technical journal. Details on basic theory, additional information on experimental procedures, and supportive data and figures, which are not included in the papers, are presented as Appendices at the end of the respective chapters. All references are listed collectively at the end of the dissertation.

Chapter 2

Studying Colloid Transport in Porous Media using Geocentrifuges

2.1 Abstract

Movement of colloids in the subsurface is a major concern because mobile colloids may enhance the transport of contaminants. Excessive time required to conduct flow and transport experiments in porous media led to the use of geocentrifuges to evaluate subsurface transport processes. The objective of this study was to determine the suitability of geocentrifuges to study colloid transport in saturated porous media. We used sedimentation and diffusion theory to develop a functional relation between centrifugal acceleration, colloid diameter, and colloid specific density, which allows us to predict the acceleration where colloid transport will be dominated by sedimentation or diffusion. A geocentrifuge was used to run colloid transport experiments under saturated flow with polystyrene (1.05 g/cm^3), silica (2 g/cm^3),

This chapter has been submitted for publication: Sharma, P., M. Flury, and E.D. Mattson. 2007. Studying colloid transport in porous media using geocentrifuges, Water Resour. Res.

and hematite (5.26 g/cm^3), under conditions unfavorable for colloid attachment. Colloid deposition coefficients, obtained from the breakthrough curves at different centrifugal accelerations, were used to test the theory. Our results suggest that a critical acceleration can be calculated to determining an upper limit of centrifugal acceleration that should be applied to colloid transport experiments in saturated porous media. Common subsurface colloids, such as iron oxides and aluminosilicates, can be affected at accelerations that are used in geocentrifuge transport studies (5 to 300 g). Even colloids with low specific densities will be affected by centrifugal accelerations if their size is sufficiently large.

Keywords: Colloid, geocentrifuge, deposition.

2.2 Introduction

Colloids are ubiquitous in the subsurface and play an important role in contaminant fate and transport. The behavior of colloids in subsurface systems is often assessed with transport experiments in porous media. Flow and transport experiments in porous media can take a long time, particularly in unsaturated porous media where the hydraulic conductivity decreases exponentially with decreasing water saturation. Experimental time can be shortened by using centrifuges. Two types of centrifuges are used to study flow and transport phenomena in porous media, the unsaturated flow apparatus (UFA) and the so-called geocentrifuge. The UFA consists of a standard laboratory centrifuge that has been modified to accommodate porous media samples together with a water supply and drainage system [*Nimmo,* 1987]. The UFA has been used to determine hydraulic properties [*Nimmo et al.,* 1987*; Conca and Wright,* 1998], diffusion and sorption coefficients [*Celorie et al.,* 1989*; Conca and Wright,*

2000], and to study transport of solutes [*Gamerdinger and Kaplan*, 2000; *Gamerdinger et al.*, 2001] and colloids [*McGraw*, 2000; *Gamerdinger and Kaplan*, 2001].

Geocentrifuges are large-scale centrifuges (≈1.5 to 9-m radius) which have loading capacities up to 200 g-tons. These centrifuges have mainly been used for geotechnical applications [*Wu et al.*, 1996; *Mitchell*, 1998; *Dewoolkar et al.*, 1999], but are being increasingly applied to study flow and transport, like contaminant remediation by air sparging [*Marulanda et al.*, 2000], or transport of NAPL [*Culligan et al.*, 2002; *Levy et al.*, 2002]. Geocentrifuges allow the use of larger samples than possible in the UFA, but at lower accelerations. Typical accelerations in geocentrifuge studies reach up to 300 g [*Mitchell*, 1998; *ISSMGE-TC2*, 1998].

The major advantage of using centrifuges for flow and transport experiments is that the driving force can be varied without affecting the moisture content, experiments can be conducted with materials of low hydraulic conductivity, and the experimental time can be shortened [*Nimmo et al.*, 1987]. Accelerations larger than 1 g may limit the suitability of centrifuges to study colloid transport, because the centrifugal body force may bias colloid transport in such a way that the results cannot be scaled back to a 1 g system. Several studies on colloid transport in porous media have been conducted with centrifuges [*McGraw*, 2000; *Gamerdinger and Kaplan*, 2001; *McGraw*, 1996; *McGraw and Kaplan*, 1997]; however, the effect of centrifugal force on colloid transport has not been considered explicitly. As colloid deposition, specifically deposition by sedimentation, is impacted by the body force acting on colloids, it is expected that colloid transport will be different in a centrifuge experiment as compared to one conducted under normal gravity, if the colloid deposition becomes sufficiently biased by the centrifugal acceleration.

The objectives of this study were to test the suitability of geocentrifuges for colloid trans-

port in porous media, and to determine the critical accelerations when colloid transport through a saturated porous media is altered compared to normal gravity. We used sedimentation and diffusion theory to determine the effect of the centrifugal force on retention of colloids during transport. We predicted the threshold centrifugal acceleration above which colloid transport will be altered as compared to normal gravity conditions, as a function of colloid diameter and colloid specific density. Theoretical calculations were complemented with column transport experiments carried out on a geocentrifuge.

2.3 Theory

Colloid removal from the fluid phase during transport in porous media under favorable attachment conditions can be described by filtration theory [*Yao et al.,* 1971*; Rajagopalan and Tien,* 1976*; Logan et al.,* 1995*; Tufenkji and Elimelech,* 2004a]. Under such conditions, filtration theory could be used to derive critical centrifugal accelerations beyond which colloid filtration is significantly altered as compared to normal gravity. However, under conditions unfavorable for colloid attachment, it has been observed that colloid concentration profiles in porous media do not follow the exponential decrease expected from filtration theory [*Tufenkji and Elimelech,* 2004b*; Tufenkji and Elimelech,* 2005*; Tong and Johnson,* 2007], and the deposition rates of colloids decrease with increasing flow rate [*Li et al.,* 2005*; Johnson and Tong,* 2006*; Tong and Johnson,* 2006]. Both of these observation suggest that filtration theory does not apply for colloid transport under conditions of unfavorable colloid attachment.

No theory is currently available to predict colloid deposition under unfavorable conditions. However, it is expected that sedimentation and diffusion play an important role in the

deposition process. Interception may be important as well, but for submicron-sized particles, it can often be neglected [*Yao et al.,* 1971*; O'melia,* 1980]. To assess the effect of acceleration on colloid transport under unfavorable conditions, we consider the relative importance of sedimentation and diffusion as affected by acceleration.

The root mean square displacement $\overline{x}$ of a colloid by diffusion is [*Hiemenz and Rajagopalan,* 1997]:

$$\overline{x} = \sqrt{2Dt} \tag{2.1}$$

where D is the diffusion coefficient, given by the Stokes-Einstein relationship $D = kT/(3\pi\eta d_c)$, k is the Boltzmann constant, T is absolute temperature, η is the dynamic viscosity, d_c is the colloid diameter, and t is time. The apparent velocity of diffusion v_{diff} can be expressed as function of time or space [*Hiemenz and Rajagopalan,* 1997]:

$$v_{\text{diff}} = \sqrt{\frac{2D}{t}} = \frac{2D}{x} \tag{2.2}$$

where x is travel distance. The apparent velocity of diffusion is time- or scale-dependent. Here we consider the velocity associated with the travel distance of one particle diameter, so that $x = d_c$. The sedimentation velocity of a colloid v_{sed} is given by Stokes law as [*Hiemenz and Rajagopalan,* 1997]:

$$v_{\text{sed}} = \frac{{d_c}^2 a(\Delta\rho)}{18\eta} \tag{2.3}$$

where a is the acceleration, and $\Delta\rho$ is the density difference between the colloid and the fluid.

The random motion of colloids due to diffusion counteracts the linear motion due to sedimentation. In a centrifugation experiment, diffusion is not affected, but sedimentation increases with acceleration, thereby the balance between the two processes changes. We

assume that applying a centrifugal acceleration will not affect the transport results (i.e., colloid deposition) as long as the sedimentation velocity is much less than the diffusion velocity:

$$v_{\text{sed}} \ll v_{\text{diff}} \tag{2.4}$$

As acceleration increases, sedimentation velocity increases, and sedimentation and diffusion velocities become equal ($v_{\text{sed}} = v_{\text{diff}}$) at an acceleration $a_{\text{diff=sed}}$:

$$a_{\text{diff=sed}} = \frac{36\eta D}{d_c^3(\Delta\rho)} = \frac{12kT}{\pi d_c^4(\Delta\rho)} \tag{2.5}$$

where the two right-hand terms are related to each other by the Stokes-Einstein relationship. It is difficult to predict the exact acceleration at which sedimentation starts to become important for colloid deposition in a porous medium, but it is likely that this happens much before $a_{\text{diff=sed}}$ is reached. We assume that as long as the sedimentation velocity is at least two orders of magnitude smaller than the diffusion velocity, diffusion will dominate. Then, based on Equation (2.5), we can estimate the critical acceleration a_{critical} beyond which centrifugation affects colloid transport by:

$$a_{\text{critical}} \approx \frac{a_{\text{diff=sed}}}{100} \tag{2.6}$$

The approximate sign indicates that there is no exact value of a_{critical}, but that rather the order of magnitude of a_{critical} is important.

2.4 Experimental Methods

2.4.1 General Approach

We tested the theoretical predictions with colloid transport experiments using water-saturated columns. A geocentrifuge was used to vary the centrifugal acceleration and to determine the threshold acceleration beyond which colloid deposition was altered. Colloid transport was assessed from colloid breakthrough curves at the column outflow, from which we determined colloid deposition coefficients, K_c. All experiments were carried out at 20 to 22°C and were triplicated.

2.4.2 Types of Colloids

We used three types of colloids: hydrophilic polystyrene particles with COOH surface groups (Bangs Laboratories Inc., Fishers, IN), fluorescent silica particles (Gbr KisKer, Steinfurt, Germany), and hematite (synthesized in our laboratory according to *Schwertmann and Cornell* [2000, *p. 121-129*]). The hematite stock suspension was kept in a polypropylene bottle at pH 1.5, and was diluted with the experimental solution before the beginning of the transport experiments. Polystyrene and silica beads were diluted from the commercial stock solutions.

We verified hematite mineralogical stability during the course of the experiments with XRD (Philips XRG 3100, Philips Analytical Inc., Mahwah, NJ). The shape and size of the colloids were examined by scanning and transmission electron microscopy (Hitachi S-570 SEM, JEOL 1200EX TEM). Electrophoretic mobility of the colloids was measured by dynamic light scattering (ZetaSizer 3000HSa, Malvern Instruments Ltd., Malvern, UK), at the pH and ionic strength used in the transport experiments.

2.4.3 Column Transport Experiments

We conducted a series of colloid filtration experiments using an acrylic column of 1.5-cm ID and 6.4-cm length. The end pieces were made of Teflon with a nylon membrane at both ends. The nylon membrane had a bubbling pressure of 60-cm of H_2O, with a pore opening of 53 μm (square pores). Flow was driven by a peristaltic pump (Ismatec IP4, Glattburg, Switzerland) and a custom-built fraction collector was used to collect the effluent suspensions. A CO_2 trap containing 100 mM NaOH was employed to maintain constant pH of the inflow solutions. The column was packed with silica sand (Mallinckrodt Baker, Inc., Phillipsburg, NJ). The sand was fractionated by dry sieving, and the fraction between 425 and 500 μm in diameter was used in the columns. The sand was pretreated with 2 M HCl at 90^{o}C temperature for 24 hours, to remove impurities, such as Fe-oxides, organic matter and carbonates, and was rinsed with deionized water eight times. The average bulk density of the packed columns was 1.75 g/cm^3, and the porosity was 0.34 cm^3/cm^3.

Colloid suspensions with particle concentrations of 7.5 mg/L (polystyrene of 161-nm diameter), 864 mg/L (polystyrene of 786-nm diameter), 20 mg/L (fluorescent silica), and 8 mg/L (hematite) were prepared, which correspond to a number concentration of 3.16×10^{12} particles/L in all cases. Colloids were suspended in deionized water buffered at pH 10 using 1.67 mM Na_2CO_3/$NaHCO_3$. The ionic strength of the solutions was adjusted with NaCl. Colloid suspensions were introduced into the columns for four pore volumes (approximately 16 mL) for each breakthrough curve. The hydrodynamics of the column experiments was checked with a colloid-free tracer ($NaNO_3$) experiment. The experimental conditions for the experiments are summarized in Table 2.1. Flow rates and ionic strength were selected

from preliminary experiments, such that we obtained about 20 to 40% deposition of colloids under normal gravity (1 g), which we considered optimal for testing the anticipated increased deposition under higher gravity. The flow rate was constant for all experiments, and flow was from top to bottom, in direction of gravity or centrifugal acceleration.

The entire column set up was placed on the platform of a 2-m geocentrifuge (Model C61-3 Civil Engineering Centrifuge, Actidyn Systèmes, France) at the geocentrifuge laboratory of the Idaho National Laboratory, Idaho Falls, ID (Figure 2.1). We first conducted the experiments at 1 g (normal gravity) without spinning the centrifuge to obtain a data set in which to compare the centrifugal results. For experiments conducting using the centrifuge, the column influent was switched from a background solution containing no colloids to a solution that contained the colloids once the centrifuge reached its target centrifugal acceleration. When four pore volumes of the colloid suspension passed through the column, the flow was stopped and the centrifuge was allowed to spin-down. Preliminary tests were run to find optimal centrifugal accelerations, and the finally selected accelerations are shown in Table 2.1. After each experiment, the sand was removed from the column, rinsed thoroughly with deionized water, and repacked into the column.

Effluent nitrate, polystyrene, and hematite concentrations were measured at a wavelength of 220, 300, and 366 nm, respectively, using a spectrophotometer (HP 8452A, Hewlett-Packard), while fluorescent silica concentrations were determined with a fluorescent spectrometer (Hitachi-F3010, excitation bandpass: 10 nm, emission bandpass: 10 nm, scan speed: 120 nm/min). The excitation and emission peaks of the fluorescent silica particles are at 354 and 450 nm, respectively.

For the experiments on the geocentrifuge, it is important to make sure that the colloidal

suspension in the column inflow is stable, i.e., no settling of the colloids in the inflow suspension occurs. We verified the colloidal stability of the different colloidal suspensions in the respective background solutions with a laboratory centrifuge (Beckman, Model J2-21) at a centrifugal acceleration of $a/g = 96$. The sedimentation velocities resulting from an acceleration of $a/g = 96$ were between 0.02 and 0.78 cm/h for the different colloids used, implying that the colloids did not move a considerable distance in the inflow beaker during the course of the experiments. These results indicated that all four colloids remained in stable suspension at least for 50 minutes of centrifugation, suggesting that the colloids should remain in a stable suspension for all the geocentrifuge experiments (maximum acceleration was $a/g = 20$, and maximum time was 26 min).

2.4.4 Force Calculations

We calculated DLVO interaction energies for the colloid-silica sand system using equations for sphere-plate geometry. The electrostatic interaction energy is given as [*Gregory*, 1975]:

$$\Delta G_{\mathrm{el}} = 64\pi\epsilon R \left(\frac{kT}{ze}\right)^2 \Upsilon_1 \Upsilon_2 \exp(-\kappa h) \tag{2.7}$$

and Υ_i for $i = 1, 2$ is defined as

$$\Upsilon_i = \tanh\left(\frac{ze\psi_{0,i}}{4kT}\right) \tag{2.8}$$

where ϵ is the dielectric permittivity of the medium; R is the radius of the colloids; k is the Boltzmann constant; T is absolute temperature; z is the ion valence, e is the electron charge; $\psi_{0,i}$ is the surface potential of the colloids and the sediments, which is taken as the colloid and sediment ζ-potentials, h is the separation distance; κ is the inverse Debye-Hückel length,

which is calculated as:

$$\kappa = \sqrt{\frac{e^2 \sum n_j z_j^2}{\epsilon k T}} \tag{2.9}$$

where n_j is the number concentration of the ions in solution, and z_j is the ion valence.

The van der Waals interaction energy was calculated as [*Gregory*, 1981]:

$$\Delta G_{\text{vdw}} = -\frac{AR}{6h}\left[1 - \frac{5.32h}{\lambda_0}\ln\left(1 + \frac{\lambda_0}{5.32h}\right)\right] \tag{2.10}$$

where A is the effective Hamaker constant; and λ_0 is a characteristic length of 100 nm.

The parameters used for the DLVO calculations are summarized in Table 2.2 and the results are shown in Figure 2.4. The effective Hamaker constants (for sediment-water-colloids) were calculated using the individual Hamaker constants for homogeneous interactions [*Hiemenz and Rajagopalan*, 1997, *page 493*]. The DLVO profiles show differences in the interaction profiles among the colloids. Polystyrene (161 nm) had a small repulsive energy peak (7 kT) and a secondary minimum of about -6 kT (weakly unfavorable conditions), polystyrene (786 nm) had a large repulsive peak and a weak secondary minimum of -3 kT (unfavorable conditions), silica and hematite had repulsive peaks (>125 kT) and weak secondary minima (unfavorable conditions).

The DLVO forces were calculated as

$$F_{\text{ad}} = \frac{\mathrm{d}}{\mathrm{d}h}\left(\Delta G_{\text{tot}}\right) = \frac{\mathrm{d}}{\mathrm{d}h}\left(\Delta G_{\text{el}} + \Delta G_{\text{vdw}}\right) \tag{2.11}$$

where the separation distances h were chosen according to the expected positions of the colloids based on the DLVO interaction energy profiles. We calculated the forces required to remove the colloids from the sediment surface. For polystyrene (161 nm) we used $h > 2$ nm (location of secondary minimum at $h = 1.7$ nm), for polystyrene (786 nm) $h > 12$ nm

(location of secondary minimum at $h = 11.3$ nm), and for silica $h > 4$ nm (location of secondary minimum at $h = 3.5$ nm). For hematite the secondary minimum was at 36 nm and we used a distance > 36 nm to calculate the DLVO forces.

Centrifugation may cause colloids to detach from solid surfaces. Centrifugation is indeed used to measure adhesion forces of colloid attachment. The detachment force F_{det} in a centrifuge is [*Zimon,* 1969]:

$$F_{\text{det}} = V(\Delta\rho)a \tag{2.12}$$

where V is the volume of the colloid, $\Delta\rho$ is the density difference between the colloid and the fluid, and a is the centrifugal acceleration. As long as the adhesive force (Equation 4.4) dominates the detachment force, a deposited colloid will not detach [*Zimon,* 1969].

2.4.5 Data Analysis

The colloid breakthroughs were analyzed with the advection-dispersion model (ADE) including a first-order colloid deposition term. The experimental pore water velocity v was calculated from the measured water flux, as J_w/θ. We used CXTFIT 2.1 [*Toride et al.,* 1995] to fit the ADE to the experimental data, using the effective hydrodynamic dispersion coefficient $D_{\text{hydrodynamic}}$, and the deposition coefficient K_{c} as fitting parameters. Note that the effective hydrodynamic dispersion coefficient $D_{\text{dispersion}}$ is the sum of hydrodynamic dispersion and molecular diffusion, whereas for our experiments, dispersion was in the order of 10^{-7} to 10^{-6} m^2/s, and diffusion in the order of 10^{-12} m^2/s. Diffusion had therefore a negligible effect on hydrodynamic dispersion.

The deposition coefficient was also calculated using the breakthrough data by [*Kret-*

zschmar et al., 1999]:

$$K_c = \frac{v}{L} \ln\left(\frac{C_0}{C}\right) \tag{2.13}$$

where L is the length of column, C is the steady-state outflow and C_0 the inflow colloid concentration. The steady-state outflow was calculated as the mean of the outflow concentration once breakthrough was completed.

The statistical differences between estimated model parameters obtained from the triplicated experiments were evaluated with a one-way ANOVA and Tukey pairwise comparison using SAS [*SAS*, 1990]. A significance level of $p = 0.05$ was chosen for these tests.

2.5 Results and Discussion

2.5.1 Colloid Characterization

Selected properties of the colloids are listed in Table 2.3. All the colloids had a net negative electrophoretic mobility at the experimental conditions (Figure 2.2). The DLVO calculations indicated unfavorable attachment for all the four colloids, i.e., there was a repulsive energy barrier present (Figure 2.4). The polystyrene (161 nm) repulsive barrier, however, was only about 10 kT, i.e., in the range of thermal energy. The scanning and transmission electron microscopy showed that the colloids had spherical shape (Figure 2.3).

2.5.2 Colloid Filtration Experiments

Experimental breakthrough curves for 1 and 20 g, together with the fitted ADE model, are shown in Figure 2.5 (results for all experimental accelerations are presented in the Appendix A). The fitted model parameters and the results of the statistical significance tests are

summarized in Table 2.4. The model could describe the experimental data well, and the fitted deposition coefficients were similar to the ones obtained with Equation (2.13), and showed the same statistical dependencies. The data also showed that the experiments were reproducible.

The hydrodynamic dispersion coefficient ($D_{\text{dispersion}}$) was not affected by acceleration, no significant differences among different accelerations were observed for nitrate and any colloids (Table 2.4). The deposition coefficient K_c, however, showed that acceleration did affect colloid transport for some cases. We did not observe any effect of centrifugal acceleration on breakthrough curves of polystyrene with 161-nm diameter at 20 g (Figure 2.5a,b) and the deposition coefficients were not statistically different between 1 and 20 g (Table 2.4). We noticed the effect of centrifugal acceleration between 10 and 20 g for polystyrene with 786 nm, between 10 and 20 g for silica, and between 10 and 15 g for hematite (Figure 2.5, see Figures 2.11–2.13 in Appendix A). Note that the hematite deposition at 1 g was less than for polystyrene and silica, because we used a lower ionic strength and higher flow rate for the hematite experiments (Table 2.1).

The deposition coefficients for polystyrene with 786-nm diameter at 1, 5, and 10 g were not significantly different, but were different from the one at 20 g, although the absolute differences were small (Table 2.4). For silica, deposition coefficients at 1, 5, and 10 g were not statistically different, but at 20 g the deposition coefficient was significantly larger. For hematite, deposition of colloids at 1, 5, and 10 g was not statistically different, but there was a significant increase of deposition at 15 and 20 g.

The force calculations using Equations (4.4) and (4.2) showed that for all the four colloids, the accelerations, for which $F_{\text{det}} \geq F_{\text{ad}}$, were greater than $10^3 g$. Therefore, colloid detach-

ment due to centrifugation should not be important in our experiments, where accelerations did not exceed 20 g.

2.5.3 Comparison of Experiments and Theory

The deposition coefficients obtained from the ADE fits are plotted as a function of acceleration in Figure 2.6. The figure shows that the colloid transport behavior was not affected by acceleration up to a critical acceleration, beyond which colloid deposition increased significantly. Although polystyrene (786 nm) showed a significantly higher deposition for the 20 g case, the absolute differences in deposition among all the polystyrene (786 nm) experiments were small compared to the other colloids. As discussed below, this is likely because the critical acceleration for polystyrene (786 nm) was of the same order of magnitude as the experimental accelerations.

Table 2.3 shows the critical accelerations obtained from theory (Equations 2.5 and 2.6) and experiments. For polystyrene (161 nm), the expected critical acceleration was in the order of 470, and our largest experimental acceleration was far below that value. From our experiments, we only can say that the critical acceleration is larger than 20 g. For silica and hematite, the theory agrees fairly well with the experimental observations. Indeed, our experimental critical accelerations are in the range of the theoretical predictions. For polystyrene (786 nm), the critical acceleration was in the order of 1 g, i.e., already under normal gravity, the sedimentation velocity is in the range where it affects colloid behavior. Consequently, any increase in acceleration would further enhance sedimentation, and sedimentation should increase linearly with acceleration, as is indeed indicated in Figure 2.6.

Equations (2.6) implies that as long as the sedimentation velocity is more than about

two orders of magnitude smaller than the diffusive velocity, there should be no change in the colloid transport behavior as compared to normal gravity. Diffusion will keep the colloids in suspension. Our experimental data do support this assertion, although we cannot pinpoint the exact critical accelerations because of the limited experimental data available. Deviations between our theory and experimental observations can also be caused by processes not considered in our theory. Our theory only considers diffusion and sedimentation, and does not include any specific colloid filtration mechanisms, such as those used in filtration theory. Indeed, for favorable conditions, we can use filtration theory [*Rajagopalan and Tien,* 1976*; Logan et al.,* 1995] to derive a critical acceleration similar to the one in Equation (2.5) (shown in Appendix A). However, for the case of our experiments, where colloid deposition occurred under unfavorable conditions, no filtration theory currently exists.

The pore water velocity is an important factor for colloid deposition. We can estimate the effect of the pore water velocities for our experimental system by considering the magnitude of the velocities: the pore water velocities (1 to 4 cm/min) were many orders of magnitude larger than both sedimentation and diffusion velocities (10^{-3} to 10^{-12} cm/min) for the accelerations used. For the saturated column experiments described in this study, pore water velocity was controlled at a constant rate using a peristaltic pump, and was independent of the centrifugal acceleration.

The general relationship between the critical acceleration, colloid size, and colloid density as outlined in Equations (2.5) and (2.6) is shown in Figure 2.7. For colloids of the same size, dense colloids exhibit a lower critical acceleration than less dense colloids. For instance, the critical accelerations for 200-nm diameter colloids are 2.5 g for iron oxide (density 5 g/cm^3), 10 g for aluminosilicate (density 2 g/cm^3), and 200 g for polystyrene (density 1.05 g/cm^3).

The figure also shows the relationship between colloid density and size where sedimentation is already an important process at normal gravity, i.e., critical acceleration $a_{\text{critical}}/g = 1$. In these cases, using a geocentrifuge will exceed the critical acceleration, and bias colloid transport.

2.6 Implications

Theoretical calculations illustrated that centrifuge colloid transport experiments are the most appropriate for colloids with low specific density and small diameter. We expect colloid deposition due to sedimentation to become the dominant trapping mechanism as acceleration exceeds a critical value. This critical acceleration is determined by the density difference between colloid and the fluid, and by the colloid size. Other factors, such as pore size and hydrodynamics, will also play role, but are currently not considered in our theory.

The colloids used in our experiments are representative for many subsurface colloids (bacteria, silicates and aluminosilicates, and (hydro)oxides). For inorganic subsurface colloids, such as silicates and iron oxides, colloid transport can be biased in geocentrifuge experiments as compared to normal gravity conditions at fairly low accelerations. Under our experimental conditions (temperature, flow velocities, porous media size, fluid chemical composition, colloid sizes), centrifugal accelerations as low as 10 g changed the filtration behavior of colloidal hematite and silica. Because of their high specific density, (hydro)oxides will be more affected by centrifugal acceleration than silicates.

Organic colloids, which have densities close to that of water, i.e., $\approx$ 1 to 1.4 g/cm^3, are less susceptible to sedimentation. However, natural organic colloids vary a lot in size.

For instance, for viruses (specific density: 1.3 to 1.5 g/cm^3, diameter: 24 to 81 nm [*Jin and Flury,* 2002]) critical accelerations will be in the range of 700 to 10^5 g, so that most geocentrifuge experiments will not affect the transport behavior. Bacteria (specific density: 1.02 g/cm^3, diameter: 1 to 4 μm [*Campbell and Mutharasan,* 2005*; Salyers and Whitt,* 2001]), however, because of their large size, have critical accelerations between 1 and 80 g. Because bacteria have a density close to water, the most sensitive parameter determining the critical acceleration is the bacteria diameter.

2.7 Tables and Figures

Table 2.1: Experimental conditions for geocentrifuge experiments.

Tracer/Colloids	Ionic strength[b] (mM)	pH (–)	Concentration (mM or particles/L)	Pore water velocity (cm/min)	Centrifugal acceleration[c], a/g (−)
Nitrate	0.2	6	0.2 mM	1.58	1, 20
Polystyrene (161 nm[a])	582	10	3.16×10^{12}	1.58	1, 20
Polystyrene (786 nm[a])	57	10	3.16×10^{12}	1.60	1, 5, 10, 20
Silica	307	10	3.16×10^{12}	1.58	1, 5, 10, 20
Hematite	7	10	3.16×10^{12}	3.97	1, 5, 10, 15, 20

[a]Diameter of polystyrene colloid from Scanning Electron Microscopy.

[b]Ionic strength adjusted by NaCl for colloids and by $NaNO_3$ for tracer.

[c]Centrifugal acceleration a normalized by gravitational acceleration g.

Table 2.2: Parameters used for DLVO calculations.

Colloid/ Sediment Pair	Particle radius[a] (nm)	Ionic strength[b] (mM)	Electrophoretic mobility[c] (μm/s)/(V/cm)	ζ-potential[d] (mV)	Hamaker constant (J)
Polystyrene (161 nm)/	80.5	582	-2.31 ± 0.22	-29.1 ± 2.8	5.59×10^{-21} [e]
Silica sand		582	-2.23 ± 0.15	-28.5 ± 1.9	
Polystyrene (786 nm)/	393	57	-6.57 ± 0.03	-82.9 ± 0.4	5.59×10^{-21} [e]
Silica sand		57	-5.50 ± 0.16	-69.3 ± 1.9	
Silica/	91	307	-3.45 ± 0.15	-43.9 ± 1.8	4.67×10^{-21} [e]
Silica sand		307	-3.33 ± 0.04	-42.0 ± 0.4	
Hematite/	49	7	-3.50 ± 0.02	-44.2 ± 0.3	8.12×10^{-21} [f]
Silica sand		7	-5.93 ± 0.07	-74.8 ± 0.9	

[a]Radius of colloid from Scanning Electron Microscopy/Transmission Electron Microscopy. [b]Ionic strength adjusted with NaCl and Na_2CO_3/$NaHCO_3$. [c]Measured using ZetaSizer 3000HSa (Malvern Instruments Ltd., Malvern, UK) at given chemical conditions. [d]Obtained from measured electrophoretic mobilities using the von Smoluchowski equation [*Hiemenz and Rajagopalan*, 1997]. [e]Calculated from data in *Gregory* [1969] and *Hiemenz and Rajagopalan* [1997]. [f]Calculated from data in *Gregory* [1969], *Hiemenz and Rajagopalan* [1997], and *Plaza et al.* [2002].

Table 2.3: Selected properties of colloids and critical accelerations.

Colloids	Specific density (g/cm^3)	Colloid diameter (nm)	Diffusion coefficient[e] (m^2/s)	Electrophoretic mobility[f] ($\mu m/s)/(V/cm$)	Critical acceleration, $a_{critical}/g$	
					theory[g] (–)	experiment (–)
Polystyrene	1.05[a]	161±5[c]	2.66×10^{-12}	−2.31±0.22	≈ 470	>20
Polystyrene	1.05[a]	786±26[c]	5.46×10^{-13}	−6.57±0.03	≈ 1	10–20
Silica	2.0[a]	182±20[c]	2.36×10^{-12}	−3.45±0.15	≈ 14	10–20
Hematite	5.26[b]	98±22[d]	4.38×10^{-12}	−3.50±0.02	≈ 40	10–15

[a]Provided by manufacturer. [b]According to Schwertmann and Taylor [*Schwertmann and Taylor*, 1977]. [c]Measured by Scanning Electron Microscopy (n=20), where n is the number of particles selected randomly for size measurement. [d]Measured by Transmission Electron Microscopy (n=20). [e]Calculated using Stokes-Einstein equation, viscosity of water at 20^{o}C. [f]Measured using ZetaSizer 3000HSa (Malvern Instruments Ltd., Malvern, UK) at the chemical conditions shown in Table 2.1. [g]Calculated with Equations (2.5) and (2.6).

Table 2.4: Parameters for colloid breakthrough curves.

	Experimental parameters		Model parameters[a]		
	Centrif. acceler.	Pore water velocity	Hydrodynamic dispersion[b]	Deposition coefficient[b]	Deposition coefficient[c]
Tracer/ Colloids	a/g (−)	v (cm/min)	$D_{\text{dispersion}}$ (cm^2/min)	K_c (1/min)	K_c (1/min)
Nitrate	1	1.58	0.26±0.01, A	0	0
	20	1.58	0.32±0.06, A	0	0
Polystyrene (161 nm)	1	1.58	0.95±0.10, A	0.061±0.005, A	0.059±0.002, A
	20	1.58	0.87±0.07, A	0.058±0.003, A	0.059±0.002, A
Polystyrene (786 nm)	1	1.60	0.79±0.05, A	0.128±0.002, A	0.125±0.002, A
	5	1.60	0.63±0.06, A	0.131±0.004, A	0.129±0.004, A
	10	1.60	0.65±0.04, A	0.145±0.005, A	0.141±0.005, A
	20	1.60	0.88±0.43, A	0.169±0.010, B	0.158±0.014, B
Silica	1	1.58	0.76±0.10, A	0.153±0.001, A	0.147±0.001, A
	5	1.58	0.71±0.13, A	0.157±0.009, A	0.151±0.008, A
	10	1.58	0.75±0.25, A	0.160±0.008, A	0.153±0.009, A
	20	1.58	0.74[d]	0.590±0.049, B	0.517±0.038, B
Hematite	1	3.97	1.13±0.03, A	0.094±0.015, A	0.087±0.012, A
	5	3.97	1.07±0.01, A	0.063±0.012, A	0.079±0.030, A
	10	3.97	1.15±0.07, A	0.166±0.041, A	0.156±0.037, A
	15	3.97	0.93±0.04, A	1.141±0.055, B	1.016±0.048, B
	20	3.97	1.09±0.43, A	1.277±0.089, B	1.144±0.091, B

[a]The parameters (by column) for particular tracer/colloids followed by the same letter (A or B) are not significantly different at the 95% confidence level within each group of colloids. [b]Obtained by fitting ADE. [c]Obtained from Equation (2.13) using relative concentration from individual breakthrough cures and considering column length = 6.4 cm and experimental pore water velocities. [d]Parameter fixed because of high parameter correlation.

Figure 2.1: The 50 g-ton, 2-m radius geocentrifuge at the Idaho National Laboratory in Idaho Falls, ID. (a) platform, (b) control room, (c) overview, (d) column filling.

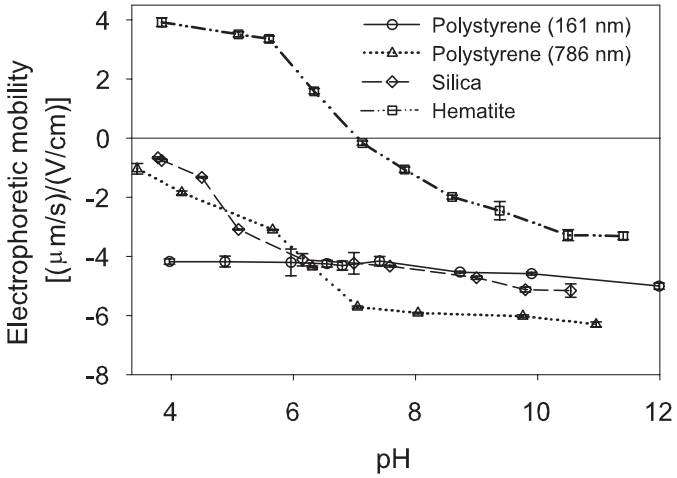

Figure 2.2: Electrophoretic mobility of the colloids as a function of pH measured in a weak electrolyte solution (1.67 mM $NaHCO_3$/1.67 mM Na_2CO_3). Error bars denote ± one standard deviation.

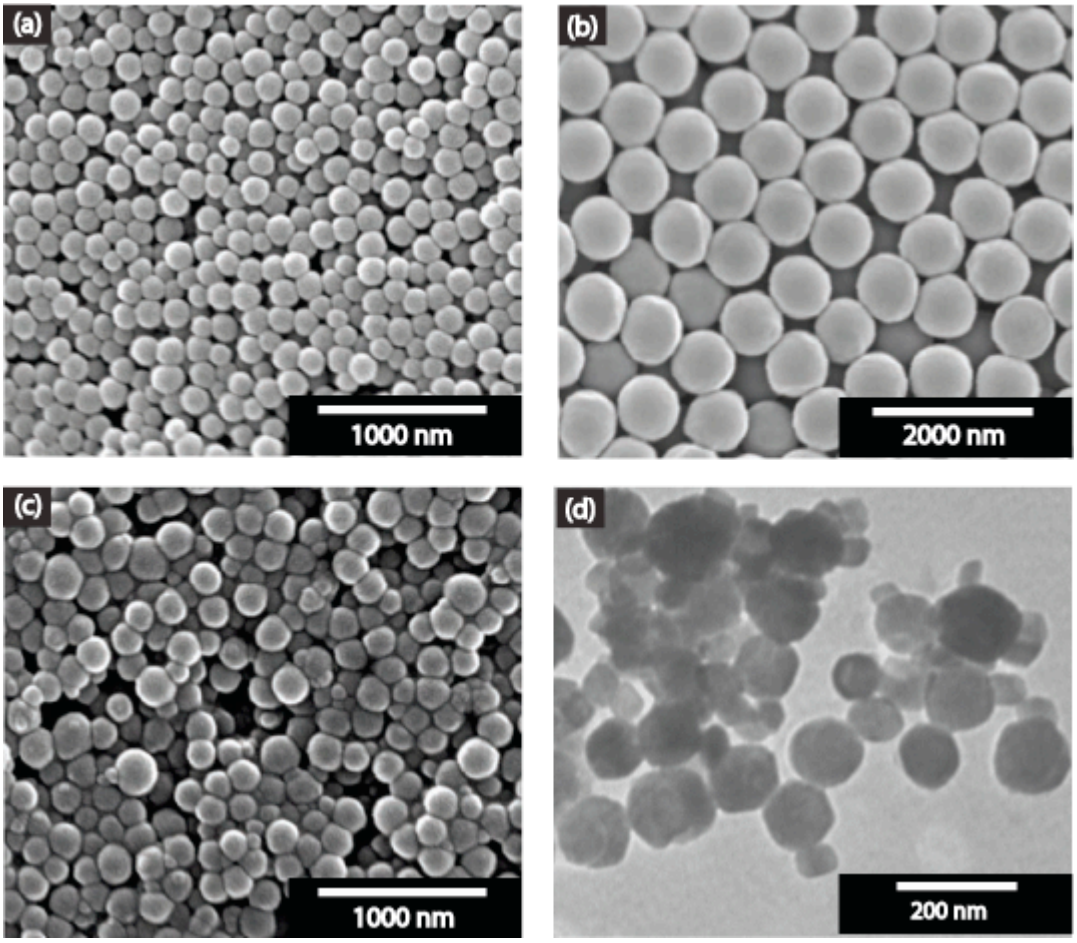

Figure 2.3: Colloid images for (a) polystyrene of 161-nm diameter (Scanning Electron Microscope, SEM), (b) polystyrene of 786-nm diameter (SEM), (c) silica (SEM), and (d) hematite (Transmission Electron Microscope).

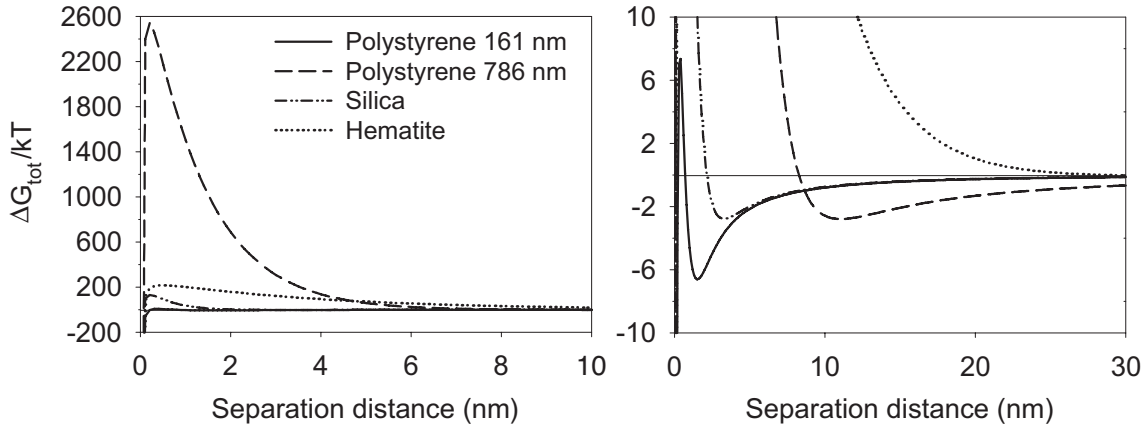

Figure 2.4: DLVO interaction energy profiles for colloids used in the column experiments (left: large-scale view of repulsive peaks; right: detailed view of secondary minima).

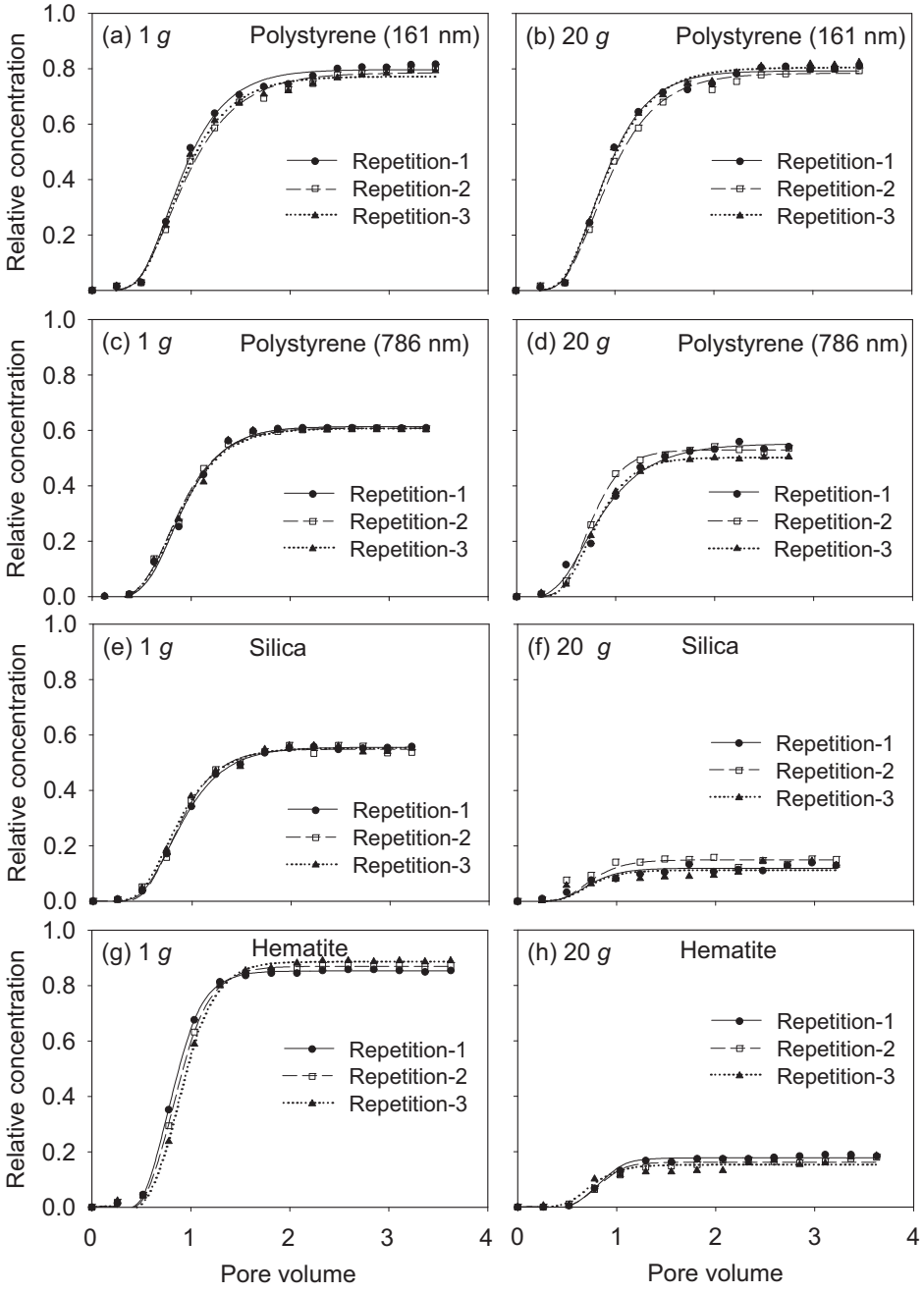

Figure 2.5: Breakthrough curves for (from top to bottom): polystyrene (1.05 g/cm^3 density, 161-nm diameter), polystyrene (1.05 g/cm^3 density, 786-nm diameter), silica (2 g/cm^3 density), and hematite (5.3 g/cm^3 density) at centrifugal accelerations of 1 g (left column) and 20 g (right column) in triplicate. Symbols are the measured data and lines are fitted ADE model.

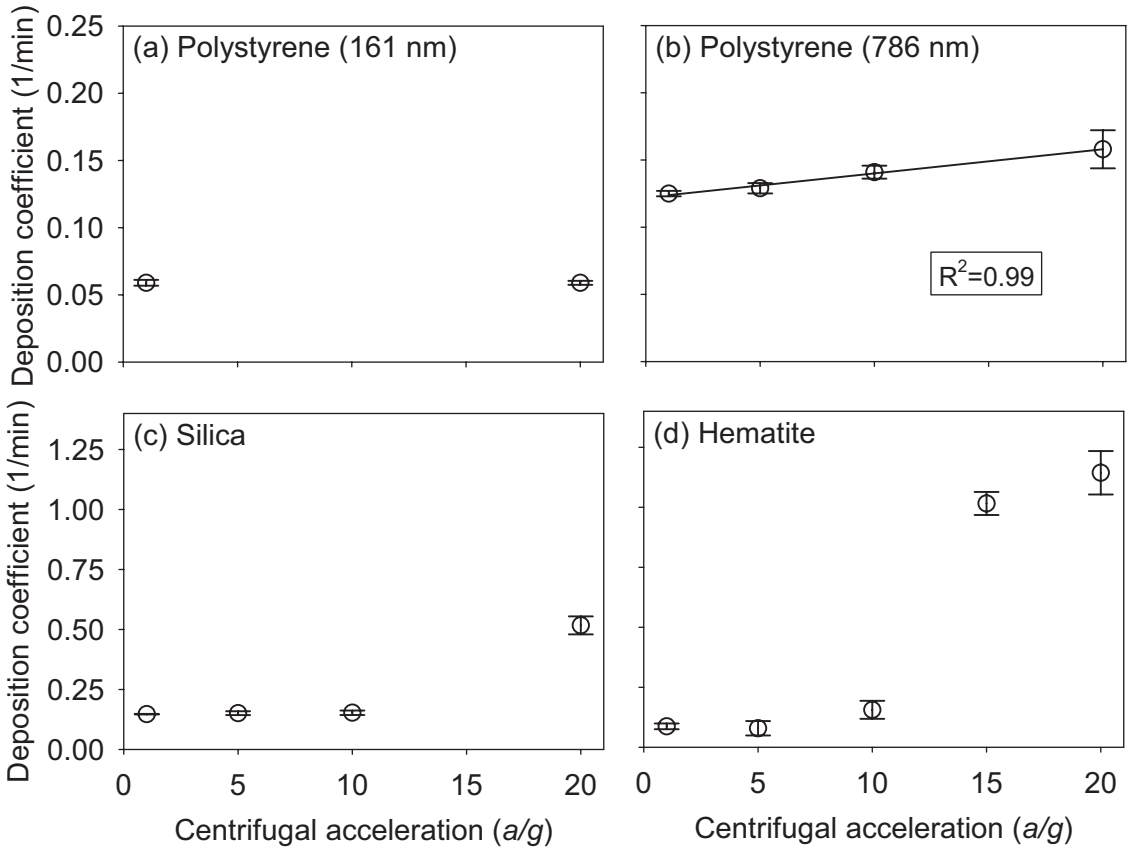

Figure 2.6: Effect of centrifugal acceleration on deposition of colloids: (a) polystyrene (161-nm diameter), (b) polystyrene (786-nm diameter), line shows linear regression, (c) silica, and (d) hematite. Error bars denote ± one standard deviation.

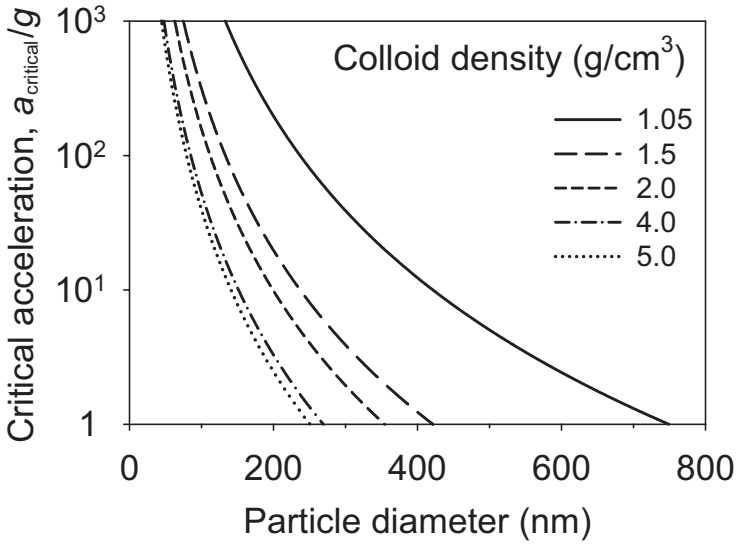

Figure 2.7: Relationship between dimensionless critical acceleration a_{critical}/g and particle diameter for different colloid densities (Equations 2.5 and 2.6) in aqueous suspension at room temperature.

2.8 Appendix A

2.8.1 Filtration Theory

Filtration theory describes the mechanisms of colloid transport to the solid collector (collector efficiency) and the probability that colloids attach to the collector (collision efficiency). The colloid deposition coefficient, K_c, is given by [*Logan et al.,* 1995*; Kretzschmar et al.,* 1999]:

$$K_c = \frac{3}{2}\frac{(1-\theta)}{d_m}\alpha\eta_{tot}v \tag{2.14}$$

where θ is the porosity of the porous medium, d_m is the diameter of the spherical collector, η_{tot} is the total collector efficiency, α is the collision or attachment efficiency, and v is the pore water velocity.

Colloid-collector contact can occur due to interception, diffusion (Brownian motion), and sedimentation. The total collector efficiency, η_{tot}, is the sum of the single collector efficiencies by interception, η_i, sedimentation, η_s, and diffusion, η_d [*Yao et al.,* 1971]. The single collector efficiencies are given according to the RT model by [*Logan et al.,* 1995]:

$$\eta_i = A_s {N_{Lo}}^{1/8}\left(\frac{d_c}{d_m}\right)^{15/8} \tag{2.15}$$

$$\eta_s = 0.00338A_s\left(\frac{(\Delta\rho)ad_c^2}{18v\theta\mu}\right)^{6/5}\left(\frac{d_c}{d_m}\right)^{-2/5} \tag{2.16}$$

$$\eta_d = 4{A_s}^{1/3}\left(v\theta\frac{d_m}{D}\right)^{-2/3} \tag{2.17}$$

where $A_s = \frac{2(1-\gamma^5)}{2-3\gamma+3\gamma^5-2\gamma^6}$ is the Happel correction factor in which $\gamma = (1-\theta)^{1/3}$, $N_{Lo} = \frac{4H}{9\pi\mu{d_c}^2v\theta}$, H is the Hamaker constant, μ is the dynamic viscosity, d_c is colloid diameter, $\Delta\rho$ is the difference between colloid and fluid densities, a is the acceleration (usually due to earth's gravity), and D is the colloid diffusion coefficient, which can be calculated by

the Stokes-Einstein equation [*Hiemenz and Rajagopalan,* 1997]. Depending on pore water velocity, particle size, particle density, and collector diameter, filtration can be dominated either by interception, sedimentation, or diffusion.

We plotted single collector efficiencies due to sedimentation, diffusion and interception as function of dimensionless acceleration a/g, where a is centrifugal acceleration and g is gravitational acceleration, for colloids with different diameter and densities (Figure 2.8). The collector efficiency due to sedimentation increases with acceleration and intersects the collector efficiency due to diffusion as acceleration increases. For small, mineral colloids (density ≤ 2 g/cm^3, diameter ≤ 400 nm) in sandy media, interception can generally be neglected (Figure 2.8a). However, for particles with low density (density ≈ 1.05 g/cm^3), like polystyrene or bacteria, interception will become prominent at low accelerations (Figure 2.8b).

Out of the three single collector efficiency terms, only the sedimentation term, η_{s}, is affected by acceleration. Increasing acceleration, as is done in a centrifuge experiment, will increase colloid filtration due to sedimentation. We assume that acceleration does not affect colloid filtration as long as:

$$\eta_{\mathrm{s}} \leq \kappa \left(\eta_{\mathrm{d}} + \eta_{\mathrm{i}}\right) \tag{2.18}$$

where κ is an empirical factor used to weigh the diffusion and interception coefficients. The relationships between threshold acceleration as a function of pore water velocity and colloid density can be derived from the equality ($\eta_{\mathrm{s}} = \kappa(\eta_{\mathrm{d}} + \eta_{\mathrm{i}})$) in eq (2.18) as:

$$a = \frac{18\mu}{(\Delta\rho)} \left(\frac{\kappa}{0.00338}\right)^{5/6} \left\{ \frac{4^{5/6}(v\theta)^{4/9}}{d_{\mathrm{m}}^{8/9}\, d_{\mathrm{c}}^{5/3}} \left(\frac{D}{A_{\mathrm{s}}}\right)^{5/9} + \frac{(v\theta)}{d_{\mathrm{m}}^{91/48}} \left(\frac{N_{\mathrm{Lo}}}{d_{\mathrm{c}}}\right)^{5/48} \right\} \tag{2.19}$$

Equation 2.19 allows us to predict the centrifugal acceleration at which the filtration behavior of colloids for saturated flow will be altered compared to normal gravity conditions. If the

acceleration exceeds the one predicted by eq 2.19, we expect colloid transport to be affected by centrifugation. The effect of pore water velocity on centrifugal acceleration by considering five different particle densities and diameter = 150 nm is shown in Figure 2.9. The higher the pore water velocity, the greater can the acceleration be before sedimentation overcomes diffusion and interception.

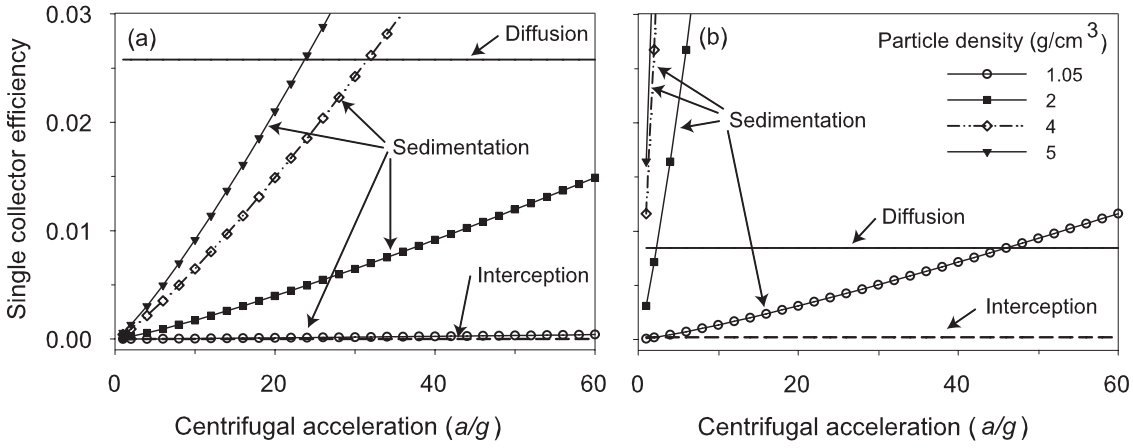

Figure 2.8: Effect of centrifugal acceleration on single collector efficiency due to interception, diffusion and sedimentation at different particle densities. Parameters for collector efficiencies: particle diameter (a) 150 nm and (b) 800 nm, collector diameter = 462.5 μm, pore water velocity = 1.58 cm/min, porosity = 0.34, and viscosity of water at 20^{o}C. The acceleration a/g is the centrifugal acceleration a normalized by gravitational acceleration g.

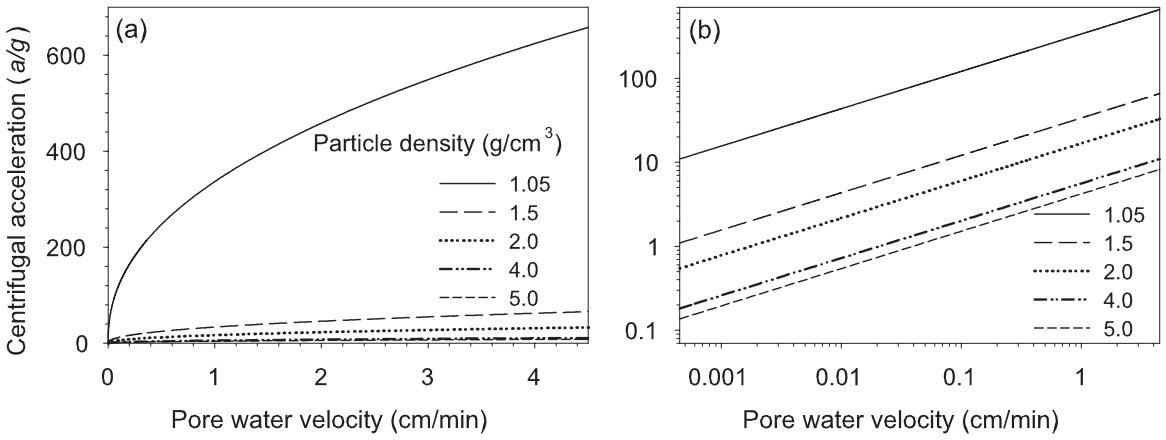

Figure 2.9: Relationship between threshold acceleration and pore water velocity for different colloids (eq 2.19 with $\kappa = 0.16$) at (a) normal scale and (b) log scale. Parameters selected: particle diameter = 150 nm, collector diameter = 462.5 μm, porosity = 0.34, and viscosity of water at 20^{o}C.

2.8.2 Breakthrough Curves from Filtration Experiments

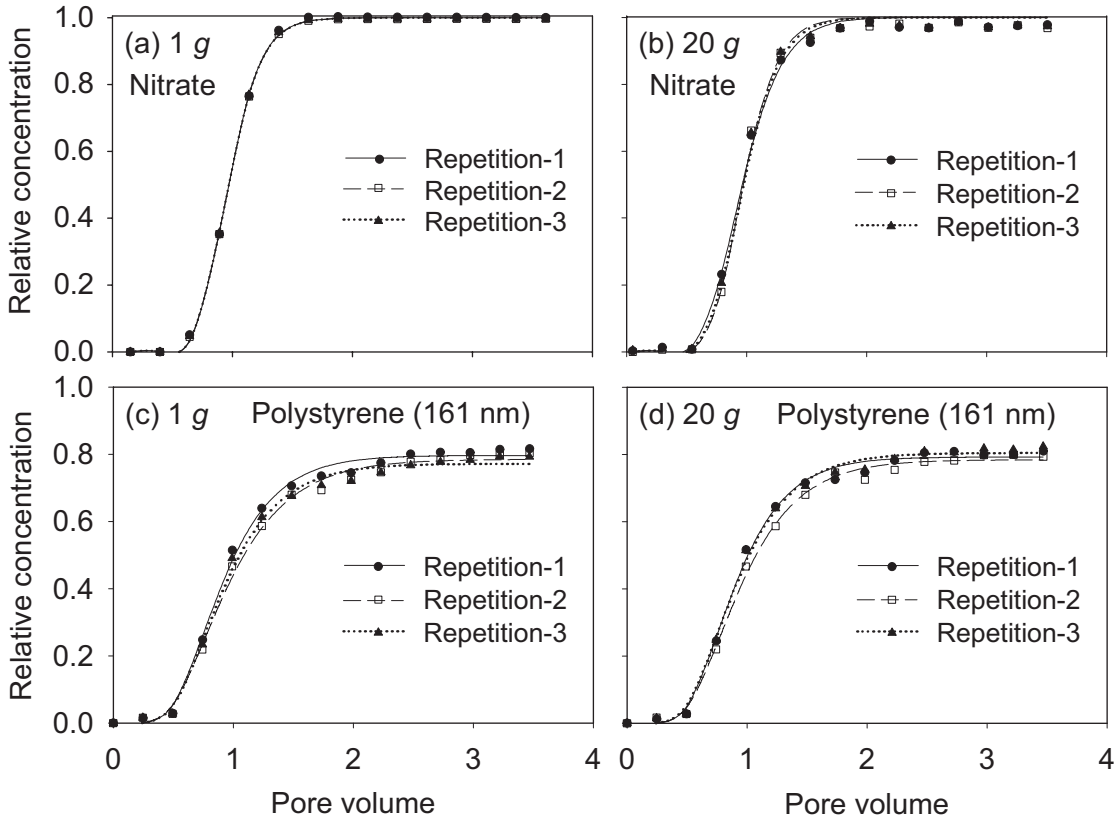

Figure 2.10: Breakthrough curves from transport experiments using tracer (nitrate) and polystyrene (1.05 g/cm^3 density) at 1 g (left) and 20 g (right), in triplicate. (a,b) nitrate, (c,d) polystyrene (161-nm diameter). Symbols are the measured data and lines are fitted ADE model.

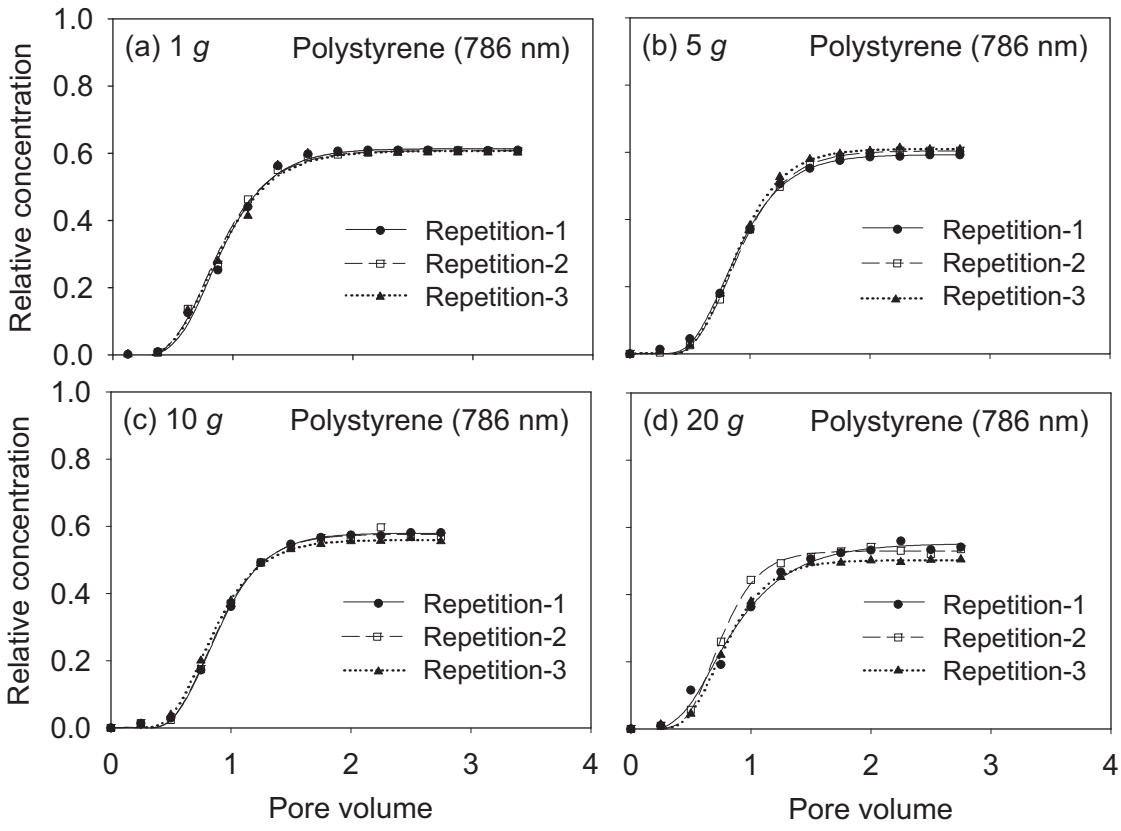

Figure 2.11: Breakthrough curves from transport experiments using polystyrene (1.05 g/cm^3 density and 786-nm diameter) at different accelerations: (a) 1 g, (b) 5 g, (c) 10 g, and (d) 20 g, in triplicate. Symbols are the measured data and lines are fitted ADE model.

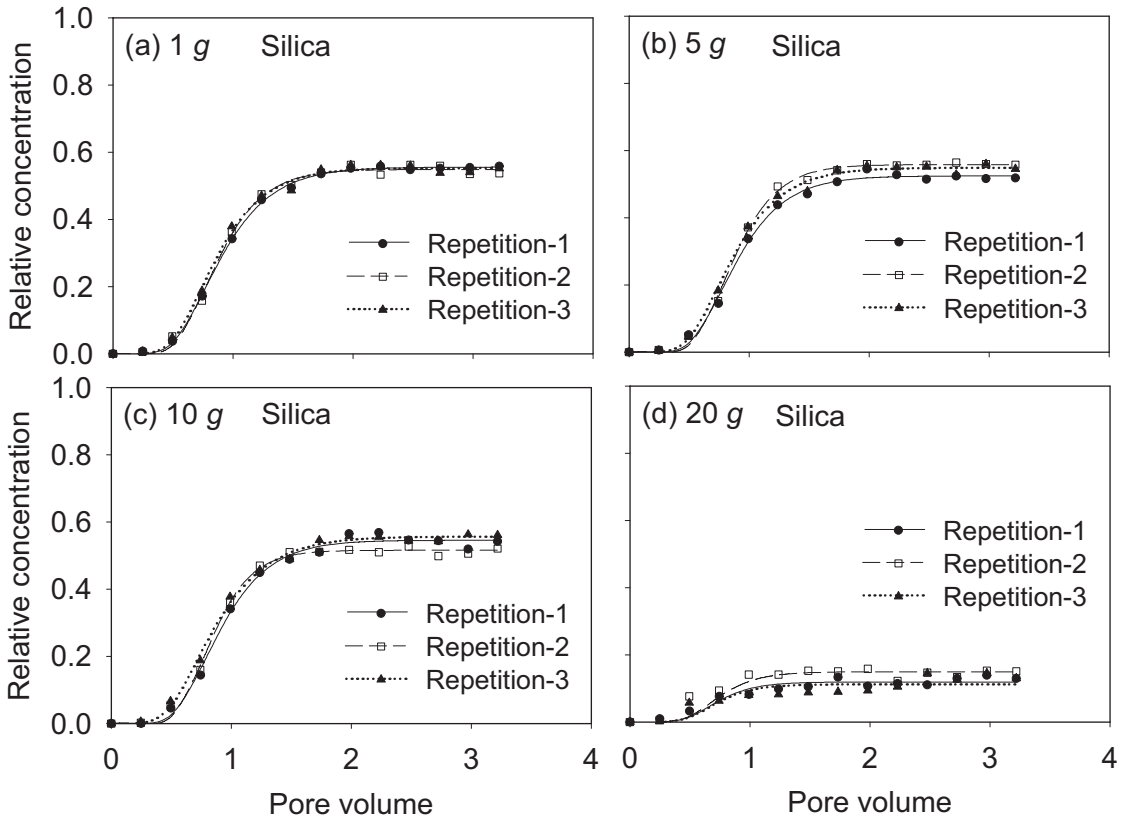

Figure 2.12: Breakthrough curves from transport experiments using silica colloids (2 g/cm^3 density) at different centrifugal accelerations: (a) 1 g, (b) 5 g, (c) 10 g, and (d) 20 g, in triplicate. Symbols are the measured data and lines are fitted ADE model.

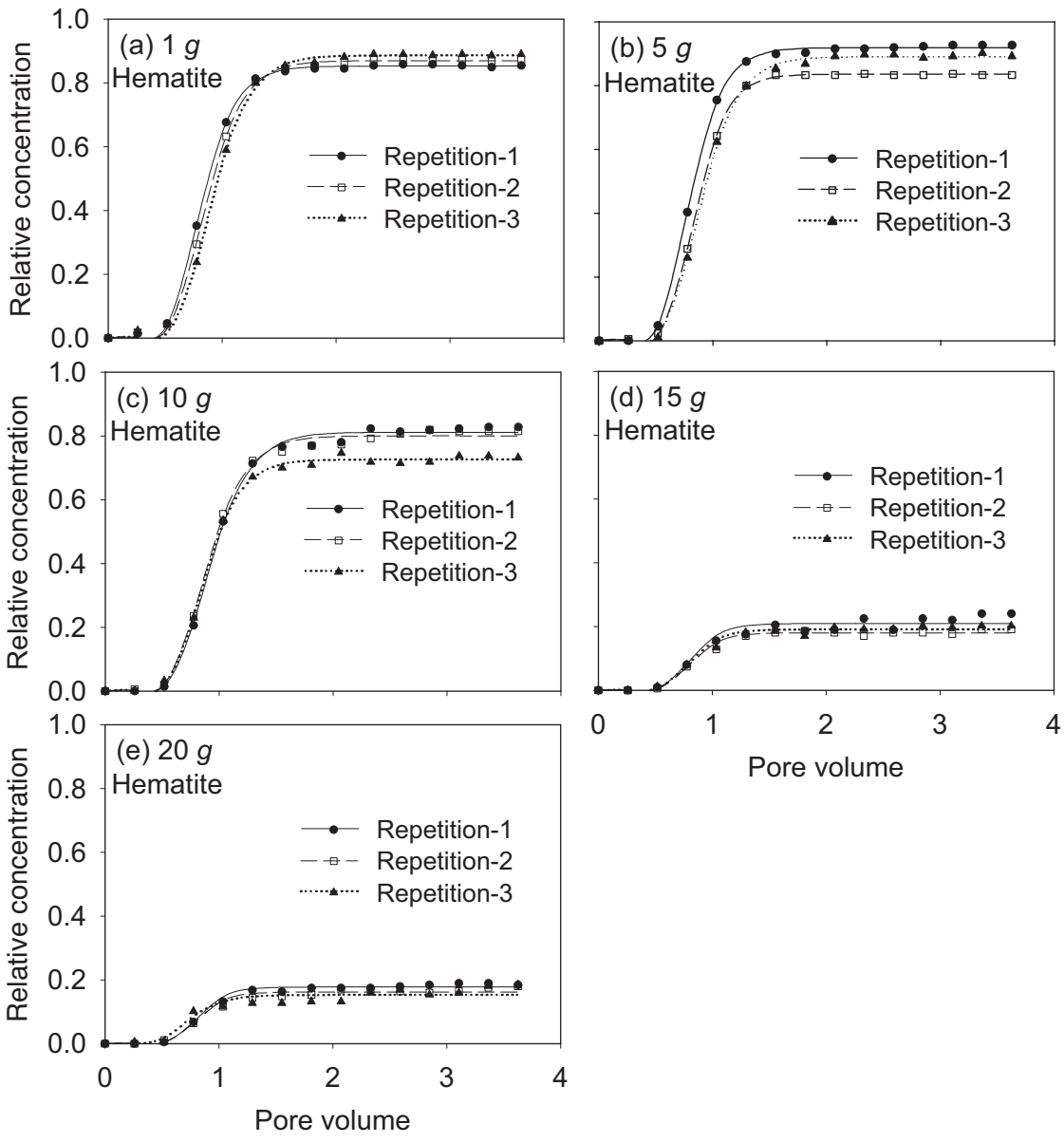

Figure 2.13: Breakthrough curves from transport experiments using hematite colloids (5.3 g/cm^3 density) at different centrifugal accelerations: (a) 1 g, (b) 5 g, (c) 10 g, (d) 15 g, and (e) 20 g, in triplicate. Symbols are the measured data and lines are fitted ADE model.

Chapter 3

Effect of the Lower Boundary Condition on Colloid Mobilization in Unsaturated Porous Media

3.1 Abstract

Colloid transport and mobilization are often investigated by column experiments. Our objective was to study *in situ* colloid mobilization during transient, unsaturated flow as affected by the boundary condition imposed at the column outflow, and to elucidate the mechanisms of colloid mobilization. We conducted colloid mobilization experiments by infiltrating unsaturated, packed sediment columns under two different bottom boundary conditions: a seepage and a suction control. Different flow rates and ionic strengths were used for the column experiments. The mechanisms of colloid mobilization were investigated theoretically using force calculations (adhesive and interfacial forces), complemented with "flotation" experiments, where colloids in the bulk fluid and at the liquid-gas interface were measured

This chapter has been submitted for publication: Sharma, P., H.M. Abdou, and M. Flury. 2007. Effect of the Lower Boundary Condition on Colloid Mobilization in Unsaturated Porous Media, Vadose Zone Journal

separately. More colloids were mobilized under seepage than under suction-controlled boundary conditions. The shape of the colloid breakthrough curves also differed: for the seepage boundary, the maximum of the colloid concentration occurred right at the beginning of the column outflow, but for the suction-controlled boundary, colloid concentrations in the outflow increased gradually before reaching a maximum. Colloid mobilization increased with flow rate and decreased with ionic strength for both boundary conditions; however, colloids were mobilized even at ionic strength exceeding the critical coagulation concentration (CCC). Flotation experiments showed that colloids were located both in the bulk fluid and at the liquid-gas interface at electrolyte concentrations less than the CCC, but only at the liquid-gas interface when the CCC was exceeded. Theoretical considerations confirmed that interfacial forces at the liquid-gas interface exceeded adhesive forces at all ionic strengths used in our experiments. Both experiments and theory showed that the liquid-gas interface had a dominant effect on colloid mobilization. As the movement and configuration of the liquid-gas interface is controlled by the lower boundary condition in column experiments, so is colloid mobilization.

Keywords: Colloid, mobilization, boundary condition, flotation.

3.2 Introduction

Colloid mobilization in the vadose zone is governed by chemical as well as physical factors. Chemical factors include pH, ionic strength, and the surface properties of colloids and sediments. Physical factors include flow rate, water content, film straining, pore size, surface heterogeneity, and capillary forces. Increasing flow rate usually leads to increasing

water content, so that these two factors cannot be separated. Increased water content can cause colloid mobilization by expanding water films [*Wan and Tokunaga,* 1997*; Crist et al.,* 2005*; Gao et al.,* 2006], by a greater fraction of pores contributing to flow [*Levin et al.,* 2006], or by a reduction of the size of immobile water zones [*Saiers and Lenhart,* 2003*; Gao et al.,* 2006]. Colloids can be attracted to the air-water interface, caused by electrostatic [*Wan and Tokunaga,* 2002], or hydrophobic forces [*Gillies et al.,* 2005]. When particles are attached to the air-water interface, usually capillary forces are dominant [*Sirivithayapakorn and Keller,* 2003*; Gillies et al.,* 2005].

Solid particles suspended in aqueous solutions strongly interact with the air-water interface. In industrial applications, air bubbles are used to separate suspended particles in aqueous solutions, a technique known as flotation. The process is based on the attachment of small particles to the surfaces of air bubbles as they rise up inside a suspension [*Scheludko et al.,* 1976*; Ralston et al.,* 1999]. Hydrophobic particles will attach more easily than hydrophilic particles to air bubbles, and will be carried by the rising bubbles to the surface of the suspension, where they can be collected [*Crawford and Ralston,* 1988]. The mechanisms and forces leading particle attachment to bubbles have been investigated by atomic force microscopy [*Gillies et al.,* 2005*; Johnson et al.,* 2006]. It was found that for negatively charged particles, Derjaguin-Landau-Verwey-Overbeek (DLVO) and hydrodynamic forces hinder attachment, but hydrophobic forces favor attachment [*Gillies et al.,* 2005]. It is expected that these forces are also controlling the colloid interactions with the air-water interface in a porous medium.

In situ colloid mobilization from unsaturated soils and sediments has been studied both under field and laboratory conditions. Colloids are usually sampled with lysimeter devices

in the field, and by collecting column outflow in the laboratory. In few cases, the column outflow was suction-controlled [*Lenhart and Saiers*, 2003; *Kjaergaard et al.*, 2004; *Levin et al.*, 2006]; in most cases, however, the bottom boundary was open to the atmosphere, i.e., a seepage boundary was used [*Jacobsen et al.*, 1997; *Ryan et al.*, 1998; *Laegdsmand et al.*, 1999; *El-Farhan et al.*, 2000a; *Schelde et al.*, 2002]. Such seepage boundaries disturb the unsaturated flow profile, because the soil or sediments have to be water saturated before outflow can occur [*Flury et al.*, 1999]. Due to heterogeneity, it is likely that the bottom will initially only locally saturate, causing water to flow horizontally until the bottom is completely saturated [*Abdou and Flury*, 2004]. This boundary-induced increase in water content may impact colloid mobilization, as it is known that more colloids are mobilized at large water contents compared with small water contents. We hypothesize that more colloids are mobilized from a system with a seepage boundary as compared to a suction-controlled boundary, and that this constitutes an experimental artifact. Further, we anticipate that the higher the flow rate, the less the impact of the bottom boundary on colloid mobilization.

Our objectives were (1) to study *in situ* colloid mobilization during transient, unsaturated flow as affected by the boundary condition imposed at the column outflow, and (2) to elucidate the mechanisms of colloid mobilization. Column experiments were carried out, where unsaturated sediments were sprinkling irrigated. Two different boundary conditions were imposed at the column outlet: a seepage boundary and a suction-controlled boundary. We used different infiltration rates to create different liquid-gas configurations inside the columns, and we varied the ionic strength of the infiltration solution to vary DLVO interactions. Theoretical considerations and flotation experiments were used to elucidate the colloid mobilization mechanisms.

3.3 Theory

Colloids are mobilized in a porous medium when the detachment force exceeds the attachment force. We can calculate the net force acting on a colloid in an unsaturated porous medium as follows. We consider the forces acting on a particle exerted by gravity, buoyancy, surface tension, pressure, and adhesion for the case when a particle in a porous medium is in contact with the liquid-gas interface. We first discuss the forces exerted by the liquid-gas interface, and then the forces exerted by adhesion (DLVO forces).

The maximum size of a particle that can float at a liquid-gas interface can be calculated by a force balance using gravity, buoyancy, and interfacial forces. The interfacial forces include surface tension and pressure forces, which, in the general case, have to be calculated numerically. We used the numerical results obtained by *Huh and Mason* [1974] to plot the maximum size of a spherical particle of 2.65 g/cm^3 density that can float at a liquid-gas interface. This density is typical for aluminosilicate-type subsurface colloids. The maximum radius of a particle, as a function of contact angle, that can float at a water-air and ethanol-air interface is shown in Figure 3.1. Water and ethanol were chosen to illustrate the effect of a fluid with high and low surface tension. As the contact angle increases, so does the maximum particle size, and the relationship is approximately linear for contact angles less than 90^o. The graph shows that, for an air-water interface and a contact angle of 30^o, particles with radii up to 650 μm can float at the interface; for a contact angle of 150^o, the maximum radius is 2,800 μm. For ethanol the radii are smaller because of the lower surface tension.

For particles with radii < 500 μm, the effect of gravity and buoyancy can be neglected,

and the force to detach a spherical particle from the liquid-gas interface into the liquid phase is given as [*Scheludko et al.,* 1976*; Preuss and Butt,* 1998*; Pitois and Chateau,* 2002]:

$$F_{\text{det}} = 2\pi R\gamma \sin^2\left(\frac{\theta}{2}\right) \tag{3.1}$$

where R is the particle radius, γ is surface tension of liquid and θ is the advancing contact angle.

The adhesion force is given by the sum of electrostatic and van der Waals forces, which can be calculated from DLVO theory. We calculated electrostatic interaction energies for a colloid-silica sand system using equations for sphere-plate geometry. The electrostatic interaction energies are [*Gregory,* 1975]:

$$\Delta G_{\text{el}} = 64\pi\epsilon R\left(\frac{kT}{ze}\right)^2 \Upsilon_1\Upsilon_2 \exp(-\kappa h) \tag{3.2}$$

and Υ_i for $i = 1, 2$ is defined as

$$\Upsilon_i = \tanh\left(\frac{ze\psi_{0,i}}{4kT}\right) \tag{3.3}$$

where ϵ is the dielectric permittivity of the medium; R is the particle radius; k is the Boltzmann constant; T is the absolute temperature; z is the ion valence, e is the electron charge; $\psi_{0,i}$ is the surface potential of particles and the sediments (taken as the particle and sediment ζ-potentials), h is the separation distance; κ is the inverse of Debye-Hückel length, which is given as:

$$\kappa = \sqrt{\frac{e^2 \sum n_j z_j^2}{\epsilon kT}} \tag{3.4}$$

where n_j is the number concentration of the ions in solution, and z_j is the ion valence.

The van der Waals interaction energies were calculated as [*Gregory,* 1981]:

$$\Delta G_{\text{vdw}} = -\frac{AR}{6h}\left[1 - \frac{5.32h}{\lambda_0}\ln\left(1 + \frac{\lambda_0}{5.32h}\right)\right] \tag{3.5}$$

where A is the effective Hamaker constant; and λ_0 is a characteristic length of 100 nm. The effective Hamaker constant was calculated using the individual Hamaker constants of the liquid (subscript 1) and solid (subscript 2) for homogeneous interactions [*Hiemenz and Rajagopalan,* 1997, *page 492*]:

$$A = A_{212} = (\sqrt{A_{11}} - \sqrt{A_{22}})^2 \tag{3.6}$$

where A_{11} is the Hamaker constant of the liquid and A_{22} is the Hamaker constant of the solid. Finally, the DLVO forces were calculated as

$$F_{\mathrm{ad}} = \frac{\mathrm{d}}{\mathrm{d}h}\left(\Delta G_{\mathrm{tot}}\right) = \frac{\mathrm{d}}{\mathrm{d}h}\left(\Delta G_{\mathrm{el}} + \Delta G_{\mathrm{vdw}}\right) \tag{3.7}$$

We assumed a separation distance of $h = 0.3$ nm [*Elimelech et al.,* 1995] to calculate the values of the DLVO forces.

During infiltration of water into a porous medium, liquid-gas interfaces are moving and exerting forces on particles. By comparing detachment forces exerted by the liquid-gas interface with DLVO forces, we can assess the likelihood that particles are scoured from sediment surfaces during infiltration.

3.4 Materials and Methods

3.4.1 Sediments

We used unconsolidated sediments from the Hanford site (south-central Washington State, USA) for our experiments. The sediments were obtained from 17-m depth below ground surface at the Environmental Restoration Disposal Facility (ERDF), which is located 8 miles from the Columbia River between the 200 East and 200 West areas of the Hanford Site. The

sediments were air dried and stored under ambient laboratory conditions until use. The bulk sediments consisted mainly of quartz, feldspar, mica, magnetite, pyroxene, hornblende, kaolinite, illite, and smectite [*Mashal et al.,* 2004]. The fine fraction (diameter < 2 μm) was mainly quartz, kaolinite, illite, and smectite [*Czigany et al.,* 2005]. The median particle diameter of the bulk sediments was 797 μm, and the sand (50–2,000 μm), silt (2–50 μm), and clay (<2 μm) fractions were 2, 6, and 92% by weight, respectively.

3.4.2 Experimental Setup

Sediments were packed into a brass column of 5.37-cm i.d. and 3-cm length. Before packing the sediments into the columns, the sediments were moisturized to a water content of 0.04 m^3/m^3 to mimic the in situ water content of the sediments at the Hanford site. In addition, the moisturizing helped to bind the fine material to the coarse fraction of the sediments. The bulk density of the packed sediments was 1.46 ± 0.03 g/cm^3 and the porosity was 0.45 ± 0.03 cm^3/cm^3. We determined the soil moisture characteristic of the packed sediments by using the hanging water column method [*Dane and Hopmans,* 2002]. The saturated hydraulic conductivity was determined by the constant-head method [*Reynolds et al.,* 2002] and found to be 2.2 ± 0.12 cm/min.

For the colloid mobilization experiments, the inflow solution was supplied from the top using a sprinkler made of 12 hypodermic needles (22 gauge) and a peristaltic pump (Ismatec IP4, Glattburg, Switzerland). A filter paper (8 μm pore opening) was placed on the top of the column to prevent splashing and to enhance uniformity of the sprinkling application. The bottom of the column consisted of two layers of a nylon membrane (45 μm pore opening, Gilson Company, Lewis Center, OH). The entire column setup was placed on an electronic

load-cell connected to a data logger (CR-7X, Campbell Scientific, Inc., Logan, UT) to monitor the overall gravimetric water content during the experiment. The outflow from the column was collected with a fraction collector.

We used two different setups for the bottom boundary: (1) a seepage and (2) suction control (Figure 3.2a,b). For the seepage boundary, we mounted the two nylon membranes at the bottom of the brass column using rubber bands. The membranes were rigid enough to support the sediments inside the column. A glass funnel was mounted below the column to collect outflow, which was then routed via Tygon tubing to a fraction collector (Figure 3.12 in Appendix C). For the suction-controlled boundary, we used the bottom piece of a Tempe Cell (Soil Measurement Systems, Tucson, AZ). The two nylon membranes, inserted into the bottom piece of the Tempe cell, and a hanging water column were used as suction-control device. Suction was varied with a hanging water column according to the sprinkling rate (Figure 3.13 in Appendix C).

3.4.3 Mobilization Experiments

The mobilization experiments were conducted by infiltrating aqueous solutions under different flow rates and different ionic strengths into the packed sediment columns. To assess the effect of the flow rates on colloid mobilization, we infiltrated deionized water (initial pH 7 and electric conductivity 1 μS/cm) at flow rates of 0.018, 0.035, 0.071, 0.142, and 0.284 cm/min. For each flow rate, new sediment was packed into the column.

We chose one flow rate (0.071 cm/min, the median flow rate) to study the effect of the ionic strength on colloid mobilization. The ionic strength of the inflow was adjusted with 1, 10, 100, 500, and 1000 mM $CaCl_2$ solutions, corresponding to ionic strengths of 3, 30, 300,

1500, and 3000 mM, respectively (Table 3.1). We measured electrical conductivity in the inflow and outflow to monitor changes in electrolyte concentrations during the experiments.

We determined the concentration of the colloids in the effluent by turbidity measurements (HP8452A Diode Array Spectrophotometer) at a wavelength of 300 nm. Before measurement, the vials containing the colloid suspensions were shaken by hand to disperse colloids. A calibration equation was developed by dispersing the Hanford sediments, and separating the colloidal fraction < 2 μm in diameter by gravity settling. Standards were then prepared by dilution of the original suspension and gravimetric measurement of colloid concentrations. Two calibration equations were developed, one for colloid concentrations between 5 and 40 mg/L, and one for 40 and 400 mg/L. Linear calibration equations were used in the two ranges, and the R^2's of the regressions were 0.97 and 1.0, respectively. Samples were diluted when concentrations exceeded the calibration range. The analytical detection limit of the concentration measurements was determined using the standard deviation from several blank measurements [*Skoog et al.*, 1996]. The detection limit was less than 0.42 mg/L and highest for the 1000 mM $CaCl_2$ solution.

All experiments were done at ambient laboratory conditions ($\approx$22°C). Each experiment was repeated three times to check reproducibility of experiments. We also tested the uniformity of the water flow by using a dye tracer to visualize the infiltration patterns. Visualization tests were carried out for each flow rate, using a Brilliant Blue FCF dye solution [*Flury and Wai*, 2003], and showed no evidence of preferential flow within the columns (Figure 3.11 in Appendix C).

The colloid concentration data are presented as averages and standard deviations of the three replicates. Breakthrough curves are plotted as a function of pore volume, i.e.,

cumulative water outflow normalized by the column pore volume. The pore volume for each experiment was estimated by the volumetric water content at steady state. For the suction-controlled boundary, there was a dead volume between the sediment column and the fraction collector, which we considered when plotting the breakthrough curves.

3.4.4 Flotation Experiments

To examine the effect of the liquid-gas interface on colloid mobilization, we conducted a series of "flotation" experiments, where the column was saturated from the bottom. The top of the column was open, and a second, empty brass cylinder was mounted on top of the sediment column, to allow the liquid to raise above the sediment surface (Figure 3.2c and 3.14 in Appendix C). We used the same solutions for these experiments as described above: 0, 1, 10, 100, 500, and 1000 mM $CaCl_2$. In addition, we used ethanol (reagent histological alcohol, ethanol 90% v/v, methanol 5% v/v, isopropanol 5% v/v; Fisher Scientific). Ethanol was used because of its low surface tension ($\sigma = 22.22$ mN/m at 22°C, *Lide*, 1994), and we expected that less colloids would be mobilized because the interfacial forces are smaller at the ethanol-air interface than at the water-air interface.

The liquids were pumped into the columns from the bottom at a flow rate of 0.071 cm/min, and pumping continued until the liquid completely filled the top cylinder, just so that no overflow occurred. Due to surface tension, the liquid-gas interface protruded slightly above the brim of the cylinder without overflowing. We used a stainless-steel gliding rod attached to a collector tube to remove the top layer of the liquid by slicing the gliding rod once over the brim of the column. With this procedure, we collected about 1 mL of solution. We then inserted a hypodermic needle (18 gauge) into the bulk fluid of the top cylinder and extracted

about 1 mL of solution. The collected suspensions were then filtered through a 45 μm nylon membrane, and the colloid concentrations in the filtrate quantified by spectrophotometry as described above. The differences of colloid concentrations between and among different treatments were analyzed by a paired t-test at a significance level of $p = 0.05$ [*SAS Institute Inc.*, 1990]. The surface tensions of the fluids were measured for the inflow and outflow solutions using the Wilhelmy plate method at 20^{o}C (K100 Tensiometer, Krüss GmbH, Hamburg, Germany), and differences were analyzed with a paired t-test ($p = 0.05$).

3.4.5 Parameters for Interfacial Force Calculations

Water-solid-air contact angles were determined on sediment particles with diameters < 100 μm using the Washburn method (K100 Tensiometer). We calculated the ζ-potentials from the electrophoretic mobilities using the von Smoluchowski equation [*Hiemenz and Rajagopalan*, 1997]. The electrophoretic mobilities of colloidal particles were measured in the different solutions used in the column experiments using a ZetaSizer 3000HSa (Malvern Instruments Ltd., Malvern, UK). The effective Hamaker constants were calculated for the different solutions and the Hanford sediment system by Eq (4.3). The Hamaker constants for Hanford sediments and colloids were assumed to be equal, and were approximated as that of silica sand, taken as 7.66 $\times 10^{-21}$ J [*Gregory*, 1969]. The Hamaker constant of water was considered to be 2.43 $\times 10^{-20}$ J [*Hiemenz and Rajagopalan*, 1997]. We assumed the Hamaker constant of ethanol to be that of other hydrocarbons, taken as 5 $\times 10^{-21}$ J [*Visser*, 1972].

3.4.6 Water Flow Modeling

We numerically simulated the infiltration of water into initially moist Hanford sediment columns using the HYDRUS-1D code [*Šimůnek et al.,* 2005]. The parameters for the soil moisture characteristic and the unsaturated hydraulic conductivity functions were obtained by fitting the Mualem-van Genuchten model to experimental water characteristic and saturated hydraulic conductivity data using the RETC code [*van Genuchten et al.,* 1991]. The upper boundary condition for the simulations was set as constant flux with the inflow rates used in the colloid mobilization experiments (Table 4.1), and the initial condition was set as a water potential of -100 cm-H_2O.

Two different cases of the lower boundary were simulated. In the first case, the lower boundary condition was set to be a seepage face, and the boundary had to reach saturation before outflow occurred. At steady-state water flow, the simulations showed that, for all flow rates, the columns were water saturated up to the surface when outflow occurred under this boundary condition. In the second case, we used a suction-controlled lower boundary condition. Different suctions, varying from 0 to -30 cm-H_2O, were applied at the lower boundary, and simulations were run until water flow was steady state. The suctions that provided a uniform water content distribution within the sediments were then used as the boundary conditions for the colloid mobilization experiments (Table 4.1).

3.5 Results and Discussion

3.5.1 Hydraulic Conditions of Mobilization Experiments

Table 4.1 summarizes the hydraulic conditions of the columns at the different flow rates and bottom boundary conditions. For the seepage boundary condition, both the simulations as well as the experimental measurements indicate that the sediments were close to saturation (measured effective saturation ranged from 93% to 97%). For the suction-controlled boundary, the water contents decreased with increasing suction, ranging from 46% to 75% effective saturation. The simulations further indicated that, for both boundary conditions, the water content distribution in the columns was uniform as a function of depth at the time when steady-state flow was reached. The water characteristic and unsaturated hydraulic conductivity functions, obtained by fitting the Mualem-van Genuchten model to the water retention data (hanging water column), are shown in Figure 3.3. Also shown in Figure 3.3 are the five data points obtained from the colloid mobilization experiments for the five flow rates (Table 4.1). These five data points were not used to determine the Mualem-van Genuchten parameters, but the data agreed well with the model curves.

3.5.2 Effect of Flow Rate and Boundary Condition on Colloid Mobilization

For both, the seepage boundary as well as the suction boundary, more colloids were mobilized as the flow rate was increased (Figures 3.4 and 3.5). As the flow rates increased from 0.018 to 0.284 cm/min, the maximum colloid concentrations in the outflow increased by a factor 5 to 6 for both the seepage and suction-controlled boundary conditions (Figure 3.5a). Similarly, the larger the flow rate, the larger was the total mass of colloids mobilized (Figure 3.5b). This

positive effect of flow rate/water content on *in situ* colloid mobilization during infiltration under unsaturated flow is consistent with previous results [*Saiers and Lenhart,* 2003*; Gao et al.,* 2006] Also under drainage conditions, where water is displaced by air, increasing drainage rates have been found to lead to increased colloid mobilization [*Saiers et al.,* 2003*; Zhuang et al.,* 2007]. However, the literature does not allow to differentiate whether the flow rate or the water content is the dominant factor for colloid mobilization.

The bottom boundary condition had a pronounced effect on the shape of the colloid breakthrough curves (Figures 3.4a,b). For the seepage boundary, the maximum colloid concentrations occured right with the first outflow sample, and colloid concentration gradually decreased afterwards. For the suction-controlled boundary, colloid concentrations in the outflow gradually increased until reaching a peak, and then decreased continuously. A second important feature is that the maximum colloid concentrations, as well as the total amounts of colloids mobilized, were considerably greater under the seepage boundary than under suction-controlled boundary conditions (Figure 3.5a,b).

Inspecting the literature on *in situ* colloid mobilization under unsaturated flow shows that under seepage boundary conditions, the colloid breakthrough curves have a similar shape as ours [*Jacobsen et al.,* 1998*; Schelde et al.,* 2002*; de Jonge et al.,* 2004]. In a few cases where suction-controlled boundaries were used, the type of colloid breakthrough-curves as shown in Figure 3.4b were observed [*Saiers and Lenhart,* 2003*; Gao et al.,* 2004].

The different outflow behavior between seepage and suction-controlled boundary is likely caused by different water contents reached at a given flow rate for the two boundary conditions: a higher effective water saturation was reached for the seepage boundary than for the suction boundary (Table 4.1). Under seepage boundary, water only flows out of the column

when the boundary is completely water saturated, causing an initial high spur of colloids to be eluted along with the first outflow of water.

Subsequent increase of the flow rate under seepage boundary condition had little effect on the shape of the breakthrough curve of colloid mobilization (Figure 3.6a). The maximum concentration occurred with the first outflow sample, and increasing flow rate did not cause pronounced mobilization of additional colloids. It appears that the first infiltration event already mobilized most of the available colloids, although the flow rates were subsequently increased. This is likely because already at the lowest flow rate, the column was close to saturation, and increasing flow rates did not increase much the column water saturation (Table 4.1properties).

For the suction-controlled boundary, the subsequent increase in flow rate resulted in subsequent flushes of colloid mobilization. The maximum concentration obtained for the first flow rate was about the same as obtained in the single flow rate experiment (≈100 mg/L), whereas for the subsequent flow rates, the concentrations did not reach the values observed in the single flow rate experiments (Figures 3.4b and 3.6b).

3.5.3 Effect of Ionic Strength and Boundary Condition on Colloid Mobilization

The electrical conductivity measurements showed that there was no significant change between inflow and outflow for solutions with ionic strengths larger than 10 mM $CaCl_2$ (Table 3.1). However, for the 0 and 1 mM $CaCl_2$ solutions, the electrical conductivity of the outflow was elevated for the first few outflow samples, and then decreased steadily (Table 3.1).

Increasing the ionic strength of the infiltration solution caused a decrease in the con-

centrations and total mass of colloids mobilized, under both seepage and suction boundary conditions (Figures 3.7 and 3.8). As the $CaCl_2$ concentration increased from 0 to 10 mM, we observed a drastic reduction of the amounts of colloids mobilized, both in terms of maximum concentrations and total mass (Figures 3.8a,b). Nonetheless, even at the highest ionic strength used, i.e., 1000 mM $CaCl_2$, we still observed colloid mobilization. The maximum concentrations were still in the range of 25 to 45 mg/L (Figure 3.7a,b insets). Under high ionic strength, colloid breakthrough curves under unsaturated flow did not show a pronounced tailing as was observed for low ionic strengths. We suspect that under high ionic strength, the mobile colloids were located mainly at the liquid-gas interface, and that they were eluted from the porous medium as the liquid-gas interface was displaced during an infiltration event. Most of the colloids were therefore eluted when the liquid-gas interface reached the bottom of the porous medium.

As will be shown in the next section, there were no colloids present in the bulk fluid at electrolyte concentrations larger than 10 mM $CaCl_2$, confirming that at high ionic strength the eluted colloids were located at the liquid-gas interface. It is expected that as the ionic concentration of the infiltration solution exceeds the critical coagulation concentration (CCC), colloids inside the bulk pore water will coagulate and sediment out [*Grolimund et al.,* 1996*; Grolimund et al.,* 2001*; Czigany et al.,* 2005].

3.5.4 Effect of the Liquid-Gas Interface on Colloid Mobilization

The results of the flotation experiments indicate that colloids were captured at the liquid-gas interface. For all solutions used, a considerable amount of colloids was found at the liquid-gas interface (Figure 3.9). The colloid concentrations at the liquid-gas interface were

significantly larger than in the bulk fluid for all cases. Although the absolute values of the colloid concentrations at the liquid-gas interface are somewhat subject to the measurement method used, our data indicate that a substantial fraction of the colloids mobilized was located at the liquid-gas interface. We would expect that the larger the surface tension, the greater the amount of colloids captured at the liquid-gas interface, because the capillary and interfacial forces increase with surface tension. There were differences in colloid concentrations at the liquid-gas interface among the different liquids (see significance matrix in Figure 3.9); however, the differences did not show a consistent trend. Unexpectedly, the solution with the lowest surface tension (ethanol) had the significantly highest concentrations of colloids at the liquid-gas interface.

The analysis of the bulk liquid showed that deionized water had the largest colloid concentration in the bulk liquid (Figure 3.9). Already at 1 mM $CaCl_2$, the colloid concentration dropped significantly, and for $CaCl_2 \geq 10$ mM, the measured colloid concentrations were below the analytical detection limit. The drop in colloid concentrations agrees with the critical coagulation concentrations (CCC) for coarse Hanford sediment colloids, which were reported to range from 0.7 to 1.4 mM $CaCl_2$ [*Czigany et al.*, 2005]. The colloid concentrations in the bulk liquid dropped with increasing ionic strength, but the interfacial concentrations did not drop. This shows that the colloids at the liquid-gas interface were protected against coagulation and sedimentation. We cannot with certainty eliminate coagulation at the liquid-gas interface, but at least, no coagulation was observed visually (aggregates larger than 11 μm should be visible by eye).

Saiers et al. [2003] reported an inverse relationship between colloid scouring by the air-water interface and ionic strength: for ionic strengths ranging from 1 to 50 mM NaCl, the

scouring probability decreased with increasing ionic strength. They hypothesized that at the higher ionic strength, colloids formed aggregates at the silica surfaces, and were then less susceptible for mobilization by the air-water interface. Our data also showed decreasing colloid mobilization with increasing ionic strength as long as the CCC was not exceeded; however, no consistent trends were evident at concentrations larger than the CCC.

For ethanol, the colloid concentrations in the bulk fluid were smaller than for 0 and 1 mM $CaCl_2$ solutions (Figure 3.9). Generally, charge-stabilized colloidal suspensions are less stable in alcohol than in water because alcohol reduces the electrical repulsion between particles [*Permien and Lagaly*, 1994]. For instance, the CCC of Na montmorillonite decreased with increasing alcohol contents of the suspensions; montmorillonite-alcohol complexes formed at high alcohol contents, and colloidal suspensions became unstable [*Permien and Lagaly*, 1994]. In our ethanol experiment, colloids were therefore not in stable suspension, and only a small amount of colloids is expected to be in the bulk fluid.

3.5.5 Interfacial Force Considerations

We calculated the forces exerted on a particle attached to the solid phase during an infiltration event. Before infiltration, the particles attached to the solid phase are partially exposed to the air phase. A thin liquid film, because of the pre-wetting of the sediments, formed strong attractive capillary forces pinning the particles to the solid surfaces. As we infiltrated fluid under saturated conditions (infiltration from the bottom), these liquid films expanded and ultimately caused a repulsive force on the particles away from the solid phase as the liquid-gas interface moved along with the displacement of the gas phase. Particles detached from the solid surface when adhesion (DLVO) forces were less than detachment (capillary)

forces. Our calculations showed that the detachment forces exceeded the adhesion forces for all particle radii (Figure 4.2). The larger the particle radius, the larger was the force difference between detachment and adhesion. We calculated the forces for all the different fluids used in our experiments, using the surface tensions and densities shown in Table 3.1. The measured contact angles for the colloids with air-water and air-ethanol were 26^o and 10^o, respectively. The measured fluid surface tensions did not significantly differ between inflow and outflow solutions. The forces among the electrolyte solutions were similar; however, both, the capillary and DLVO forces were much smaller for ethanol (Figure 4.2).

These calculations indicate that the forces exerted by the liquid-gas interface indeed can detach colloids from the sediment surface. As the liquid-gas interface moves through the porous medium, colloids that are attached to the liquid-gas interface are displaced along with the liquid-gas interface. As colloids are captured at the liquid-gas interface, they are floating on the liquid surface, like in a typical mineral flotation process [*Schulze,* 1977*; Leja,* 1982*; Ralston et al.,* 1999]. The maximum size of spherical particles that can float on a liquid-gas interface (air-water and air-ethanol) based on a force balance is shown in Figure 3.1, and the specific radii for our experimental system are listed in Table 3.1. These data show that the floatable particle size is in the order of hundreds of micrometers, consistent with what is known from mineral flotation [*Scheludko et al.,* 1976*; Pitois and Chateau,* 2002].

These force calculations support our experimental observations of high particle concentrations at the liquid-gas interface (Figure 3.9). The different ionic strengths of the aqueous solutions did not result in significant changes of the DLVO and capillary forces (Figure 4.2), which corroborates our experimental finding of a non-consistent trend of particle concentrations at the liquid-gas interface as a function of ionic strength. The force calculations also

show that particles up to a few hundred micrometers can float on the liquid-gas interface (Table 3.1). In our experiment we filtered the samples through a 45 μm membrane, eliminating larger particles. Therefore, the measured particle concentrations at the liquid-gas interface are only approximate. Nonetheless, our data show the pronounced effect of flotation.

That particles attach to liquid-gas interfaces is known from flotation and bubbling experiments [*Scheludko et al.*, 1976; *Ralston et al.*, 1999; *Wan and Tokunaga*, 1998; *Wan and Tokunaga*, 2002], and from micromodel studies [*Sirivithayapakorn and Keller*, 2003]. An important difference in our experiments is that our colloids are forced to contact the liquid-gas interface, whereas in previous bubbling and visualization experiments, colloids were in the liquid phase and had to penetrate the liquid-gas interface first before strong capillary forces become active. Our experimental scenario is more similar to the air-bubble experiments described by *Gomez-Suarez et al.* [1999a] and *Gomez-Suarez et al.* [1999b]. These latter experiments corroborate that colloids can be scoured from sediment surfaces by moving liquid-gas interfaces.

3.6 Implications

Our experiments showed that colloid mobilization was strongly affected by the type of boundary condition imposed at the column outflow. Not only the amounts of colloids mobilized differed (the colloid mass mobilized under the suction-controlled boundary was 20 to 60% less than the one under seepage), but also the shapes of the colloid breakthrough curves were different between the boundary conditions. This difference in colloid mobilization is caused by saturation of the sediments at the seepage boundary, which is an experimental artifact

for unsaturated flow experiments. The lower the water flow rates (or the lower the water content), the more pronounced will be the artifacts. This has important implications for sampling colloids in the vadose zone: any sampling device that causes local saturation, will likely cause sampling artifacts.

Our results further showed the importance of interfacial forces associated with the liquid-gas interface on colloid mobilization. Even at ionic strengths larger than the CCC, colloid mobilization still occurred. At low ionic strength, the mobilized colloids were located both in the bulk fluid and at the liquid-gas interface, whereas at high ionic strength (larger than the CCC), colloids were mainly associated with the liquid-gas interface and no colloids were found in the bulk fluid. Moving liquid-gas interfaces are effective in mobilizing colloids, and any changes in liquid-gas interface configurations, as caused by sampling devices or outflow boundaries, will cause experimental artifacts.

The results from this study point to the relevance of moving air-water interfaces for colloid mobilization and transport in the vadose zone. Such moving air-water interfaces are common in soils and near-surface sediments, where rainfall, snow melt, or irrigation cause infiltration and drainage. Current theory for colloid transport in unsaturated porous media does not consider the effect of moving air-water interfaces.

3.7 Tables and Figures

Table 3.1: Properties of solutions used in the experiments.

Background solution	$CaCl_2$ conc. (mM)	Ionic strength (mM)	Electrical conductivity		Surface tension[b]		Density (kg/m^3)	Max. flotation radius[e] (μm)
			Inflow (mS/cm)	Outflow (mS/cm)	Inflow (mN/m)	Outflow (mN/m)		
Ethanol	–	–	–	–	22.42±0.02	22.79±0.03	787.3[c]	112
DI water	0	0	0.002±0.001	0.03 to 0.15[a]	72.56±0.05	71.65±0.82	997.4[c]	567
	1	3	0.27±0.01	0.28 to 0.44[a]	72.73±0.28	71.59±0.64	1001[d]	572
	10	30	2.43±0.04	2.30±0.07	72.93±0.11	71.70±0.13	1005[d]	573
	100	300	18.7±1.3	17.7±1.2	73.22±0.09	72.46±0.34	1075[d]	596
	500	1500	71.0±0.1	67.1±1.8	74.18±0.22	73.04±0.24	1318[d]	654
	1000	3000	115±1	111±3	75.16±0.04	74.67±0.39	1508[d]	715

[a]Range of measurements for 0 to 2.5 pore volume column outflow: first number refers to the last outflow sample, second number is the first value measured.

[b]Measured with Wilhelmy plate using a Krüss K100 Tensiometer at 20^{o}C.

[c]At 25^{o}C, from *Lide* [1994].

[d]At 25^{o}C, from *Zhang et al.* [1997].

[e]Obtained from Figure 3.1; the contact angle of ethanol-colloid-air was 10^o and water-colloid-air was 26^o.

Errors are ± standard deviations.

Table 3.2: Initial and boundary conditions used for water flow modeling.

Flow rate		Seepage Boundary					Suction Controlled Boundary				
J_w	J_w/K_s[a]	Pore water velocity[b]	Suction[c]	Water content θ_v modeled[d]	Water content θ_v measured	Effective saturation measured	Pore water velocity[b]	Suction[c]	Water content θ_v modeled[d]	Water content θ_v measured	Effective saturation measured
(cm/min)	(−)	(cm/min)	(cm-H_2O)	(cm^3/cm^3)	(cm^3/cm^3)	(%)	(cm/min)	(cm-H_2O)	(cm^3/cm^3)	(cm^3/cm^3)	(%)
0.018	0.008	0.043	0	0.421	0.418	92.9	0.087	27	0.226	0.206	45.8
0.035	0.016	0.083	0	0.421	0.424	94.2	0.149	23	0.248	0.236	52.3
0.071	0.032	0.165	0	0.422	0.430	95.5	0.268	20	0.270	0.265	58.9
0.142	0.065	0.329	0	0.422	0.431	95.8	0.482	16	0.300	0.294	65.4
0.284	0.129	0.654	0	0.422	0.434	96.5	0.839	12	0.340	0.339	75.2

[a] K_s is the saturated hydraulic conductivity.

[b] Calculated by $J_w/\theta_{v,\text{measured}}$.

[c] Obtained by HYDRUS-1D modeling, and then used as experimental boundary conditions.

[d] At steady-state water flow, water contents were uniform throughout the column.

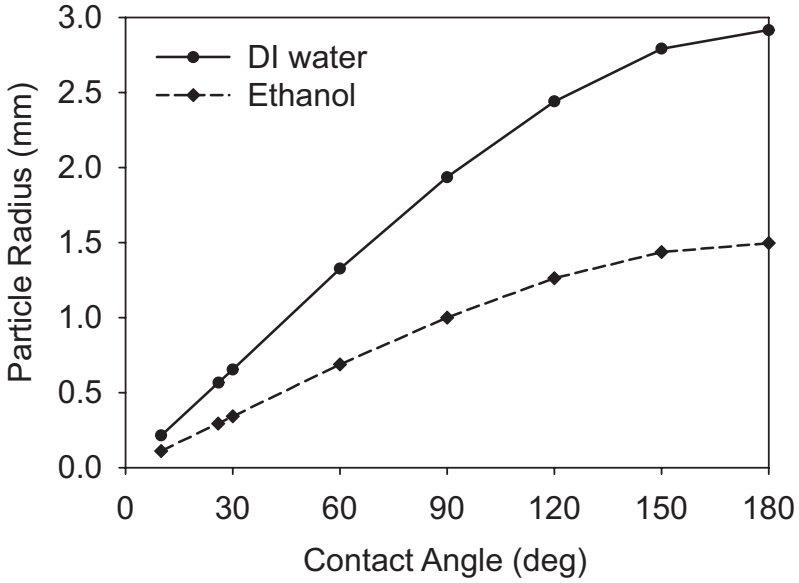

Figure 3.1: Maximum radius of a spherical particle that can float at a liquid-gas (air) interface as a function of contact angle for deionized water and ethanol. (Data points denoted by symbols were taken from Table 1 in Huh and Mason, 1974).

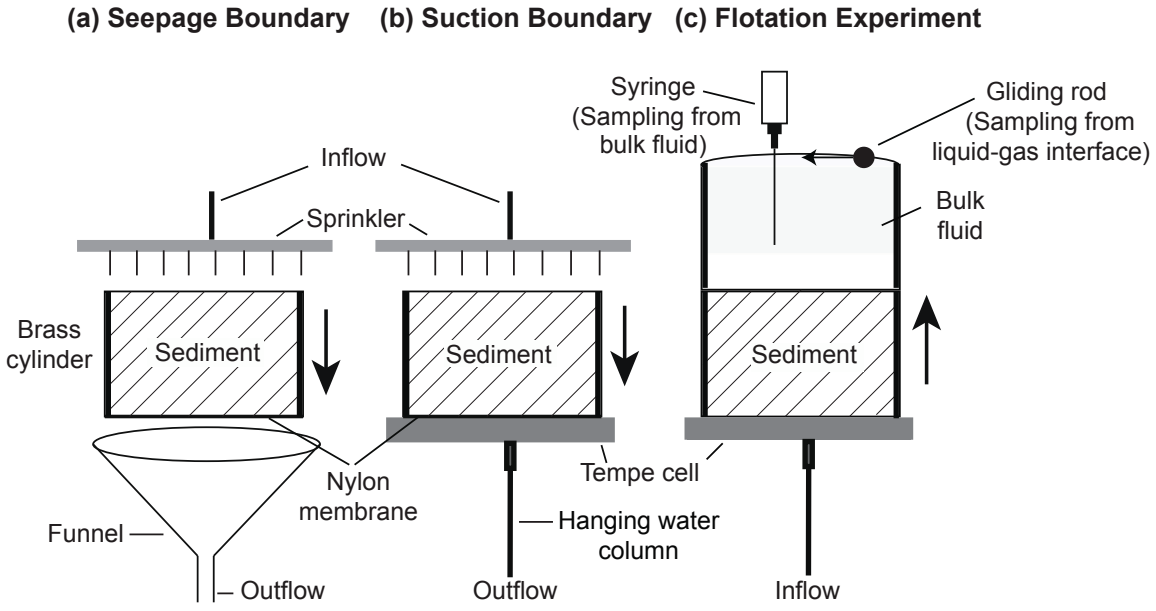

Figure 3.2: Experimental setup for the mobilization experiments: (a) seepage boundary, (b) suction boundary, and (c) flotation experiments. Vertical arrows indicate direction of flow.

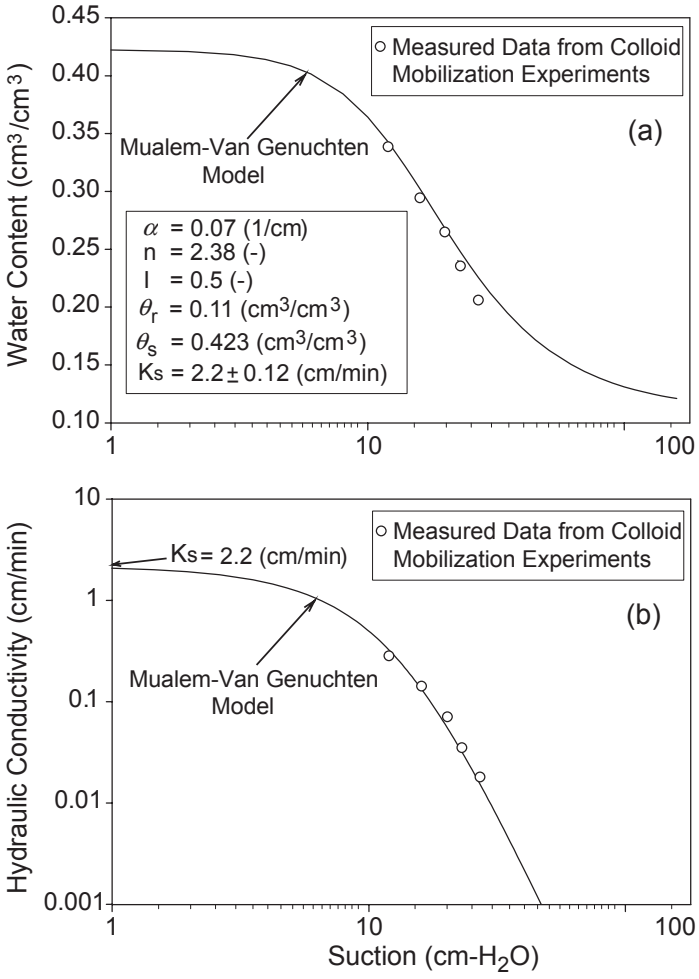

Figure 3.3: Hydraulic properties of sediment columns: (a) water characteristic function, (b) unsaturated hydraulic conductivity function.

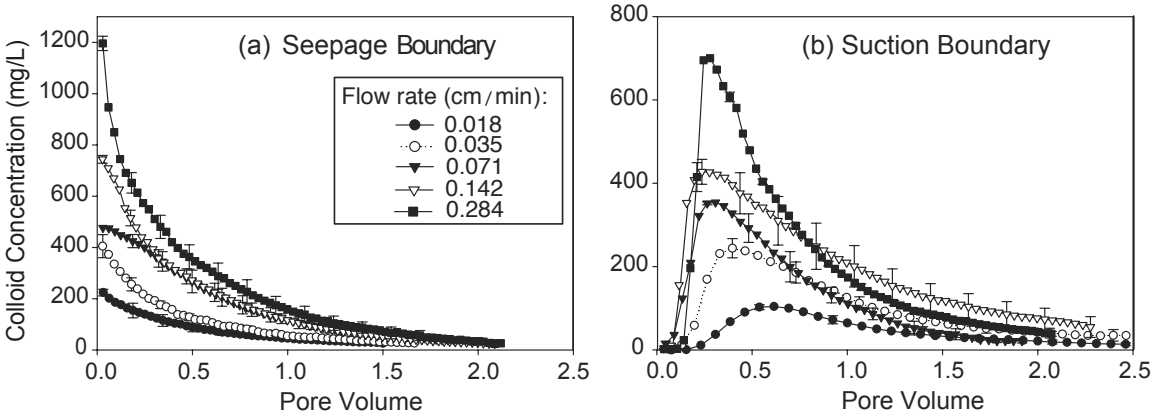

Figure 3.4: Colloid breakthrough curves from *in situ* colloid mobilization at different water flow rates for (a) seepage and (b) suction-controlled bottom boundary. Infiltration solution was deionized water. Error bars represent standard deviations of three replicates; only every fifth error bar is shown.

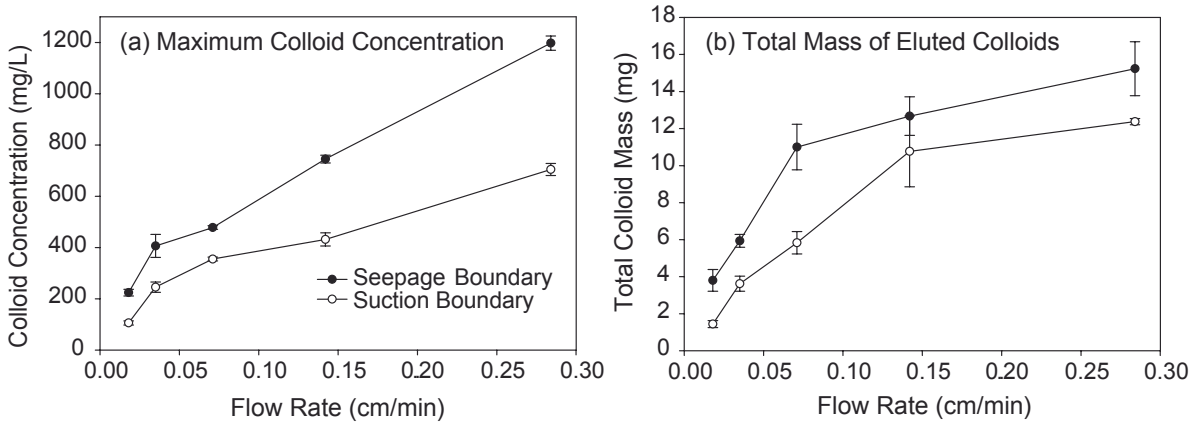

Figure 3.5: Maximum colloid concentrations (a) and total colloid masses (b) in column outflow as a function of water flow rates for seepage and suction-controlled bottom boundary conditions. Infiltration solution was deionized water. Error bars represent standard deviations of three replicates.

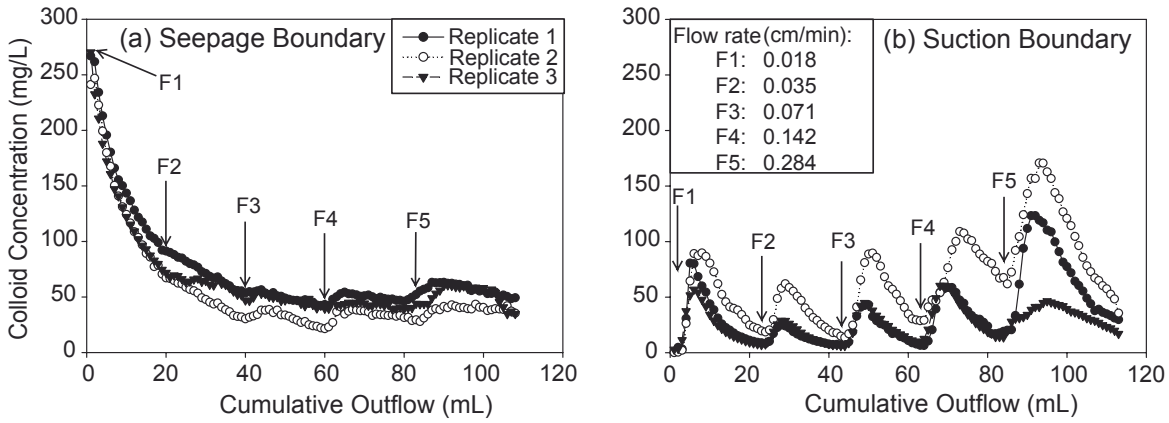

Figure 3.6: Effect of increasing flow rate on the concentration of mobilized colloid. Infiltration solution was deionized water.

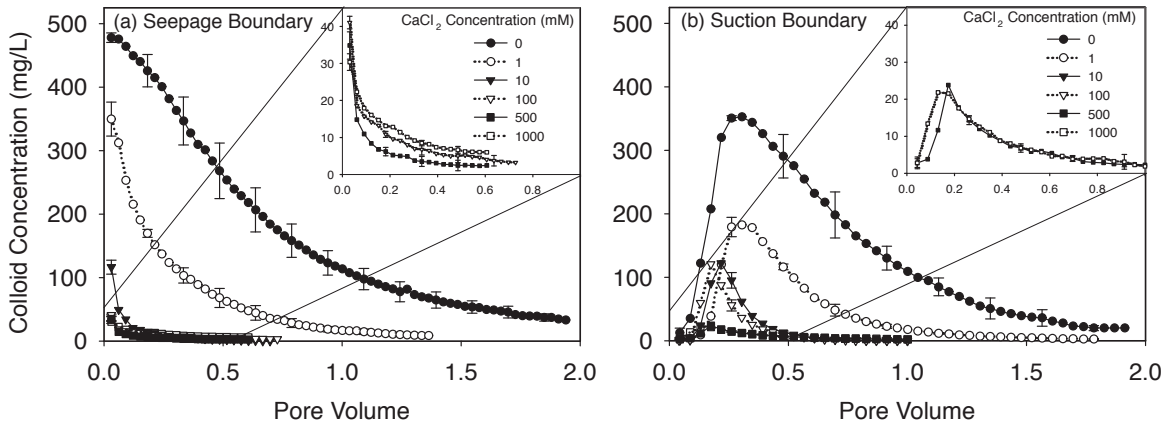

Figure 3.7: Colloid breakthrough curves from *in situ* colloid mobilization at different $CaCl_2$ concentrations for (a) seepage and (b) suction-controlled bottom boundary. Flow rate was $J_w = 0.071$ cm/min. Error bars represent standard deviations of three replicates.

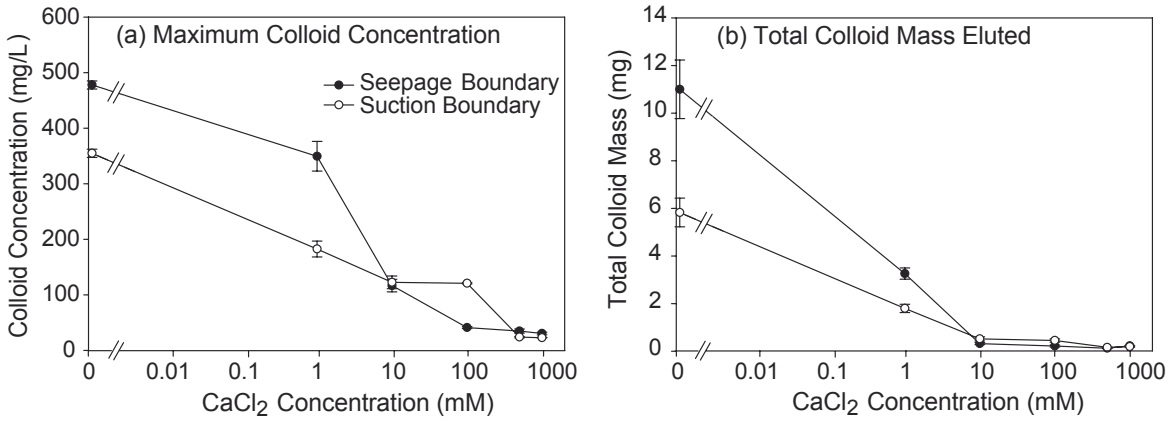

Figure 3.8: Maximum colloid concentrations (a) and total colloid masses (b) in column outflow as function of $CaCl_2$ concentrations for seepage and suction-controlled bottom boundary conditions. Flow rate was $J_w = 0.071$ cm/min. Error bars represent standard deviations of three replicates.

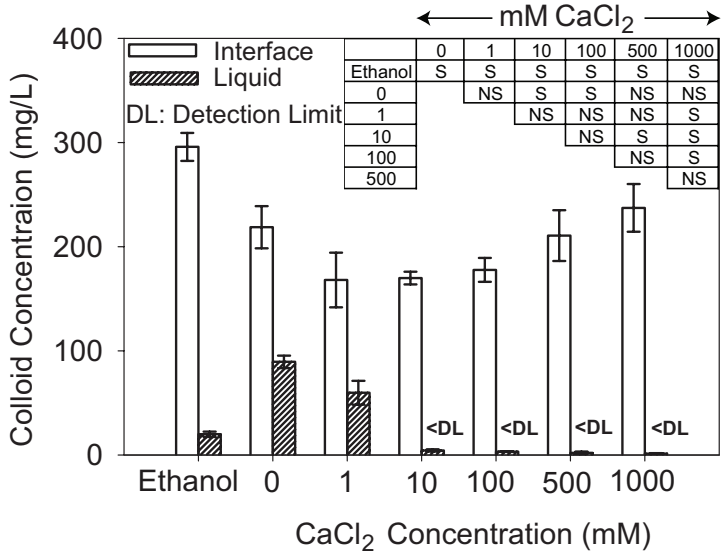

Figure 3.9: Colloid concentrations at the liquid-gas interface and in the bulk liquid measured for the flotation experiments. Error bars represent standard deviations of three replicates. Insert matrix shows statistical significance of colloid concentrations at the liquid-gas interface among different solutions (NS: not significantly different; S: significantly different; number represent $CaCl_2$ concentrations in mM).

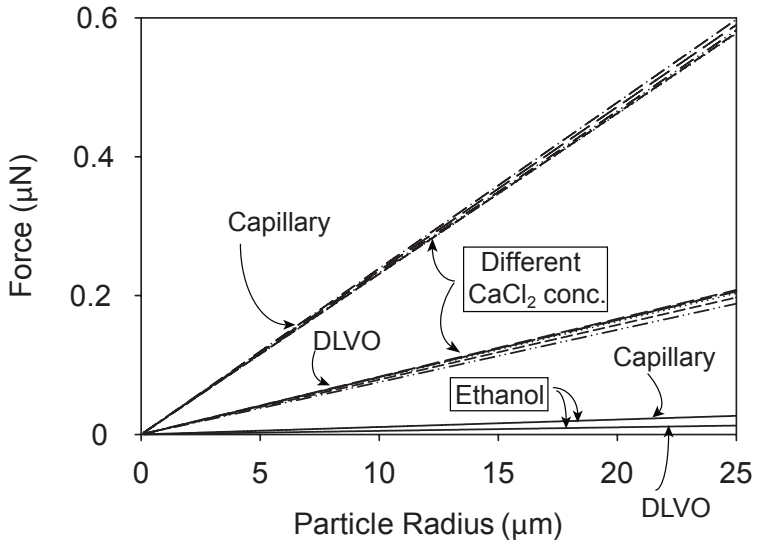

Figure 3.10: Comparison of detachment (capillary) and adhesion (DLVO) forces for our experimental system. Surface tension forces were calculated with Eq (4.5), DLVO forces with Eq (4.4).

3.8 Appendix B

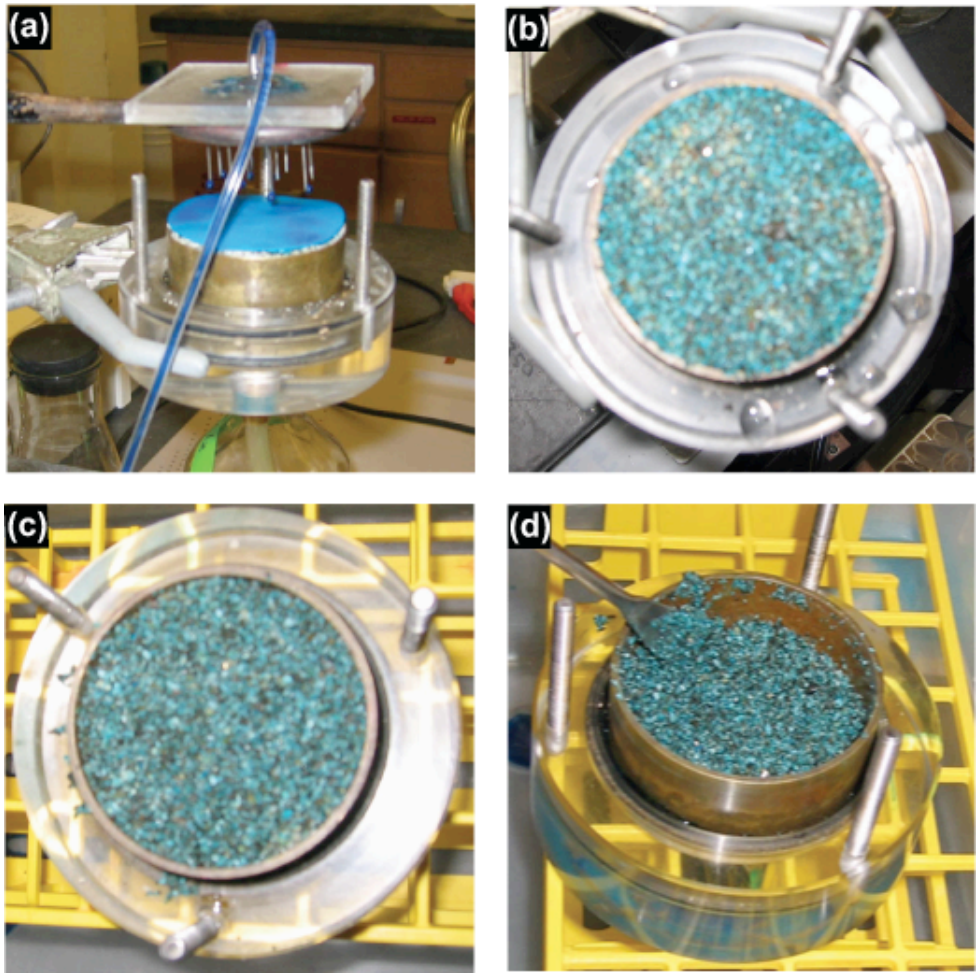

Figure 3.11: Tracer tests for uniformity of water distribution in the columns (a) sprinkling the tracer, (b) top layer, (c) 1 mm deep layer, and (d) 8 mm deep layer.

Figure 3.12: Experimental setup for mobilization experiments with seepage boundary.

Figure 3.13: Experimental setup for mobilization experiments with suction-controlled boundary.

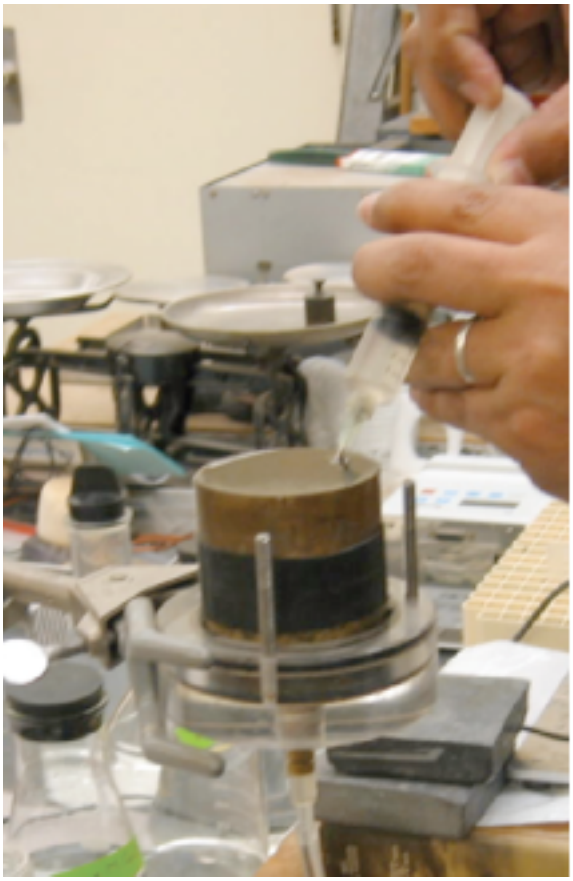

Figure 3.14: Experimental setup for flotation experiments collecting samples from bulk fluid.

Chapter 4

Detachment of Colloids from a Solid Surface by a Moving Liquid-Gas Interface

4.1 Abstract

Colloid attachment to liquid-gas interfaces is an important process used in industrial applications to separate colloids or to clean surfaces from colloidal dust. In the unsaturated soil zone, moving liquid-gas interfaces may lead to colloid mobilization. It is therefore important to understand the interactions between moving liquid-gas interfaces and colloidal particles. The main objective of this study was to quantify the effect of moving liquid-gas interfaces on the detachment of colloids deposited on an air-dried glass surface, as a function of hydrophobicity/hydrophilicity and surface charge of the colloids. We selected four types of colloids with different surface properties. The colloids were deposited on clean microscope glass slides using a flow-through deposition chamber. Liquid-gas interfaces were passed over the colloid-deposited glass slides. The amounts of colloids removed from the glass slides were

This chapter will be submitted for publication to the Journal of Colloid and Interface Science.

visualized using confocal laser scanning microscopy and quantified by image analysis. Our results showed that colloids attached under unfavorable conditions were removed in significantly greater amounts than those attached under favorable conditions. Hydrophobic and hydrophilic colloids did not show significantly different detachment. The effect of the liquid-gas interface on colloid removal was only noticeable for the first two passages of the liquid-gas interface. Multiple passages of liquid-gas interfaces over the colloid-deposited glass slide did not cause additional colloid removal. The force balances, calculated from theory, supported the experimental findings, and highlight the dominance of detachment forces (surface tension forces) over the attachment forces (DLVO forces).

Keywords: Liquid-gas interface, colloid, detachment, attachment.

4.2 Introduction

Gas bubbles in a fluid can be used to remove particles from solid surfaces. When a gas bubble moves over a particle that is adhered to a solid surface, strong capillary forces form between the bubble and the particle, and the particle may detach from the adhering surface [*Noordmans et al.,* 1997*; Gomez-Suarez et al.,* 1999a]. This principle is used in industrial applications, for instance to clean silicon wafers [*Leenaars and O'Brien,* 1989].

Various chemical and physical parameters affect the efficiency of gas bubbles to detach particles from a solid surface. Busscher and coworkers used a horizontal parallel-plate flow chamber to study detachment of Latex particles from uncoated and coated quartz or microscope glass slides [*Noordmans et al.,* 1997*; Gomez-Suarez et al.,* 1999b*; Gomez-Suarez et al.,* 1999a*; Gomez-Suarez et al.,* 2001]. They found that a moving liquid-air interface

generates a very strong detachment force on adhered particles. The surface tension-based detachment force is several orders of magnitude larger than the adhesion force [*Noordmans et al.,* 1997]. Particle detachment from surfaces by moving air-bubbles is more efficient when the liquid-air surface tension is high and the particle size is small [*Gomez-Suarez et al.,* 1999a*; Gomez-Suarez et al.,* 1999b*; Gomez-Suarez et al.,* 2001]. It was also observed that the more air-bubbles moved over a surface, the more particles were removed [*Gomez-Suarez et al.*, 1999a*; Gomez-Suarez et al.*, 1999b]

That gas bubbles form strong capillary forces with particles at the gas-liquid-solid interface is known from theory, and forces have experimentally measured by atomic force microscopy [*Preuss and Butt,* 1998*; Gillies et al.,* 2005*; Johnson et al.,* 2006]. The detachment process caused by air-bubbles involves interception, thinning of the liquid film, film rupture, formation of a three-phase line, and stabilization of particle-bubble aggregates [*Ralston and Dukhin,* 1999*; Dai et al.*, 1999*; Gomez-Suarez et al.,* 1999a]. A particle can attach to an air-bubble only when the particle-bubble contact time is larger than the induction time (necessary time to thin the liquid film and form the three-phase contact line) [*Dai et al.,* 1999]. The interaction force between a bubble and a particle is strongly dependent on the particle-bubble contact angle. This dependency is used in flotation to separate suspended particles according to particle hydrophilicity/hydrophobicity [*Gomez-Suarez et al.,* 1999a*; Dai et al.,* 1999*; Pitois and Chateau,* 2002*; Gillies et al.*, 2005].

Moving liquid-gas interfaces are also important for porous media flow and transport phenomena. It is likely that a moving liquid-gas interface can detach particles from porous media surfaces and carry particles along. In previous experiments, we have shown that a considerable amount of colloidal particles can be captured at the liquid-gas interface, and

moved through a porous medium with an infiltration front [*Sharma et al.,* 2007]. From microscopic visualization using transparent micromodels, it is known that colloids can attach to the liquid-gas interfaces during transport through porous media [*Wan and Wilson,* 1994a*; Keller and Auset,* 2007]. *Sirivithayapakorn and Keller* [2003] observed that colloids (Latex particles) attach to the air-water interface and move with them, and colloids formed clusters when air-bubbles dissolved.

The effects of moving air-bubbles on the detachment of submicron-sized particles (usually Latex particles) from initially wet solid surfaces have been investigated under different physical and chemical conditions [*Leenaars and O'Brien,* 1989*; Noordmans et al.,* 1997*; Gomez-Suarez et al.,* 1999b*; Gomez-Suarez et al.,* 1999a*; Gomez-Suarez et al.,* 2001]. However, the effects of moving liquid-gas interfaces over initially air-dried surfaces have not yet been investigated. The movement of liquid-gas interfaces over initially dry surfaces occurs frequently in unsaturated porous media (e.g., the vadose zone), when water infiltrates or imbibes dry soil or sediments. It is expected that the surface properties of colloids themselves will affect the removal of colloids from the surface. In this work, we examined the detachment of colloids, attached to a solid surface under initially air-dry conditions, when the surface is wetted and a liquid-gas interface is moved over the colloids.

Our main objective was to study the effect of moving liquid-gas interfaces on detachment of colloidal particles from an air-dried solid surface. We hypothesized that hydrophobic colloids are more easily removed than hydrophilic colloids when a liquid-gas interface moves over an air-dried surfaces. We further hypothesized that more colloids detach from the solid surface when colloids are attached under unfavorable as compared to favorable conditions. We examined the detachment of colloids adhered to solid surfaces under both favorable and

unfavorable conditions. We further investigated the effects of different hydrophobicity of colloidal particles. We calculated the capillary forces for detachment of colloids from the solid surfaces and the adhesive forces between colloids and solid surfaces. The theoretical predictions, based on capillary forces and adhesive forces, were verified by experimental observations using confocal microscopy and image analysis.

4.3 Materials and Methods

4.3.1 Colloids

We selected four different types of colloids for the experiments: hydrophilic amino-modified microspheres, hydrophilic carboxylate-modified microspheres, hydrophobic polystyrene microspheres, and hydrophobic sulfate-modified microspheres (Molecular Probes Inc., Eugene, OR). The carboxylate-modified, polystyrene, and sulfate-modified microspheres were negatively charged, the amino-modified microspheres were positively charged. All four colloids were fluorescent with an excitation wavelength of 505 nm and an emission wavelength of 515 nm (yellow-green). The specific density of all four colloids, according to the manufacturer, was 1.055 g/cm^3. The air-water contact angles of the colloids were measured by the sessile drop method with a goniometer (DSA 100, Krüss, Hamburg, Germany). Properties of the colloids are listed in Table 4.1.

4.3.2 Suspension Chemistry

We intended to deposit colloids under both favorable and unfavorable conditions onto microscope glass slides. We first determined electrophoretic mobilities and ζ-potentials at different

pH and ionic strengths for each of the colloids and glass slides (Table 4.3 in Appendix C). We then selected those solutions in which colloids did not aggregate in solution and did not form aggregates on air-dried glass slides. For example, amino-modified colloids formed aggregates up to 6-layers thick during the deposition process on the glass slide at pH 4.1 and a $CaCl_2$ concentration of 0.5 mM (Figure 4.9 in Appendix C). Based on Derjaguin-Landau-Verwey-Overbeek (DLVO) calculations using measured ζ-potentials and ionic strengths, we chose appropriate solution conditions, such that favorable and unfavorable attachment conditions were obtained.

4.3.3 Deposition Chamber

A flow chamber, an open flat channel made of Plexiglas, was used to deposit the colloids on a glass microscope slide (7.5 cm $\times$ 2.5 cm) (frosted microscope slides, precleaned, Fisher Scientific). The channel was rectangular in shape with a dimension of 16 cm $\times$ 2.7 cm $\times$ 1 cm without a top cover. Both sides of the channel were connected (length wise) with Tygon tubing, and a peristaltic pump (Ismatec IP4, Glattburg, Switzerland) was used to supply solution from an inflow bottle to the inlet port and to suck the solution out of the channel from the outlet port. For colloid deposition, the channel was filled with a specific colloid suspension (Table 4.1) and recirculated. The flow rate in the channel was 50 mL/h. A microscope slide was then placed into the flow chamber, and submerged into the suspension. The colloid suspension was recirculated for four hours to deposit colloids onto the microscope slide. Then, the inflow was switched to a colloid-free solution having the same solution chemistry as the colloid suspension for another four hours to rinse the slide free of unattached colloids. A dye tracer test showed that the flow was uniform and indicated

that four hours was sufficient to rinse the channel free of residual solution (Figure 4.10 in Appendix C). Samples of outflow were measured for colloids to verify that the four-hour rinse was sufficient to remove all unattached colloids. After the four-hour rinse, the flow was stopped and the solution in the channel was evaporated. The deposition experiments were done in a laminar air-flow chamber (Laminar Airflow Cabinets, NuAire Corp., Plymouth, MN) to prevent contamination by dust. After air-drying, we cleaned the bottom side of the glass slide with moistened Kimwipe tissue (Kimberly-Clark Corp., Roswell, GA), so that only the upper side of the slide contained deposited colloids.

4.3.4 Confocal Microscopy and Image Analysis

We visualized the colloids on the microscope slide with a laser scanning confocal microscope (Axiovert 200M equipped with LSM 510 META, Carl Zeiss Jena GmbH, Germany) (Figure 4.11 in Appendix C). We used a 10x magnification lens for visualization and image capturing, which was sufficient to see single colloidal particles. A cross mark was made with a diamond-point pen on the microscope slide, so that the slide always could be positioned at the same location on the confocal microscope. For imaging, we selected locations that had uniform colloid deposition, i.e., single particle deposition with no or few clusters (no more than one layer). We selected 18 locations on each slide for imaging, with each image covering an area of 900 μm $\times$ 900 μm.

The images captured by the confocal microscope were analyzed using the ImageJ software [*NIH,* 2007]. With ImageJ, we determined the number of individual particles as well as the percentage of area covered by particles on each image. For the data analysis, we used the number of particles; the area of the individual particles was not constant because some

particles were not exactly in the focal plane of the microscope, and therefore individual particles appeared in non-uniform size.

4.3.5 Liquid-gas Interface Displacement Experiments

After the colloids were deposited and the glass slide was dry, the slide was mounted vertically in a 200 mL glass beaker using a clamp and a laboratory stand (Figures 4.1 and 4.12 in Appendix C). A colloid-free aqueous solution of the same chemical composition as the deposition solution was then pumped into the beaker at a flow rate of 60 mL/h with a peristaltic pump (Ismatec IP4, Glattburg, Switzerland). This caused the water level in the beaker to rise with a velocity of 4 cm/h. As the water level rose, the liquid-gas interface moved over the colloid-deposited glass slide. When the solution reached the top of the beaker, we continued the pumping for 10 minutes to allow the beaker to overflow. This ensured that colloids attached to the liquid-gas interface were flushed away from the liquid-gas interface. Then, the water was pumped out of the beaker at the same flow rate. When the beaker was empty, the slide was air dried, and removed for confocal microscopy and image analysis. After image analysis, the slide was remounted and another liquid-gas interface was passed over the slide as described above. This procedure was repeated in total three times to flow, so that six to eight liquid-gas interfaces (three upward, three downward) moved over the slide.

4.4 Theory

4.4.1 DLVO Forces

The DLVO profiles for the colloids and their interaction with the glass surface were calculated according to [*Gregory*, 1975]:

$$\Delta G_{\text{el}} = 64\pi\epsilon R \left(\frac{kT}{ze}\right)^2 \left[\tanh\left(\frac{ze\psi_{0,1}}{4kT}\right)\right]\left[\tanh\left(\frac{ze\psi_{0,2}}{4kT}\right)\right]\exp(-\kappa h) \tag{4.1}$$

where ΔG_{el} is the electrostatic interaction energy, ϵ is the dielectric permittivity of the medium, R is the radius of the colloids, k is the Boltzmann constant, T is the absolute temperature; z is the ion valence, e is the electron charge, $\psi_{0,1}$ and $\psi_{0,2}$ are surface potential of the colloids and the glass slide respectively, which are taken as the colloid and the glass ζ-potentials, h is the separation distance, κ is the inverse Debye-Hückel length, $\kappa = \sqrt{\frac{e^2\sum n_j z_j^2}{\epsilon kT}}$, where n_j is the number concentration of the ions in solution, and z_j is the ion valence.

The van der Waals interaction energy was calculated by [*Gregory*, 1981]:

$$\Delta G_{\text{vdw}} = -\frac{AR}{6h}\left[1 - \frac{5.32h}{\lambda_0}\ln\left(1 + \frac{\lambda_0}{5.32h}\right)\right] \tag{4.2}$$

where A is the effective Hamaker constant of colloid-water-glass system, and λ_0 is a characteristic length of 100 nm. The effective Hamaker constant ($A = A_{123}$) was calculated using individual Hamaker constant of colloid, water, and glass [*Hiemenz and Rajagopalan*, 1997].

$$A_{123} = (\sqrt{A_{11}} - \sqrt{A_{22}})(\sqrt{A_{33}} - \sqrt{A_{22}}) \tag{4.3}$$

where A_{11} is the Hamaker constant of the colloids, A_{22} is the Hamaker constant of the fluid, and A_{33} is the Hamaker constant of the glass.

Finally, the total DLVO forces were calculated as:

$$F_{\text{DLVO}} = \frac{\mathrm{d}}{\mathrm{d}h}\left(\Delta G_{\text{tot}}\right) = \frac{\mathrm{d}}{\mathrm{d}h}\left(\Delta G_{\text{el}} + \Delta G_{\text{vdw}}\right) \tag{4.4}$$

The results of the DLVO calculations with the chosen solution chemistry are shown in Figure 4.2. The DLVO calculations showed favorable attachment for amino-modified microspheres i.e., a strong attractive force between colloids and the glass surface; and unfavorable attachment for carboxylate-modified, polystyrene, and sulfate-modified microspheres i.e., colloids attached to the glass surface in the secondary energy minimum. The repulsive peaks under the unfavorable conditions were $> 400\ kT$ and the secondary energy minima were about $-1\ kT$.

4.4.2 Surface Tension Forces

The total force exerted by a moving liquid-gas interface on a colloidal particle is the sum of gravity, buoyancy, and interfacial forces. However, the gravity and buoyancy forces can be neglected for small particles with radii $< 500\ \mu$m [*Scheludko et al.,* 1976*; Preuss and Butt,* 1998*; Pitois and Chateau,* 2002*; Sharma et al.,* 2007]. In our experimental setup, when the liquid-gas interface moves in upward direction over the vertically mounted glass slide, the horizontal component of surface tension force (F_γ) is the detachment force (F_{det}) which is opposed by the DLVO force (F_{att}) (Figure 4.3). The detachment force (the maximum horizontal surface tension force) can be calculated by [*Scheludko et al.,* 1976*; Leenaars and O'Brien,* 1989*; Preuss and Butt,* 1998*; Pitois and Chateau,* 2002]:

$$F_{\text{det}} = 2\pi R\gamma \sin^2\left(\frac{\theta}{2}\right)\cos\alpha \tag{4.5}$$

where R is the radius of the particle, γ is the surface tension of liquid, and θ and α are the advancing contact angles for colloids and the glass slide, respectively.

4.5 Results and Discussion

4.5.1 Colloid Removal during the Passage of Liquid-gas Interface

Figures 4.4 to 4.7 show the images captured by confocal microscopy for the different colloids before and after passages of the liquid-gas interface. The images represent typical patterns out of the 900 μm $\times$ 900 μm area of the 18 images taken. Image (a) represents the initial pattern of colloid deposition without passage of a liquid-gas interface. These initial patterns show that the colloids were mostly deposited as single particles (indicated by the letter "S" in the figures); but at some locations, colloids were deposited as clusters of a few particles (indicated by the letter "C"). These clusters were examined by higher-resolution confocal microscopy and found to be single layers, i.e., colloids were deposited on the glass slide in close proximity, without touching each other (Figure 4.9b in Appendix C). At the resolution of the images shown in Figures 4.4a to 4.7a, these clusters appear as single, large dots.

After the passage of the liquid-gas interface over the slides, we observed that a considerable amount of colloids was removed (Figures 4.4 to 4.7). Quantitative image analyses showed that the majority of the colloids were removed after the first two interface movements, and subsquent interface movements did not cause additional detachment of colloids. There was no significant increase in the amount of colloid detachment after two passages (one upward and one downward) (Table 4.2).

This result is in disagreement with observations reported by *Gomez-Suarez et al.* [1999b], who found a nearly linear relationship between the number of air-bubbles passed at a speed of 50 m/h over deposited colloids and the amount of colloid detachment. *Gomez-Suarez et al.* [1999b] emphasized that the speed of the air-bubble movement played an important

role in detachment of colloids; the lower the speed of the air-bubbles, the less the impact of the number of air-bubbles on colloid detachment. At a low speed (7 m/h), most colloids were detached by a single air-bubble [*Gomez-Suarez et al.,* 1999a]. The lower the velocity, the longer the contact time for bubble-colloid interaction is, and the more particles attach to the air-bubble [*Dai et al.,* 1999]. In our experiments, the speed of the liquid-gas interface was several orders of magnitude lower (0.04 m/h) than the speed used by *Gomez-Suarez et al.* [1999b] (7 to 50 m/h). The contact time in our experiments was so long, that most colloids attached to the liquid-gas interface in the first two passages of the interface, and subsequent interface movements had an insignificant effect (Table 4.2).

As Figure 4.2 shows, colloids deposited in the secondary minimum had a separation from the glass plate of about 18 nm. However, when the water on the slide evaporated, the water-film became smaller and smaller, and ultimately, the capillary forces, forming between the colloids and the glass surface, pulled the particles closer to the glass surface. The capillary forces exerted by a drying liquid film for our experimental system were in the order of 10^{-7} N, as calculated using the Young-Laplace equation. These forces were a few orders of magnitude stronger than the repulsive DLVO forces at the energy barrier of the unfavorable attachment ($\approx 10^{-14}$ N). It is therefore likely that during drying, some colloids were pulled over the repulsive energy barrier and moved into the primary energy minimum. The colloids remaining in the secondary minimum and a fraction of the colloids in the primary minimum were detached after the first two passages of the liquid-gas interface. The colloids attached strongly enough to resist detachment by the first two liquid-gas interface passages and then remained attached thereafter.

We observed that some of the colloids on the glass slide were displaced from the original

position on the slides after passage of the liquid-gas interface (Figures 4.4 to 4.6, the displaced particles are denoted by the letter "D"). The displacement was likely caused by the vertical component of the surface tension force (Figure 4.3). Because particles attachment to the liquid-gas interface is irreversible, i.e., colloids cannot be removed from the interface once they are attached [*Abdel-Fattah and El-Genk,* 1998b*; Abdel-Fattah and El-Genk,* 1998a], it is unlikely that particles from the liquid-gas interface will transfer into the bulk fluid and reattach to the glass surface.

We found significantly less detachment of the positively-charged (amino-modified) than the negatively-charged colloids (Table 4.2). All the positively-charged colloids were deposited in the primary energy minimum, but some of the negatively-charged colloids were located in the secondary energy minimum, and therefore they would be more easily removed from the surface by the moving liquid-gas interface. A similar pattern was observed by *Gomez-Suarez et al.* [1999b], who reported more removal of negatively-charged polystyrene colloids from a negatively-charged dimethyldichlorosilane (DDS) coated glass surface than from a positively-charged 3-(2-aminoethylamino)propyldimethoxysilane (APTS) coated glass surface [*Gomez-Suarez et al.,* 1999a].

Contrary to our expectation, we did not observe a difference in colloid detachment between hydrophobic and hydrophilic colloids. According to eq 4.5, the detachment force was 10^{-7} N for hydrophobic and 10^{-8} N for hydrophilic colloids. Therefore, there should have been more detachment of hydrophobic than hydrophilic colloids. *Gomez-Suarez et al.* [1999a] also found some inconsistent trends of the removal of hydrophilic colloids from a hydrophilic and hydrophobic surface as a function of the velocity of the air-bubble interface. At low velocity (<21 m/h), more colloids were removed from the hydrophilic surface than from the

hydrophobic surface, and opposite was found at high velocity (>21 m/h) (Figure 4.14 in Appendix C).

4.5.2 Force Balance and Comparison with Experimental Results

The attachment forces (eq 4.4) and the detachment forces (eq 4.5) as a function of separation distance for individual colloids with a glass surface are shown in Figure 4.8. The detachment forces dominated the attachment forces over at small separation distances and were much stronger for hydrophobic colloids than for hydrophilic colloids.

As discussed in the previous section, some of the colloids attached under unfavorable conditions were pulled into the primary energy minimum during drying of the liquid film. If we assume that these colloids have a separation distance of about 0.3 nm [*Elimelech et al.*, 1995], then we can use Figure 4.8 to compare the different forces acting on the colloids. The hydrophobic colloids (polystyrene and sulfate-modified) experienced an about 10-times stronger detachment force than the hydrophilic colloids (amino-modified and carboxylate-modified), and consequently more hydrophobic colloids should be removed by a passage of a liquid-gas interface.

For the positively-charged amino-modified colloids, which had favorable condition of attachment, the attachment forces were larger than the attachment forces for the negatively charged colloids at separation distance > 0.2 nm(Figure 4.8). Therefore, the colloid detachment from the surface was the least for the positively-charged colloids (Table 4.2). The theoretical prediction of the dominance of the detachment force over the attachment force (Figure 4.8) was corroborated by our experimental observations (Table 4.2). The detachment of amino-modified colloids was significantly less than of carboxylate-modified colloids

(Table 4.2), but the ratio of detachment to attachment forces for these two colloids was similar at a separation distance of 0.3 nm (Figure 4.8b). When the separation distance exceeded 0.3 nm, then the force ratio increased considerably for carboxylate-modified colloids, which corroborates our experimental observations that more carboxylate-modified than amino-modified colloids were removed (Table 4.2).

4.6 Implications

In subsurface systems, like soils and sediments, moving liquid-gas interfaces are common, e.g., during infiltration and drainage of water. Such moving liquid-gas interfaces have a profound effect on detachment of colloids from surfaces. As our experiments showed, colloids can be mobilized effectively by such moving liquid-gas interfaces. Our experiments suggest that the majority of the colloids is removed by the first liquid-gas interface movements, which helps to explain experimental findings on colloid mobilization from porous media reported in literature. *Zhuang et al.* [2007] found that at a constant infiltration rate, the majority of the colloids was mobilized with the first of a multiple infiltration sequence. However, *El-Farhan et al.* [2000b] showed the role of air-water interface passage on rapid colloid mobilization in transient flow conditions. The strong attachment of colloidal particles to liquid-gas interfaces may also be used as a remediation technique. Air-bubbles in the form of N_2 or other inert gases may be injected in soils or aquifers to preferentially mobilize colloidal contaminants.

Table 4.1: Selected properties of colloids and suspension chemistry.

				Experimental Conditions				
Colloids	Diameter[a]	Contact angle[b]	Surface charge[a]	$CaCl_2$ conc.	pH	Electrophoretic mobility[c]	ζ-potential[d]	Colloid conc.
	(μm)	(deg)	(meq/g)	(mM)	(–)	(μm/s)/(V/cm)	(mV)	(mg/L)
Amino-modified	1.0±0.02	20.3±1.9	0.1047	6	5.8	0.15±0.02	1.9±0.2	7.2×10^8
Carboxylate-modified	1.1±0.04	19.5±1.7	0.0175	10	4.3	−1.69±0.03	−21.5±0.4	2.7×10^9
Polystyrene	1.1±0.04	79.7±2.6	n.a.	10	4.3	−1.79±0.04	−22.8±0.5	2.0×10^9
Sulfate-modified	1.0±0.03	104.9±1.3	0.0017	10	4.3	−2.18±0.17	−27.8±2.1	3.6×10^9

[a]Values provided by manufacturer.

[b]Measured with a goniometer (DSA 100, Krüss, Hamburg, Germany).

[c]Measured with a ZetaSizer 3000HSa (Malvern Instruments Ltd., Malvern, UK) at the electrolyte concentration and pH indicated in the table.

[d]Obtained from measured electrophoretic mobilities using the von Smoluchowski equation [*Hiemenz and Rajagopalan,* 1997].

n.a.: not available.

Table 4.2: Percent colloids attached to the glass slide after movement of liquid-gas interface.

Colloids	Number of liquid-gas interfaces passing over deposited colloids				
	0	2	4	6	8
	Percent colloids remaining deposited on the glass slide (%)				
Amino-modified	100 Aa	35.3±3.9 Ab	33.6±3.9 Ab	32.9±3.8 Ab	32.4±3.7 Ab
Carboxylate-modified	100 Aa	14.6±4.8 Bb	10.5±3.2 Bb	10.7± 2.9 Bb	nd
Polystyrene	100 Aa	13.9±4.6 Bb	12.7±3.2 Bb	12.0±1.7 Bb	11.7±1.7 Bb
Sulfate-modified	100 Aa	12.0±4.7 Bb	11.9±4.9 Bb	11.6±4.8 Bb	nd

Data are means and standard deviations from 18 measurements.

nd: not determined.

Different capital letters (A and B) denote statistical differences column-wise; and different lower cases (a and b) denote statistical differences row-wise; both at a significance level of 0.05 (t-test).

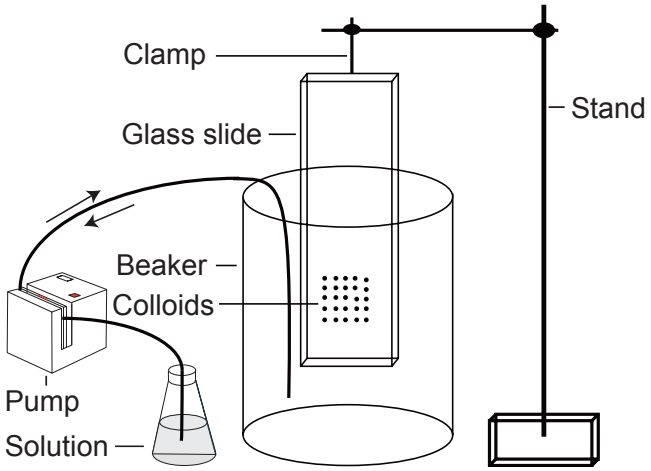

Figure 4.1: Setup for the moving liquid-gas interface experiments (arrows pointing to the right and left indicate the directions of flow during up- and downward movement of the liquid-gas interface, respectively).

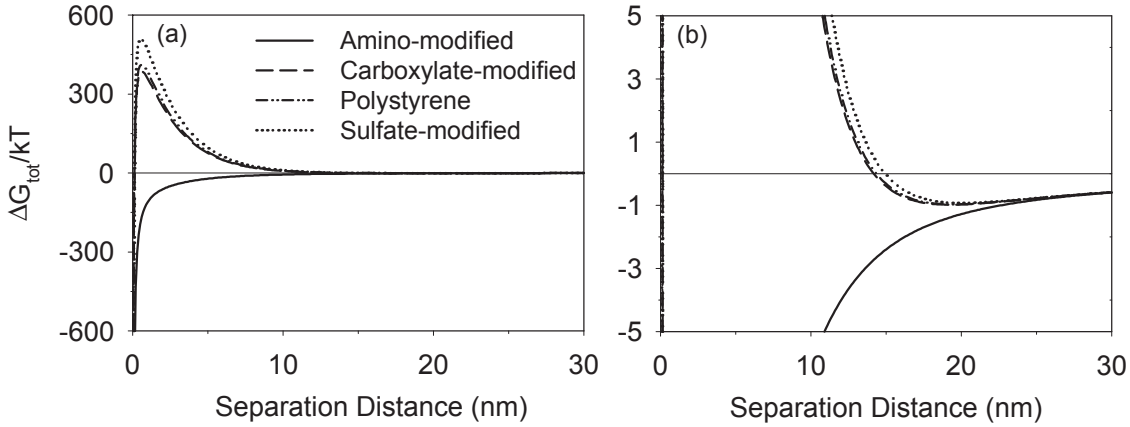

Figure 4.2: Normalized DLVO energy profiles for different colloids interacting with glass surface for the experimental conditions used in our experiments: (a) full view and (b) detailed view of secondary minima.

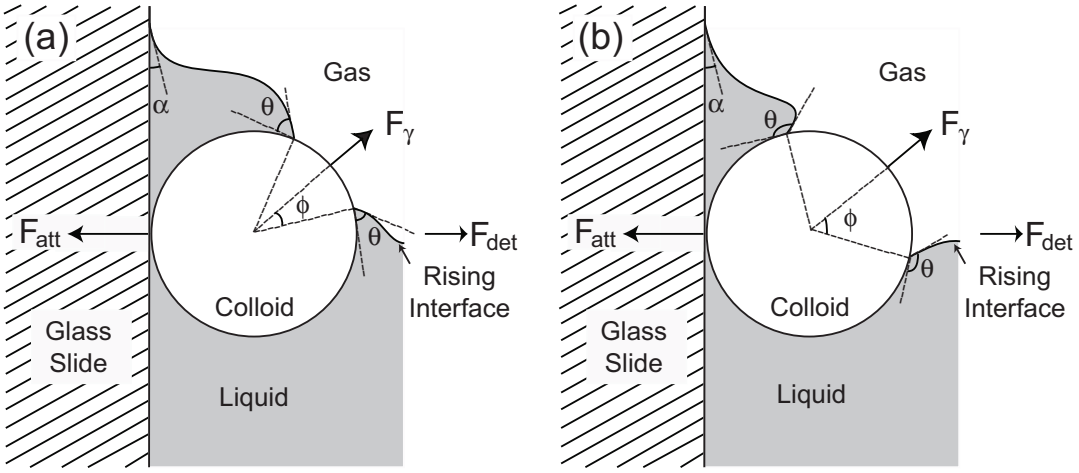

Figure 4.3: Schematic of forces exerted on an adhered particle: (a) hydrophilic and (b) hydrophobic, in contact with a liquid-gas interface. (F_{det}: detachment force, F_{att}: attachment force, F_γ: surface tension force, θ: contact angle for colloids, α: contact angle for glass surface, ϕ: filling angle) (modified from Leenaars and O'Brien, 1989)

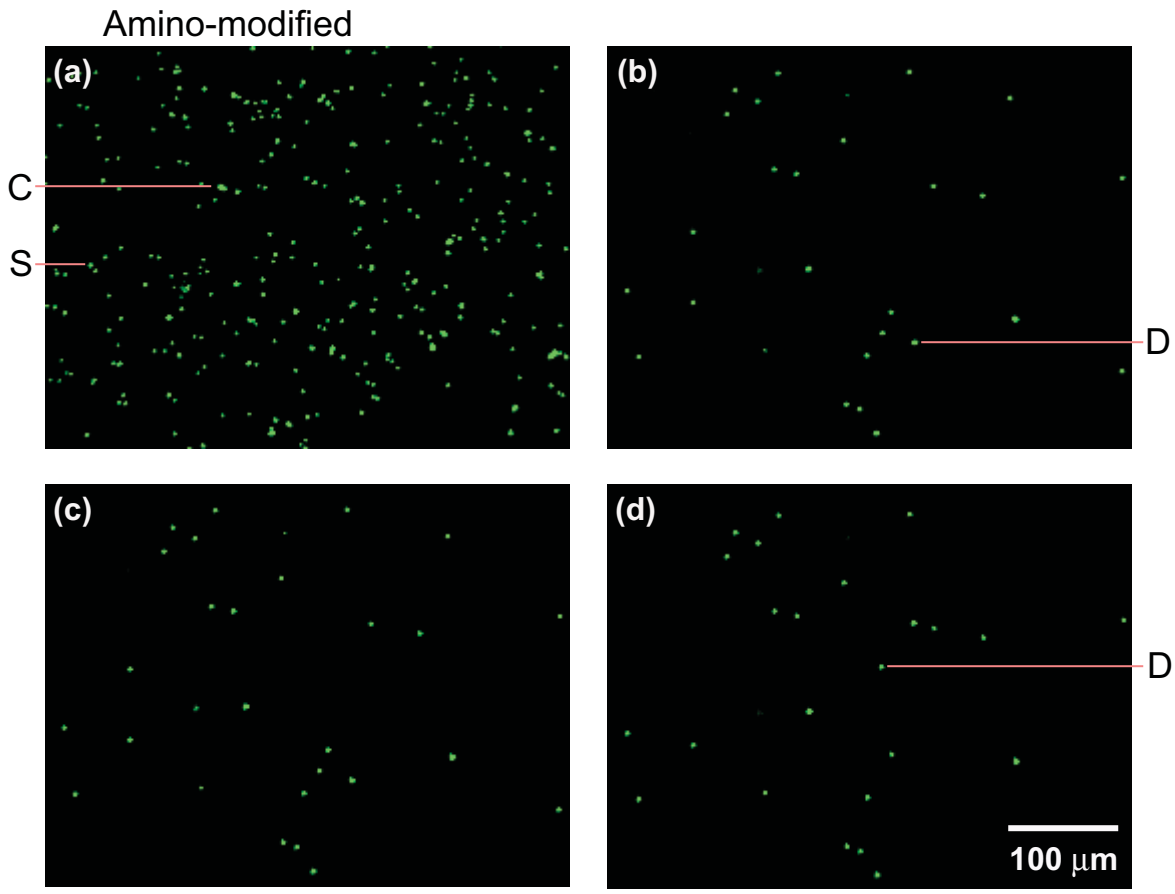

Figure 4.4: Detachment of amino-modified microspheres from glass slide after moving the liquid-gas interface: (a) no interface movement, (b) 2 interface movements, (c) 4 interface movements, and (d) 6 interface movements. S: single colloidal particle, C: colloid cluster, and D: displaced colloidal particle.

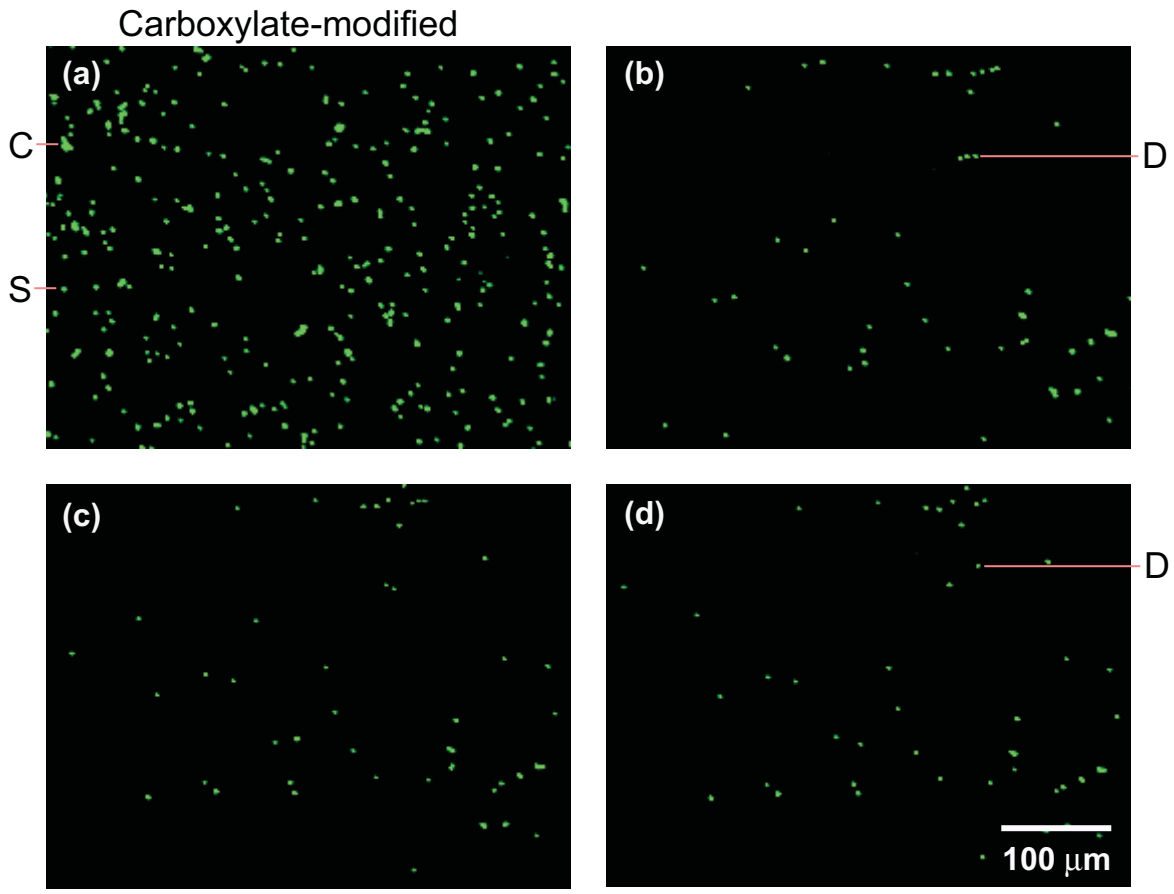

Figure 4.5: Detachment of carboxylate-modified microspheres from glass slide after moving the liquid-gas interface: (a) no interface movement, (b) 2 interface movements, (c) 4 interface movements, and (d) 6 interface movements. S: single colloidal particle, C: colloid cluster, and D: displaced colloidal particle.

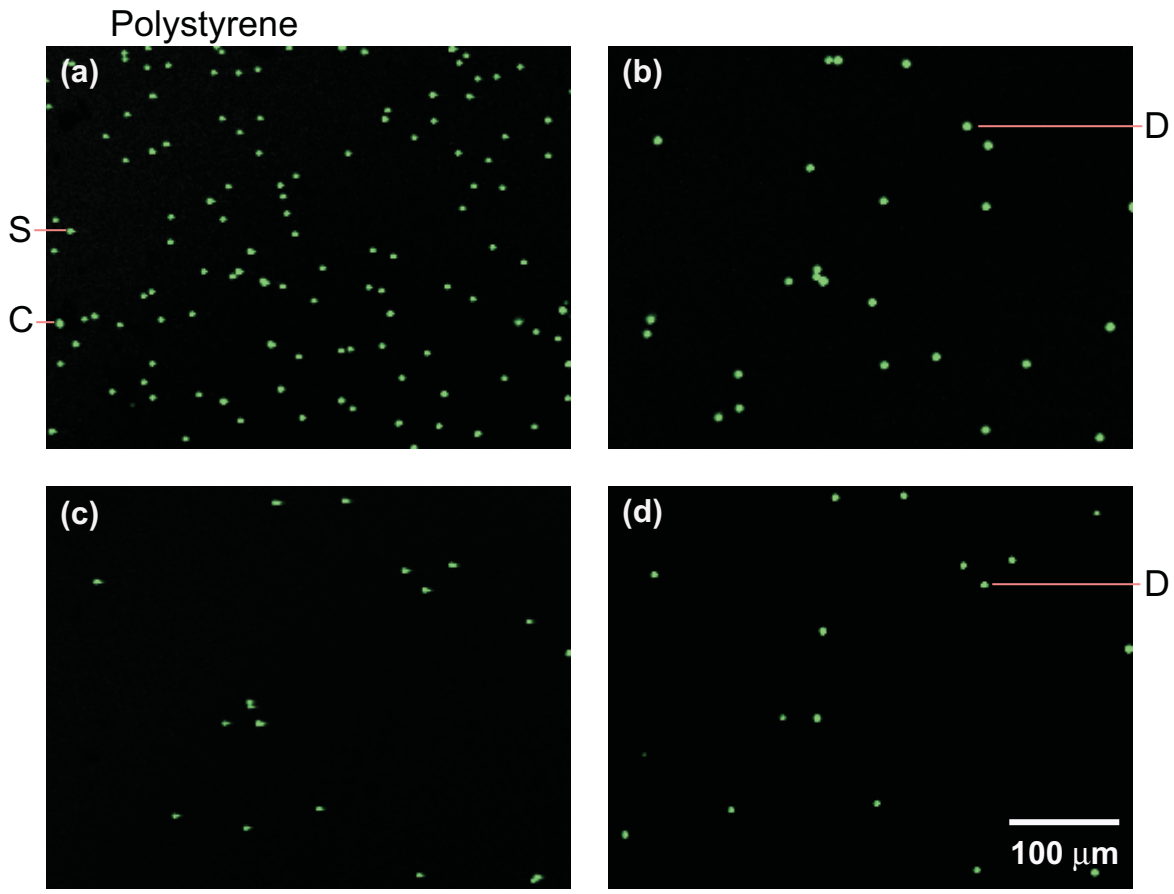

Figure 4.6: Detachment of polystyrene microspheres from glass slide after moving the liquid-gas interface: (a) no interface movement, (b) 2 interface movements, (c) 4 interface movements, and (d) 6 interface movements. S: single colloidal particle, C: colloid cluster, and D: displaced colloidal particle.

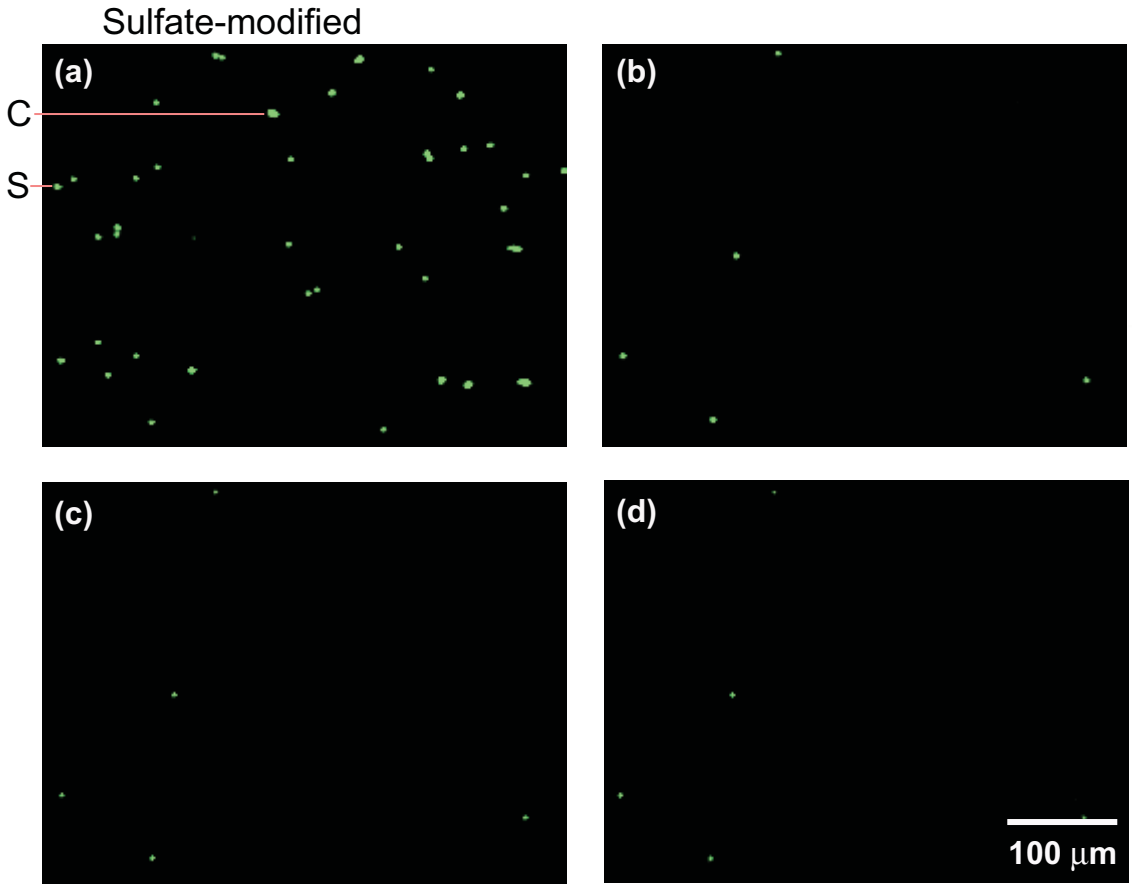

Figure 4.7: Detachment of sulfate-modified microspheres from glass slide after moving the liquid-gas interface: (a) no interface movement, (b) 2 interface movements, (c) 4 interface movements, and (d) 6 interface movements. S: single colloidal particle and C: colloid cluster.

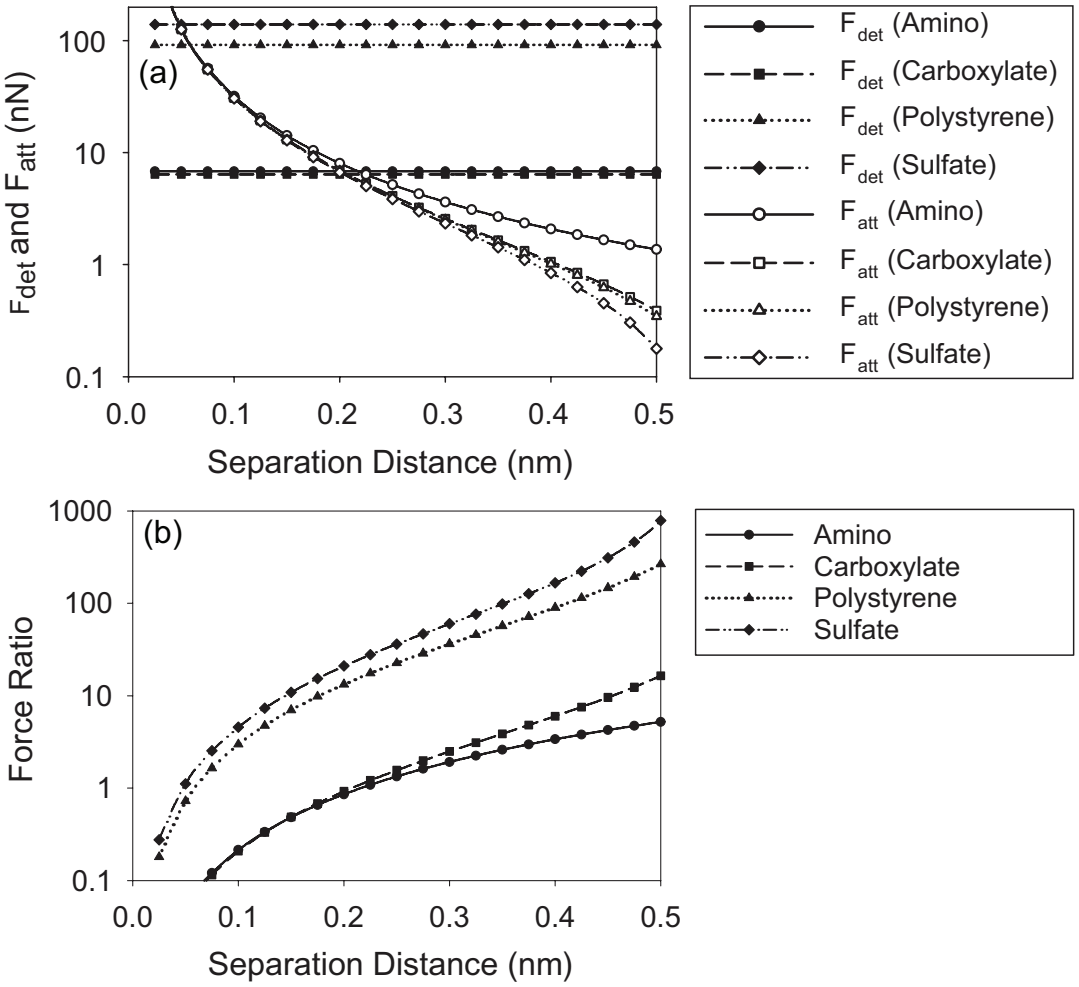

Figure 4.8: (a) Detachment and attachment forces and (b) ratio of detachment and attachment force, in relation to separation distance for the different colloids.

4.7 Appendix C

4.7.1 Single Liquid-gas Interface

We examined the effect of a single interface movement on detachment of colloids from the glass slide. We followed the same procedure for upward movement of the liquid-gas interface as described in the main text, but then we placed the glass slide horizontally inside the liquid-filled beaker without taking the slide out of the solution. We then pumped the solution out from the beaker until there was about 2 mm of standing solution over the glass slide. This standing solution was evaporated by air drying, and the slide then used for confocal microscopy and image analysis.

The confocal images for the colloids before and after the single interface experiments are shown in Figure 4.13. The quantitative results of the image analysis indicate that the amounts of colloid detachment by a single interface were significantly larger than the amounts detached by two interfaces (Table 4.4). This result was unexpected and we attribute it to an experimental artifact. The movement of the slide, while it is inside the fluid, from the vertical position to the horizontal position, may have caused disturbance of colloids remaining on the slides. Indeed, we did not find uniform removal of colloids from the slides.

4.7.2 Effect of Liquid-gas Interface Velocity

The removal of colloids from the solid surface by the moving liquid-gas interface depends on the three different steps: interception of the particle, attachment or thinning of the liquid film in between the colloid and the liquid-gas interface, and stabilization of the colloid on the liquid-gas interface [*Dai et al.,* 1999*; Gomez-Suarez et al.,* 1999a]. The detachment

probability (P_d) is defined as:

$$P_d = P_i \times P_a \times P_s \tag{4.6}$$

where P_i is interception probability, P_a attachment probability, and P_s is stability probability. The interception probability was $P_i = 1$ in our experiments because the liquid-gas interface was forced to intercept all the particles. The attachment probability depended on velocity of the liquid-gas interface. The colloidal particles attached to the liquid-gas interface only if the contact time was larger than the induction time. The induction time is the time for the liquid film between the particle and the liquid-gas interface to thin and form a three-phase contact line. Therefore, the detachment of colloids from the solid surfaces only happens if the velocity of the liquid-gas interface is low enough that the contact time with the colloid is greater than the induction time. The stability probability was also considered as $P_s = 1$ because of the irreversibility of the colloid attachment to the liquid-gas interface, i.e., once the particle attached to the liquid-gas interface, it remained there.

From air-bubble experiments, *Gomez-Suarez et al.* [1999a] found a linear increase in the detachment of colloids (upto 80%) by decreasing the air-bubble velocity in the range of 50 m/h to 7 m/h (Figure 4.14). But this linear relationship may not hold for velocities less than 7 m/h. We expect that there is a critical limit after which the decrease in air-bubble velocity will have no significant effect on detachment of colloids, because the induction time to thin a liquid-film and form a three-phase contact line is much larger than the interface velocity. Our results show that the maximum detachment of colloids was 88% for the hydrophobic and negatively-charged colloids at a liquid-gas interface velocity several orders of magnitude lower than the velocity used by *Gomez-Suarez et al.* [1999a] (Figure 4.14).

Table 4.3: Electrophoretic mobilities and ζ-potentials for the different colloids at different pH and $CaCl_2$ solutions.

Amino-modified microspheres				Polystyrene microspheres				Sulfate-modified microspheres			
pH	$CaCl_2$ conc.	EM[a]	ζ-potential[b]	pH	$CaCl_2$ conc.	EM[a]	ζ-potential[b]	pH	$CaCl_2$ conc.	EM[a]	ζ-potential[b]
(–)	(mM)	(μm/s)/(V/cm)	(mV)	(–)	(mM)	(μm/s)/(V/cm)	(mV)	(–)	(mM)	(μm/s)/(V/cm)	(mV)
5.86	0	−1.07±0.04	−13.6±0.4	6.07	0	−3.85±0.07	−49.0±0.9	6.07	0	−3.77±0.17	−48.0±2.3
5.43	0	−0.78±0.05	−9.9±0.7	6.07	5	−2.53±0.26	−32.2±3.3	6.07	5	−2.64±0.06	−33.6±0.8
4.89	0	−0.09±0.06	−1.1±0.7	6.07	50	−1.24±0.06	−15.8±0.8	6.07	10	−2.46±0.28	−31.3±3.6
4.52	0	0.58±0.22	7.4±2.8	6.07	100	−0.76±0.04	−9.6±0.5	6.07	50	−1.40±0.04	−17.9±0.5
4.02	0	1.43±0.12	18.2±1.6	6.07	200	−0.56±0.04	−7.1±0.6	6.07	100	−0.84±0.21	−10.8±2.8
4.11	0.5	4.35±0.26	55.4±3.3	4.25	200	−0.48±0.05	−6.2±0.6	6.07	200	−0.61±0.02	−7.7±0.3
5.82	6	0.15±0.02	1.9±0.2	4.32	10	−1.79±0.04	−22.8±0.5	4.32	10	−2.18±0.16	−27.8±2.1

[a] Electrophoretic mobility measured with a ZetaSizer 3000HSa (Malvern Instruments Ltd., Malvern, UK) at the electrolyte concentration and pH indicated in the table.

[b] Obtained from measured electrophoretic mobilities using the von Smoluchowski equation [*Hiemenz and Rajagopalan*, 1997].

Table 4.4: Percent colloids attached to the glass slide after movement of liquid-gas interface.

Colloids	Number of liquid-gas interfaces passing over deposited colloids		
	0	1	2
	Percent colloids remaining deposited on the glass slide (%)		
Amino-modified	100 Aa	28.3±6.3 Ab	35.3±3.9 Ac
Carboxylate-modified	100 Aa	8.1±2.6 Bb	14.6±4.8 Bc
Polystyrene	100 Aa	5.8±1.5 Bb	13.9±4.6 Bc
Sulfate-modified	100 Aa	7.6±3.2 Bb	12.0±4.7 Bc

Data are means and standard deviations from 18 measurements.

nd: not determined.

Different capital letters (A and B) denote statistical differences column-wise; and different lower cases (a, b, and c) denote statistical differences row-wise; both at the significance level of 0.05 from t-test.

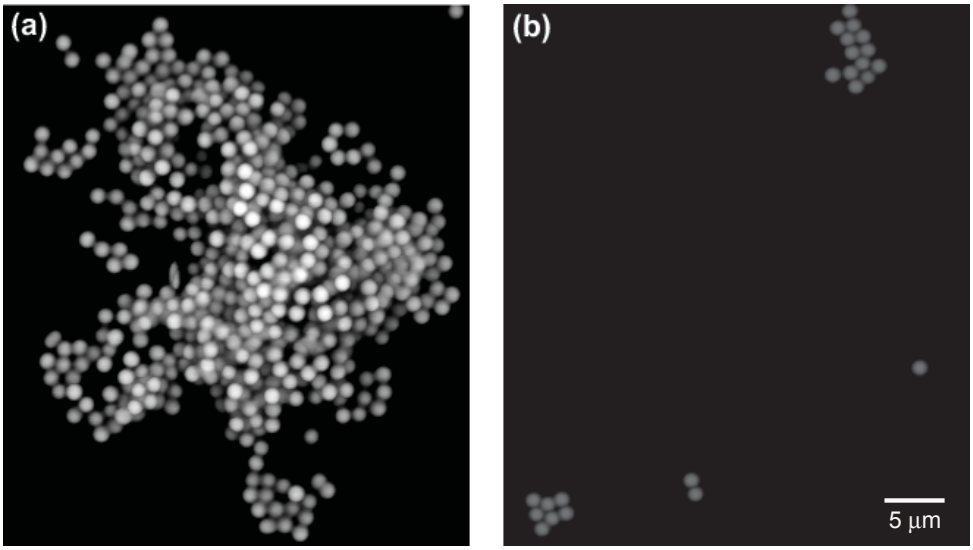

Figure 4.9: Attachment of amino-modified microspheres at different chemical conditions: (a) clusters (>2 layers), pH 4.1 and 0.5 mM $CaCl_2$; (b) no clusters (1 layer), pH 5.8 and 6 mM $CaCl_2$.

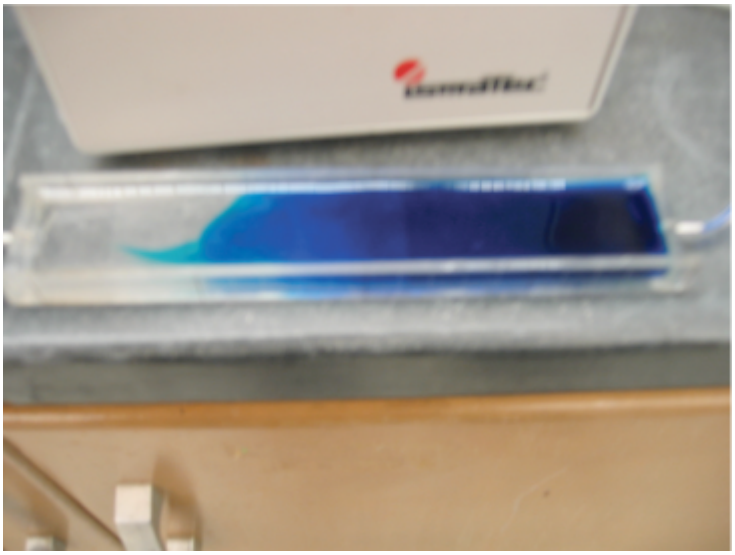

Figure 4.10: Deposition chamber during the dye tracer test.

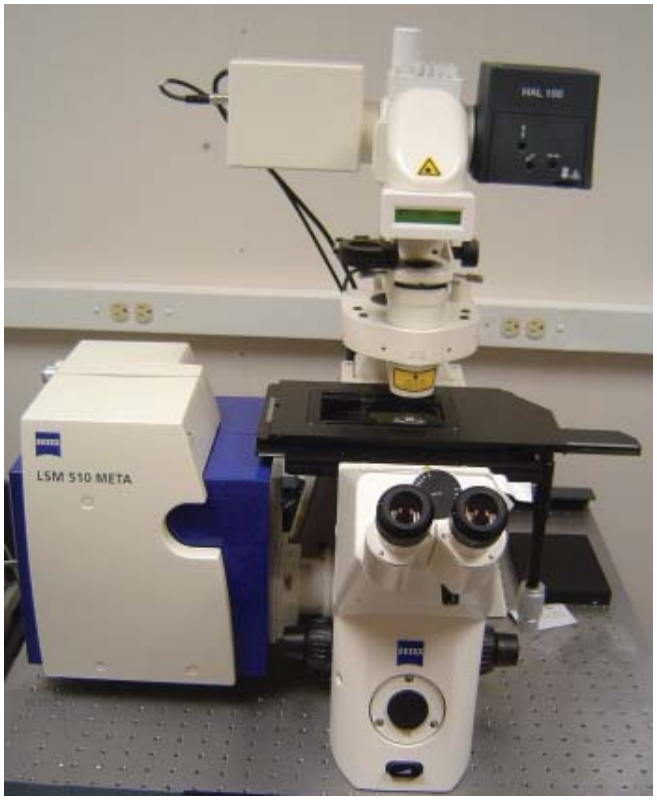

Figure 4.11: Laser scanning confocal microscope for capturing the images (photo taken in WSU's Franceschi Microscopy and Imaging Center).

Figure 4.12: Experimental setup for the liquid-gas interface experiments.

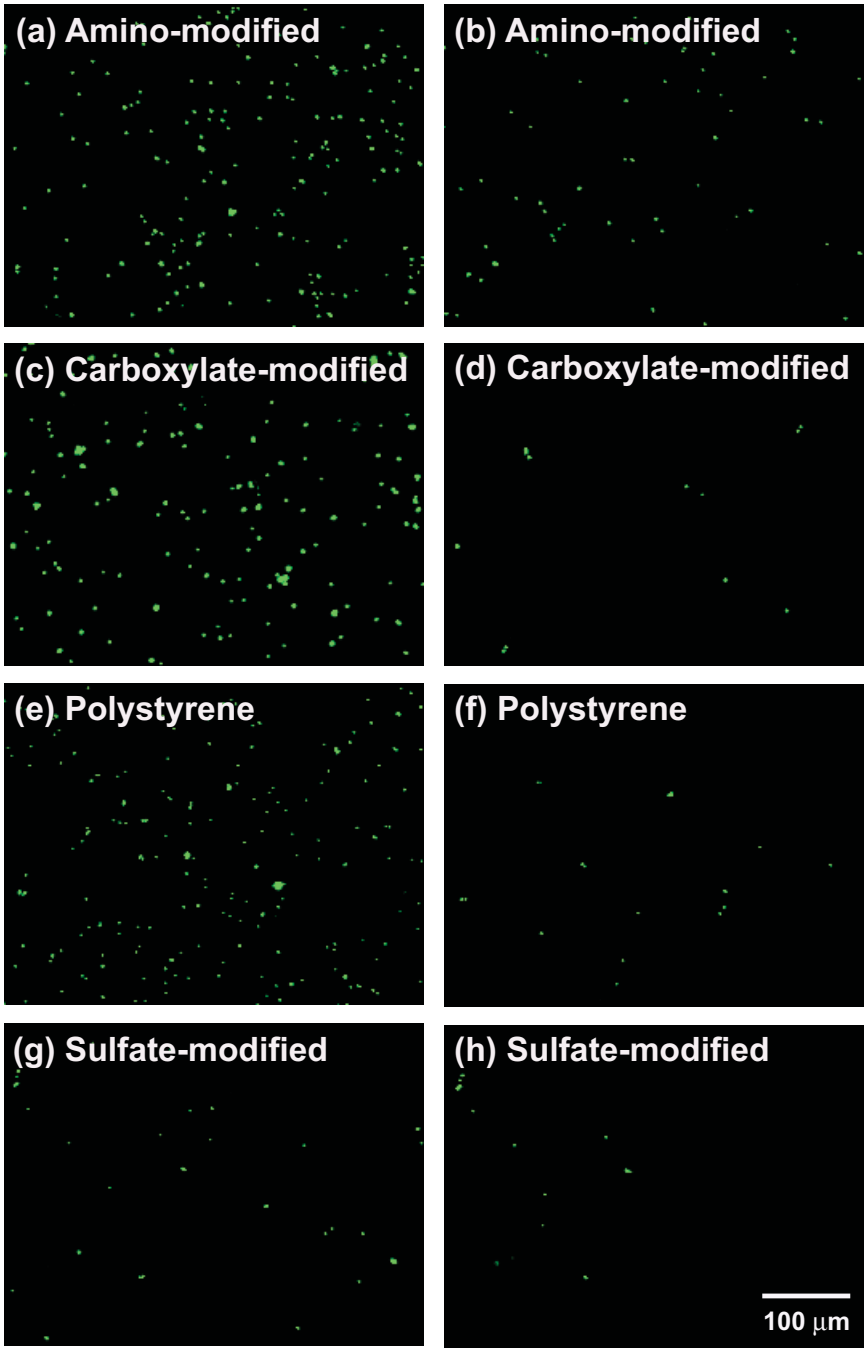

Figure 4.13: Detachment of colloids from the glass slide before and after a single interface movement for: (a) before and (b) after, amino-modified; (c) before and (d) after, carboxylate-modified; (e) before and (f) after, polystyrene; and (g) before and (h) after, sulfate-modified.

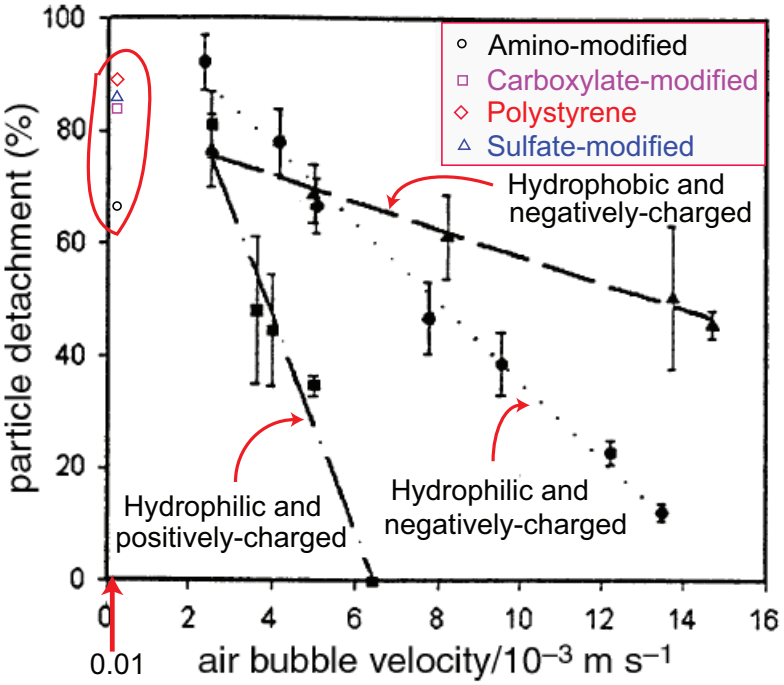

Figure 4.14: Detachment of colloids from solid surfaces as a function of the air-bubble velocity (from Gomez-Suarez et al., 1999a). Circled data are our measurements.

Chapter 5

Summary and Conclusions

In this dissertation, three studies on colloid fate and transport in porous media are presented. The studies are centered on the different types of forces responsible for the deposition and mobilization of colloids in porous media. The following paragraphs summarize these studies.

I developed a theoretical relationship for predicting whether colloid transport in geocentrifuges is altered as compared to normal gravity. It is expected, based on theoretical and experimental results, that the filtration behavior changes after a critical acceleration is exceeded. Two theories were developed in this work to determine this critical acceleration for favorable (based on sedimentation and diffusion) as well as unfavorable conditions for colloid deposition (based on filtration theory). Due to experimental limitations, the theory was tested for colloid deposition under unfavorable conditions only. The density and size of the colloids were varied for these experiments; the chosen colloids were representative of many subsurface colloids, such as viruses, bacteria, alumino-silicates, and iron oxides. The results showed that at common accelerations (5 to 300 g) used in geocentrifuges, the transport of alumino-silicates and iron oxides can be affected by acceleration. Hematite and silica colloids deposition will be affected at centrifugal accelerations as low as 10 g. Low-density

colloids in large sizes (e.g., bacteria) can be affected at even lower centrifugal accelerations.

Centrifuges were used in the past to study colloid transport in porous media [*McGraw,* 2000*; Gamerdinger et al.,* 2001*; Gamerdinger and Kaplan,* 2001]. However, in those experiments, the effect of acceleration on colloid transport was not considered explicitly on the colloid transport. The colloid types and centrifugal acceleration used for these colloid transport experiments are listed in Table 5.1. Also shown are the critical acceleration for each experiment, calculated with eq 2.6. The centrifuge used for those studies was the so-called unsaturated flow apparatus (UFA). The accelerations (a/g) used for these colloid transport experiments were calculated from the rotational speed of the centrifuge and the distance from the center of rotation. I could not find the exact radius of rotation of the UFA in the literature. Therefore, the acceleration was calculated as follows:

Darcy's law in a centrifugation experiment can be written as [*Conca and Wright,* 1990]:

$$q = -K\left(\frac{d\Psi}{dr} - \rho\omega^2 r\right) \tag{5.1}$$

where q is the water flux density, K is the hydraulic conductivity, Ψ is the matric potential, ρ is the fluid density, ω is the angular velocity, and r is the distance to center of the column from the center of rotation. At high speed, when $\frac{d\Psi}{dr} \ll \rho\omega^2 r$ [*Conca and Wright,* 1990], the distance from the center of rotation can be calculated as:

$$r = \frac{q}{K\rho\omega^2} \tag{5.2}$$

Using the values for q, K, ρ, and ω reported by *Conca and Wright* [1990], one obtains $r =$ 3.8 cm for the UFA.

Table 5.1 shows that the accelerations used for the colloid transport in most of the studies were larger than the critical centrifugal accelerations. For instance, colloid transport

Table 5.1: Centrifugal accelerations used in previous studies and the critical centrifugal acceleration calculated with eq 2.6.

References	Colloid type	Colloid density (g/cm^3)	Colloid diameter (nm)	Acceleration used a/g	Critical acceleration a/g
Gamerdinger and Kaplan (2001b)	Polystyrene latex	1.05	280	2–200	51
McGraw (2000)	Polystyrene latex	1.05	52	51–95	43000
McGraw (2000)	Polystyrene latex	1.05	189	51–95	250
McGraw (2000)	Polystyrene latex	1.05	545	51–95	4
McGraw (2000)	Polystyrene latex	1.05	910	51–95	<1
McGraw (2000)	Polystyrene latex	1.05	1900	51–95	<1

experiments in crushed tuff material from Yucca Mountain, there was a considerable amount of colloid deposition at low water content [*Gamerdinger and Kaplan*, 2001]. But these results may have been biased by centrifugal acceleration (Table 5.1). The experimental results from *McGraw* [2000] showed clear evidence of colloid deposition for colloids $\geq$ 545 nm, where the acceleration used in the experiments exceeded the critical centrifugal acceleration (Table 5.1).

I further investigated the effect of the lower boundary condition on the mobilization of colloids from unsaturated porous media. Unsaturated column experiments were conducted and the lower boundary of the columns was set to either seepage or suction-controlled conditions. The amounts of mobilized colloids were significantly larger for the seepage boundary compared to the suction-controlled boundary. The shapes of the breakthrough curves were also different for the two boundary conditions; the highest colloid concentration occurred at the beginning of the column outflow for the seepage boundary; however, colloid con-

centration increased gradually and reached a distinct maximum for the suction-controlled boundary conditions. Furthermore, mobilization experiments conducted in laboratory led to the explanation of experimental artifacts caused by the outflow boundary in unsaturated column transport experiments. The flow rate and ionic strength of the infiltrating solution were also varied for the column experiments. Colloid mobilization was greater for high flow rates and low ionic strength solutions. Several "flotation" experiments were conducted to elucidate the role of the liquid-gas interface in colloid mobilization, and the results suggested that a considerable amount of colloids was captured at the moving liquid-gas interface. I also examined the mechanisms of colloid mobilization using theoretical relationships based on force balances, which showed the dominance of the detachment force over the adhesive force for all ionic strength solution.

I designed and implemented an experimental technique to determine the detachment of colloidal particles from a solid surface by a moving liquid-gas interface. Different types of colloids were used based on their hydrophobicity/hydrophilicity and surface charges. The colloids were deposited onto a glass slide in a deposition chamber, and images were captured using confocal microscopy. Liquid-gas interfaces were passed over the slide and the slide was then analyzed to determine the percentage of detachment of colloids from the slide. The results showed that colloids attached under favorable conditions did not detach as much as colloids attached under unfavorable conditions. The removal of hydrophobic and hydrophilic colloids from the hydrophilic glass slide was not significantly different after the liquid-gas movement. There was also no significant colloid removal from the glass slide after one-upward and one-downward movement of the liquid-gas interface, i.e., some of the colloids attached so strongly that they could not be removed by multiple liquid-gas interface movements.

Experimental data were supported by theoretical analysis based on a force balance of surface tension and adhesive forces.

The main conclusions of this dissertation are:

- Colloid transport was affected by centrifugal acceleration; the greater were the density differences (between colloid and medium) and colloid diameter, the lower was the "sedimentation tolerance" of the particles towards acceleration.

- The threshold accelerations from the experiments conducted in this dissertation were 5–10 g for polystyrene (786 nm), 10–20 g for silica, and 10–15 g for hematite.

- The outflow boundary in unsaturated column experiments significantly affected the colloid mobilization from porous media because of change in water content near the outflow boundary.

- Colloid mobilization decreased as ionic strength increased; however, colloid mobilization under unsaturated conditions still occurred at ionic concentrations larger than the Critical Coagulation Concentration, because colloids attached to the moving liquid-gas interface.

- Positively charged colloids were detached in greater amount than negatively-charged colloids by a moving liquid-gas interface, but no significant differences were observed between the detachment of hydrophobic and hydrophilic colloids.

- The colloids remaining on the glass slide, after one upward and one downward movement of the liquid-gas interface, were attached so strongly to the surface that they could not be removed further after multiple passages of liquid-gas interfaces.

This research increased our understanding of several mechanisms associated with colloid transport in saturated and unsaturated porous media. The centrifugal and the interfacial forces on the colloidal particles are important for their transport through porous media. The body force, created by centrifugal acceleration, was not considered in previous colloid-transport experiments using centrifuges. In previous experiments, the centrifugal accelerations used likely exceeded the critical acceleration, and the results are likely biased. The theory developed in this dissertation can be used to obtain a range of critical accelerations for proper design of colloid transport experiments in centrifuges. The interfacial forces exerted on a colloidal particle were used to estimate the colloid mobilization in unsaturated porous media. For the column experiments conducted in unsaturated porous media, the colloid mobilization was strongly dependent on the type of outflow boundary condition. This finding has important implications for vadose-zone colloid sampling. For instance, data obtained with zero-tension lysimeters may not be the representative for unsaturated zone colloid behavior. Therefore, it is necessary to consider applying suction at the outflow boundary to maintain the unsaturated column conditions during colloid sampling. Moving liquid-gas interfaces are common in unsaturated porous media, which has important implications for vadose-zone colloid transport. The strength of the moving liquid-gas interfaces for colloid detachment from the surface was studied quantitatively in this dissertation. The results imply that moving liquid-gas interfaces tend to dominate colloid movement during water infiltration into soils and sediments. The strong forces associated at the liquid-gas interface can overcome colloid aggregation and settling, which otherwise dominate colloid dispersion and mobility in porous media.

Bibliography

Abdel-Fattah, A. I., and M. S. El-Genk, On colloidal particle sorption onto a stagnant air-water interface, *Adv. Colloid. Interface Sci.*, *78*, 237–266, 1998a.

Abdel-Fattah, A. I., and M. S. El-Genk, Sorption of hydrophobic, negatively charged microsphere onto a stagnant air/water interface, *J. Colloid Interface Sci.*, *202*, 417–429, 1998b.

Abdou, H. M., and M. Flury, Simulation of water flow and solute transport in free-drainage lysimeters and field soils with heterogeneous structures, *Eur. J. Soil Sci.*, *55*, 229–241, 2004.

Campbell, G. A., and R. Mutharasan, Detection of pathogen Escherichia coli O157:H7 using self-excited PZT-glass microcantilevers, *Biosensors and Bioelectronics*, *21*, 462–473, 2005.

Celorie, J. A., S. L. Woods, T. S. Vinson, and J. D. Istok, A comparison of sorption equilibrium distribution coefficients using batch and centrifugation methods, *J. Environ. Qual.*, *18*, 307–313, 1989.

Conca, J. L., and J. Wright, Diffusion coefficients in gravel under unsaturated conditions, *Water Resour. Res.*, *26*, 1055–1066, 1990.

Conca, J. L., and J. Wright, The UFA method for rapid, direct measurements of unsaturated soil properties, *Aust. J. Soil Res.*, *36*, 291–315, 1998.

Conca, J. L., and J. Wright, The UFA method for characterization of vadose zone behavior, in *Vadose Zone Science and Technology Solutions*, vol. Additional case studies on CD-Rom, edited by B. B. Looney, and R. W. Falta, pp. 4–24, Battelle Press, Columbus, 2000.

Crawford, R., and J. Ralston, The influence of particle size and contact angle in mineral flotation, *Int. J. Miner. Process.*, *23*, 1–24, 1988.

Crist, J. T., Y. Zevi, J. F. McCarthy, J. A. Troop, and T. S. Steenhuis, Transport and retention mechanisms of colloids in partially saturated porous media, *Vadose Zone J.*, *4*, 184–5, 2005.

Culligan, P. J., K. Banno, D. A. Barry, T. S. Steenhuis, and J. Y. Parlange, Preferential flow of nonaqueous phase liquid in dry sand, *J. Geotech. Geoenviron. Eng.*, *128*, 327–337, 2002.

Czigany, S., M. Flury, and J. B. Harsh, Colloid stability in vadose zone Hanford sediments, *Environ. Sci. Technol.*, *39*, 1506–1512, 2005.

Dai, Z., D. Fornasiero, and J. Ralston, Particle-bubble attachment in mineral flotation, *J. Colloid Interface Sci.*, *217*, 70–76, 1999.

Dane, J. H., and J. W. Hopmans, Hanging water column, in *Methods of Soil Analysis, Part 4, Physical Methods*, edited by J. H. Dane, and G. C. Topp, pp. 680–683, Soil Science Society of America, Madison, WI, 2002.

de Jonge, L. W., P. Moldrup, G. H. Rubk, K. Schelde, and J. Djurhuus, Particle leaching and particle-facilitated transport of phosphorus at field scale, *Vadose Zone J.*, *3*, 462–470, 2004.

Dewoolkar, M. M., H.-Y. Ko, and A. T. Stadler, Substitute pore fluid for seismic centrifuge modeling, *Geotechnical Testing J.*, *22*, 196–210, 1999.

El-Farhan, Y. H., N. M. Denovio, J. S. Herman, and G. M. Hornberger, Mobilization and transport of soil particles during infiltration experiments in an agricultural field, Shenandoah valley, Virginia, *Environ. Sci. Technol.*, *34*, 3555–3559, 2000a.

El-Farhan, Y. H., N. M. Denovio, J. S. Herman, and G. M. Hornberger, Mobilization and transport of soil particles during infiltration experiments in an agricultural field, Shenandoah valley, Virginia, *Environ. Sci. Technol.*, *34*, 3555–3559, 2000b.

Elimelech, M., J. Gregory, X. Jia, and R. A. Williams, *Particle deposition and aggregation*, 1st ed., Butterworth-Heinemann, Woburn, MA, 1995.

Flury, M., and N. N. Wai, Dyes as tracers for vadose zone hydrology, *Rev. Geophys.*, *41*, 1002, doi:10.1029/2001RG000109, 2003.

Flury, M., M. V. Yates, and W. A. Jury, Numerical analysis of the effect of lower boundary condition on solute transport in lysimeters, *Soil Sci. Soc. Am. J.*, *63*, 1493–1499, 1999.

Gamerdinger, A. P., and D. I. Kaplan, Application of a continuous-flow centrifugation method for solute transport in disturbed, unsaturated sediments and illustration of mobile-immobile water, *Water Resour. Res.*, *36*, 1747–1755, 2000.

Gamerdinger, A. P., and D. I. Kaplan, Physical and chemical determinants of colloid transport and deposition in water-unsaturated sand and Yucca Mountain tuff material, *Environ. Sci. Technol.*, *35*, 2497–2504, 2001.

Gamerdinger, A. P., D. I. Kaplan, D. M. Wellman, and R. J. Serne, Two-region flow and rate-limited sorption of uranium (VI) during transport in an unsaturated silt loam, *Water Resour. Res.*, *37*, 3147–3153, 2001.

Gao, B., J. E. Saiers, and J. N. Ryan, Deposition and mobilization of clay colloids in unsaturated porous media, *Water Resour. Res.*, *40*, W08602, doi:10.1029/2004WR003189, 2004.

Gao, B., J. E. Saiers, and J. N. Ryan, Pore-scale mechanisms of colloid deposition and mobilization during steady and transient flow through unsaturated granular media, *Water Resour. Res.*, *42*, W01410, doi:10.1029/2005WR004233, 2006.

Gillies, G., M. Kappl, and H. Butt, Direct measurements of particle-bubble interactions, *Adv. Colloid. Interface Sci.*, *114–115*, 165–172, 2005.

Gomez-Suarez, C., J. Noordmans, H. C. van der Mei, and H. J. Busscher, Detachment of colloidal particles from collector surfaces with different electrostatic charge and hydrophobicity by attachment to air bubbles in a parallel plate flow chamber, *Phys. Chem. Chem. Phys*, *1*, 4423–4427, 1999a.

Gomez-Suarez, C., J. Noordmans, H. C. van der Mei, and H. J. Busscher, Removal of colloidal particles from quartz collector surfaces as simulated by the passage of liquid-air interfaces, *Langmuir*, *15*, 5123–5127, 1999b.

Gomez-Suarez, C., J. Noordmans, H. C. van der Mei, and H. J. Busscher, Air bubble-induced detachment of polystyrene particles with different sizes from collector surfaces in a parallel plate flow chamber, *Colloids Surf.*, *186*, 211–219, 2001.

Gregory, J., The calculation of Hamaker constants, *Adv. Colloid. Interface Sci.*, *2*, 396–417, 1969.

Gregory, J., Interaction of unequal double layers at constant charge, *J. Colloid Interface Sci.*, *51*, 44–51, 1975.

Gregory, J., Approximate expressions for retarded van der Walls interaction, *J. Colloid Interface Sci.*, *83*, 138–145, 1981.

Grolimund, D., K. Barmettler, and M. Borkovec, Release and transport of colloidal particles in natural porous media. 2. Experimental results and effects of ligands, *Water Resour. Res.*, *37*, 571–582, 2001.

Grolimund, D., M. Elimelech, M. Borkovec, K. Barmettler, and H. Sticher, Transport of *in situ* mobilized colloidal particles in packed soil columns, *Environ. Sci. Technol.*, *32*, 3562–3569, 1996.

Hiemenz, P. C., and R. Rajagopalan, *Principles of Colloid and Surface Chemistry*, Marcel Dekker Inc., New York, 1997.

Huh, C., and S. G. Mason, The flotation of axisymmetric particles at horizontal liquid interfaces, *J. Colloid Interface Sci.*, *47*, 271–288, 1974.

ISSMGE-TC2 *Geotechnical Centrifuges Worldwide*, Centrifuge and Physical Model Testing Technical Committee of the International Society of Soil Mechanics and Geotechnical Engineering, on-line at http://geo.citg.tudelft.nlallersma/tc2/cents.htm, accessed in July 2007, 1998.

Jacobsen, O. H., P. Moldrup, C. Larson, L. Konnerup, and L. W. Petersen, Particle transport in macropores of undisturbed soil columns, *J. Hydrol. (Amsterdam)*, *196*, 185–203, 1997.

Jacobsen, O. H., P. Moldrup, H. de Jonge, and L. W. de Jonge, Mobilization and transport of natural colloids in a macroporous soil, *Phys. Chem. Earth.*, *23*, 159–162, 1998.

Jin, Y., and M. Flury, Fate and transport of viruses in porous media, *Adv. Agron.*, *77*, 39–102, 2002.

Johnson, D. J., N. J. Miles, and N. Hilal, Quantification of particle-bubble interactions using atomic force microscopy: A review, *Adv. Colloid. Interface Sci.*, *127*, 67–81, 2006.

Johnson, W. P., and M. Tong, Observed and simulated fluid drag effects on colloid deposition in the presence of an energy barrier in an impinging jet system, *Environ. Sci. Technol.*, *40*, 5015–5021, 2006.

Keller, A., and M. Auset, A review of visualization techniques of biocolloid transport processes at the pore scale under saturated and unsaturated conditions, *Adv. Water Resour.*, *30*, 1392–1407, 2007.

Kjaergaard, C., T. Poulsen, P. Moldrup, and L. W. de Jonge, Colloid mobilization and transport in undisturbed soil columns. I. Pore structure characterization and tritium transport, *Vadose Zone J.*, *3*, 413–423, 2004.

Kretzschmar, R., M. Borkovec, D. Grolimund, and M. Elimelech, Mobile subsurface colloids and their role in contaminant transport, *Adv. Agron.*, *66*, 121–3, 1999.

Laegdsmand, M., K. G. Villholth, M. Ullum, and K. H. Jensen, Processes of colloid mobilization and transport in macroporous soil monoliths, *Geoderma*, *93*, 33–59, 1999.

Leenaars, A. F. M., and S. B. G. O'Brien, Particle removal from silicon substrates using surface tension forces, *Philips J. Res.*, *44*, 183–209, 1989.

Leja, J., *Surface chemistry of froth flotation*, pp. 1–14, Plenum Press, New York, 1982.

Lenhart, J. J., and J. E. Saiers, Colloid mobilization in water-saturated porous media under transient chemical conditions, *Environ. Sci. Technol.*, *37*, 2780–2787, 2003.

Levin, J. M., J. S. Herman, G. M. Hornberger, and J. E. Saiers, Colloid mobilization from a variably saturated, intact soil core, *Vadose Zone J.*, *5*, 564–569, 2006.

Levy, C., P. J. Culligan, and J. T. Germaine, Use of the geotechnical centrifuge as a tool to model dense nonaqueous phase liquid migration in fractures, *Water Resour. Res.*, *38*, 10.1029/2001WR000660, 2002.

Li, X., P. Zhang, C. L. Lin, and W. P. Johnson, Role of hydrodynamic drag on microsphere deposition and re-entrainment in porous media under unfavorable conditions, *Environ. Sci. Technol.*, *39*, 4012–4020, 2005.

Lide, D. R., *CRC Handbook of Chemistry and Physics*, 75th ed., CRC Press, Boca Raton, FL, 1994.

Logan, B. E., D. G. Jewett, R. G. Arnold, E. J. Bouwer, and C. R. O'Melia, Clarification of clean-bed filtration models, *J. Environ. Eng.*, *121*, 869–873, 1995.

Marulanda, C., P. J. Culligan, and J. T. Germaine, Centrifuge modeling of air sparging – a study of air flow through saturated porous media, *J. Hazard. Mater.*, *72*, 179–215, 2000.

Mashal, K., J. B. Harsh, M. Flury, A. R. Felmy, and H. Zhao, Colloid formation in Hanford sediments reacted with simulated tank waste, *Environ. Sci. Technol.*, *38*, 5750–5756, 2004.

McGraw, M. A., *The effect of colloid size, colloid hydrophobicity, and volumetric water content on the transport of colloids through porous media*, Ph.D. Diss. No. 77503, University of California, Berkeley, CA, 1996.

McGraw, M. A., The effect of colloid size, colloid hydrophobicity, and volumetric water content on the transport of colloids through unsaturated porous media, in *Vadose Zone Science and Technology Solutions*, vol. 2, edited by B. B. Looney, and R. W. Falta, pp. 928–938, Battelle Press, Columbus, 2000.

McGraw, M. P., and D. I. Kaplan, 1997. Colloid suspension stability and transport through unsaturated porous media, *Technical Report PNNL–11565*, Pacific Northwest National Laboratory, Richland, WA.

Mitchell, R. J., The eleventh annual R. M. Hardy Keynote Address, 1997: Centrifugation in geoenvironmental practice and education, *Can. Geotech. J.*, *35*, 630–640, 1998.

NIH *ImageJ*, A public domain Java image processing program from National Institute of Healths, on-line at http://rsb.info.nih.gov/ij, accessed in August 2007, 2007.

Nimmo, J. R., Unsaturated flow in a centrifugal field: Measurement of hydraulic conductivity and testing of Darcy's law, *Water Resour. Res.*, *23*, 124–134, 1987.

Nimmo, J. R., J. Rubin, and D. P. Hammermeister, Unsaturated flow in a centrifugal field: Measurement of hydraulic conductivity and testing of Darcy's law, *Water Resour. Res.*, *23*, 124–134, 1987.

Noordmans, J., P. J. Wit, H. C. van der Mei, and H. J. Busscher, Detachment of polystyrene particles from collector surfaces by surface tension forces induced by air-bubble passage through a parallel plate flow chamber, *J. Adhesion Sci. Technol.*, *11*, 957–969, 1997.

O'melia, C. R., Aquasols: the behavior of small particles in aquatic systems, *Environ. Sci. Technol.*, *14*, 1052–1060, 1980.

Permien, T., and G. Lagaly, The rheological and colloidal properties of bentonite dispersions in the presence of organic compounds III. The effect of alcohols on the coagulation of sodium montmorillonite, *Colloid Polym. Sci.*, *272*, 1306–1312, 1994.

Pitois, O., and X. Chateau, Small particles at a fluid interface: effect of contact angle hysteresis on force and work of detachment, *Langmuir*, *18*, 9751–9756, 2002.

Plaza, R. C., A. Quirantes, and A. V. Delgado, Stability of dispersions of colloidal hematite/yttrium oxide core-shell particles, *J. Colloid Interface Sci.*, *252*, 102–108, 2002.

Preuss, M., and H. Butt, Measuring the contact angle of individual colloidal particles, *J. Colloid Interface Sci.*, *208*, 468–477, 1998.

Rajagopalan, R., and C. Tien, Trajectory analysis of deep-bed filtration the sphere-in-cell porous media model, *AIChE J.*, *22*, 523–533, 1976.

Ralston, J., and S. S. Dukhin, The interaction between particles and bubbles, *Colloids Surf.*, *151*, 3–14, 1999.

Ralston, J., D. Fornasiero, and R. Hayes, Bubble–particle attachment and detachment in flotation, *Int. J. Miner. Process.*, *56*, 133–164, 1999.

Reynolds, W. D., D. E. Elrick, E. G. Y. andA. Amoozegar, H. W. G. Booltink, and J. Bouma, Saturated and field-saturated water flow parameters, in *Methods of Soil Analysis, Part 4, Physical Methods*, edited by J. H. Dane, and G. C. Topp, pp. 797–817, Soil Science Society of America, Madison, WI, 2002.

Ryan, J. N., T. H. Illangasekare, M. I. Litaor, and R. Shannon, Particle and plutonium mobilization in macroporous soils during rainfall simulations, *Environ. Sci. Technol.*, *32*, 476–482, 1998.

Saiers, J. E., and J. J. Lenhart, Colloid mobilization and transport within unsaturated porous media under transient-flow conditions, *Water Resour. Res.*, *39*, 1019, doi:10.1029/2002WR001370, 2003.

Saiers, J. E., G. M. Hornberger, D. B. Gower, and J. S. Herman, The role of moving air-water interfaces in colloid mobilization within the vadose zone, *Geophys. Res. Lett.*, *30*, 2083, doi:10.1029/2003GL018418, 2003.

Salyers, A. A., and D. D. Whitt, *Microbiology Diversity, Disease, and the Environment*, Fitzgerald Science Press, Bethesda, Maryland, 2001.

SAS *STAT User's Guide*, vol. 1, fourth ed., SAS Institute Inc., Cary, NC, 1990.

SAS Institute Inc. *SAS/STAT User's Guide, Vers. 6*, vol. 2, 4th ed., SAS Institute Inc., Cary, NC, 1990.

Schelde, K., P. Moldrup, O. H. Jacobsen, H. de Jonge, L. W. de Jonge, and K. Komatsu, Diffusion-limited mobilization and transport of natural colloids in unsaturated macroporous soil, *Vadose Zone J.*, *1*, 125–136, 2002.

Scheludko, A., B. V. Toshev, and D. T. Bojadjiev, Attachment of particles to a liquid surface (Capillary theory of flotation), *J. Chem. Soc. Faraday Trans. I*, *72*, 2815–2828, 1976.

Schulze, H. D., New theoretical and experimental investigations on the stability of bubble/particle aggregates in flotation: a theory on the upper particle size on floatability, *Int. J. Miner. Process.*, *4*, 241–259, 1977.

Schwertmann, U., and R. M. Cornell, *Iron Oxides in the Laboratory: Preparation and Characterization*, 2nd ed., Wiley-VCH, Weinheim, 2000.

Schwertmann, U., and R. M. Taylor, Iron oxides, in *Minerals in Soil Environments*, edited by J. B. Dixon, S. B. Weed, J. A. Kittrick, M. H. Milford, and J. L. White, pp. 145–180, Soil Science Society of America, Madison, Wisconsin, 1977.

Sharma, P., H. Abdou, and M. Flury, Effect of the lower boundary condition on colloid mobilization in unsaturated porous media, *Vadose Zone J.*, pp. submitted, 2007.

Sirivithayapakorn, S., and A. Keller, Transport of colloids in unsaturated porous media: a pore-scale observation of processes during the dissolution of air-water interface, *Water Resour. Res.*, *39*, 1346, doi:10.1029/2003WR002487, 2003.

Skoog, D. A., D. M. West, and F. J. Holler, *Fundamentals of Analytical Chemistry*, 7th ed., Saunders College Publishing, Fort Worth, 1996.

Tong, M., and W. P. Johnson, Excess colloid retension in porous media as a function of colloid size, fluid velocity, and grain angularity, *Environ. Sci. Technol.*, *40*, 7725–7731, 2006.

Tong, M., and W. P. Johnson, Colloid population heterogeneity drives hyperexponential deviation from classic filtration theory, *Environ. Sci. Technol.*, *41*, 493–499, 2007.

Toride, N., F. J. Leij, and M. T. van Genuchten, *The CXTFIT Code for Estimating Transport Parameters from Laboratory or Field Tracer Experiments, Version 2.1*, Research Report 137, U.S. Salinity Laboratory, USDA-ARS, Riverside, CA, 1995.

Tufenkji, N., and M. Elimelech, Correlation equation for predicting single-collector efficiency in physicochemical filtration in saturated porous media, *Environ. Sci. Technol.*, *38*, 529–536, 2004a.

Tufenkji, N., and M. Elimelech, Deviation from the classical colloid filtration theory in the presence of repulsive DLVO interactions, *Langmuir*, *20*, 10818–10828, 2004b.

Tufenkji, N., and M. Elimelech, Breakdown of colloid filtration theory: role of the secondary energy minimum and surface charge heterogeneities, *Langmuir*, *21*, 841–852, 2005.

Šimůnek, J., M. T. van Genuchten, and M. Sejna, *The HYDRUS-1D software package for simulating the one-dimensional movement of water, heat, and multiple solutes in variably-saturated media, Version 3.0*, Department of Environmental Sciences, University of California, Riverside, CA, 2005.

van Genuchten, M. T., F. J. Leij, and S. R. Yates, *The RETC Code for Quantifying the Hydraulic Functions of Unsaturated Soils*, U.S. Environmental Protection Agency, EPA/600/2-91/065, Washington, DC, 1991.

Visser, J., On Hamaker constants: a comparison between Hamaker constants and Lifshitz–van der Waals constants, *Adv. Colloid. Interface Sci.*, *47*, 331–363, 1972.

Wan, J., and J. L. Wilson, Visualization of the role of the gas-water interface on the fate and transport of colloids in porous media, *Water Resour. Res.*, *30*, 11–23, 1994a.

Wan, J., and T. K. Tokunaga, Measuring partition coefficients of colloids at air-water interfaces, *Environ. Sci. Technol.*, *32*, 3293–3298, 1998.

Wan, J., and T. K. Tokunaga, Partitioning of clay colloids at air-water interfaces, *J. Colloid Interface Sci.*, 2002.

Wan, J. M., and J. L. Wilson, Colloid transport in unsaturated porous media, *Water Resour. Res.*, *30*, 857–864, 1994b.

Wan, J. M., and T. K. Tokunaga, Film straining of colloids in unsaturated porous media: conceptual model and experimental testing, *Environ. Sci. Technol.*, *31*, 2413–2420, 1997.

Wu, T. H., A. T. Stadler, and C. Low, Erosion and stability of a mine soil, *ASCE J. Geotech. Eng.*, *122*, 445–453, 1996.

Yao, K. M., M. T. Habibian, and C. R. O'Melia, Water and waste water filtration: concepts and applications, *Environ. Sci. Technol.*, *5*, 1105–1112, 1971.

Zhang, H. L., G. H. Chen, and S. J. Han, Viscosity and density of H_2O + NaCl + $CaCl_2$ and H_2O + KCl + $CaCl_2$ at 298.15 K, *J. Chem. Eng. Data*, *42*, 526–530, 1997.

Zhuang, J., J. F. McCarthy, J. S. Tyner, E. Perfect, and M. Flury, In-situ colloid mobilization in Hanford sediments under unsaturated transient flow conditions: Effect of irrigation pattern, *Environ. Sci. Technol.*, *41*, 3199–3204, 2007.

Zimon, A. D., *Adhesion of Dust and Powder*, Plenum Press, New York, NY, 1969.